Controlling translational and vortical transport in classical driven lattices

Dissertation

zur Erlangung des Doktorgrades

an der Fakultät für Mathematik,

Informatik und Naturwissenschaften

Fachbereich Physik

der Universität Hamburg

vorgelegt von Aritra Kumar Mukhopadhyay
geboren am 19 Okober 1990 in Asansol, Indien

Hamburg, 2020

Dedicated to my parents.

Abstract

In this thesis, we study the directed transport of an ensemble of classical particles in periodic potentials driven out of equilibrium by unbiased time-dependent forces. We consider both one and two dimensional setups and explore their transport properties in the underdamped as well as the Hamiltonian regime.

For the setups operating in the dissipative regime, we investigate the role of lattice geometry and the physical properties of particles on the directed transport. We show that the physical properties, for e.g. size and mass, of the particles in a driven two-dimensional (2D) lattice, strongly influence the behavior of the underlying dynamical attractors in the phase space. This allows us to develop a scheme to induce directed transport of a multi-species particle mixture where the different species are transported at different angles depending on the mass or size of the particles. This also provides a simultaneous segregation mechanism of more than two particle species differing in their physical properties by using driven lattices. In another study, we demonstrate that a superposition of 2D driven Bravais lattices having arbitrary geometries can break the spatial reflection symmetries and allow directed transport of particles along specific directions. By controlling the geometry of the lattice along with the orientation of the driving force, we are able to control the average velocities of the dynamical attractors in the system's phase space. This allows us to transport the particles parallel to the driving axis, perpendicular to it as well as in an oblique direction for different lattice geometries.

In the Hamiltonian setups without the presence of any dissipation, we focused on the time-dependent control of the transport velocity of the particle ensemble. In one study, we consider two superimposed driven lattices and show that the directed transport can be accelerated, frozen and slowed down by a time-dependent switching of the potential height and driving phase of one lattice. The parameter switches allow us to control the structure of the underlying phase space in real-time, resulting in a time-dependent change of the transport velocity. In two other works, we demonstrate that such a time-dependent control of directed transport is also possible without any explicit switching of parameter values. Here, the transport direction could be reversed dynamically multiple times in 2D driven lattices simply due to the coupled nature of the underlying potential landscape in the two dimensions.

Lastly, we demonstrate a mechanism to control the rotational or vortical motion of neutral particles in driven superlattices. The superlattice consists of a superpo-

sition of individual lattices whose potential depths are driven periodically in time but with different phases. We show that such a driving scheme breaks the spatial reflection symmetries and allows an ensemble of particles to rotate with a non-zero average angular velocity. A periodic arrangement of particles in space rotating with different angular velocities is also realized by controlling the driving amplitude of the individual lattices.

Zusammenfassung

In dieser Arbeit untersuchen wir den gerichteten Transport eines Ensembles von klassischen Teilchen in periodischen Potentialen, die durch unvoreingenommene zeitabhängige Kräfte aus dem Gleichgewicht gebracht werden. Wir betrachten sowohl ein- als auch zweidimensionale Anordnungen und untersuchen ihre Transporteigenschaften sowohl im unterdämpften als auch im Hamiltonian Regime.

Für die Anordnungen, die im dissipativen Regime arbeiten, haben wir die Rolle der Gittergeometrie und die physikalischen Eigenschaften der Teilchen auf den gerichteten Transport untersucht. Wir zeigen, dass die physikalischen Eigenschaften, z.B. Größe und Masse, der Teilchen in einem getriebenen zweidimensionalen (2D) Gitter das Verhalten der zugrundeliegenden dynamischen Attraktoren im Phasenraum stark beeinflussen. Dies ermöglichte uns die Entwicklung eines Schemas zur Induktion eines gerichteten Transports einer Multispeziespartikelmischung, bei der die verschiedenen Spezies je nach Masse oder Größe der Partikel unter verschiedenen Winkeln transportiert werden. Dies ermöglicht auch einen simultanen Separationsmechanismus von mehr als zwei Partikelspezies, die sich in ihren physikalischen Eigenschaften unterscheiden, durch Verwendung getriebener Gitter. In einer weiteren Studie zeigen wir, dass eine Überlagerung von 2D-getriebenen Bravais-Gittern mit beliebigen Geometrien die räumlichen Reflexionssymmetrien brechen und einen gerichteten Transport der Partikel entlang bestimmter Richtungen ermöglichen kann. Indem wir die Geometrie des Gitters zusammen mit der Orientierung der Antriebskraft kontrollierten, konnten wir die mittleren Geschwindigkeiten der dynamischen Attraktoren im Phasenraum des Systems steuern. Dies erlaubte es uns, die Partikel parallel zur Antriebsachse, senkrecht dazu sowie in einer schrägen Richtung für verschiedene Gittergeometrien zu transportieren.

In den Hamiltonian-Anordnungen ohne jegliche Dissipation lag der Schwerpunkt auf der zeitabhängigen Steuerung der Transportgeschwindigkeit des Teilchenensembles. In einer Studie betrachten wir zwei überlagerte getriebene Gitter und zeigen, dass der gerichtete Transport durch ein zeitabhängiges Umschalten der potentiellen Höhe und der Antriebsphase eines Gitters beschleunigt, eingefroren und verlangsamt werden kann. Mit den Parameterschaltern können wir die Struktur des zugrundeliegenden Phasenraums in Echtzeit steuern, was zu einer zeitabhängigen Änderung der Transportgeschwindigkeit führt. In zwei weiteren Arbeiten zeigen wir, dass eine solche zeitabhängige Steuerung des gerichteten

Transports auch ohne explizites Umchalten der Parameterwerte möglich ist. Hier konnte die Transportrichtung in 2D-getriebenen Gittern einfach aufgrund der Kopplung der zugrundeliegenden Potentiallandschaft in den beiden Dimensionen mehrfach dynamisch umgekehrt werden.

Schließlich demonstrieren wir einen Mechanismus zur Steuerung der Rotations- oder Wirbelbewegung von neutralen Teilchen in angetriebenen Übergittern. Das Übergitter besteht aus einer Überlagerung von einzelnen Gittern, deren Potentialtiefen periodisch in der Zeit, aber mit unterschiedlichen Phasen angetrieben werden. Wir zeigen, dass ein solches Antriebsschema die räumlichen Reflexionssymmetrien bricht und einem Ensemble von Teilchen erlaubt, mit einer von Null verschiedenen mittleren Winkelgeschwindigkeit zu rotieren. Eine periodische Anordnung von Teilchen im Raum, die mit unterschiedlichen Winkelgeschwindigkeiten rotieren, wird auch durch die Steuerung der Antriebsamplitude der einzelnen Gitter realisiert.

Contents

Preface

This cumulative dissertation contains the following list of papers, which will be cited as [*A*...] in the main text.

[*A*1] Mukhopadhyay, A. K., Liebchen, B. & Schmelcher, P. *"Simultaneous Control of Multispecies Particle Transport and Segregation in Driven Lattices"*. Phys. Rev. Lett. **120**, 218002 (2018).

[*A*2] Mukhopadhyay, A. K. & Schmelcher, P. *"Controlling transport of underdamped particles in two-dimensional driven Bravais lattices"*. Phys. Rev. Research **2**, 013290 (2020).

[*A*3] Mukhopadhyay, A. K., Liebchen, B., Wulf, T. & Schmelcher, P. *"Freezing, accelerating, and slowing directed currents in real time with superimposed driven lattices"*. Phys. Rev. E **93**, 052219 (2016).

[*A*4] Mukhopadhyay, A. K., Xie, T., Liebchen, B. & Schmelcher, P. *"Dimensional coupling-induced current reversal in two-dimensional driven lattices"*. Phys. Rev. E **97**, 050202 (2018).

[*A*5] Mukhopadhyay, A. K. & Schmelcher, P. *"Multiple Current Reversals Using Superimposed Driven Lattices"*. Applied Sciences **10**, 1357 (2020).

[*A*6] Mukhopadhyay, A. K. & Schmelcher, P. *"Controlling vortical motion of particles in two-dimensional driven superlattices"*. Phys. Rev. B **102**, 094309 (2020).

Personal contributions to scientific publications:

The numerical simulations of all the manuscripts were performed by me except for [A4], for which it was jointly performed with T. Xie. I was responsible for the analysis and explanation of the data along with the writing of all the manuscripts, which were then discussed with all the remaining authors. Additionally, I had conceptualized the projects which led to the publications [A2], [A5] and [A6].

Outline of this thesis:

In the Chapter 1, we provide an introduction to the concept of directed transport and ratchets in non-equilibrium systems. We provide a motivation for research on this topic, explain the general mathematical framework and discuss the different types of ratchets along with their applications and experimental realizations. In Chapter 2, we provide a brief overview of our scientific contributions towards controlling directed transport in classical driven lattices and relate them to the existing literature. The actual manuscripts are presented in Chapter 3. Finally in the Chapter 4, we present our conclusions and provide an outlook for future research.

1

Directed transport and ratchets

1.1 Introduction

Can thermal energy be converted into useful mechanical work? Clearly this would be impossible in a system which is at equilibrium without violating the Second Law of Thermodynamics. On the other hand, if there are net forces which drive the system away from equilibrium, such a conversion is definitely possible. However, would it be possible in a system driven out of equilibrium with any net force bias? The answer is not obvious anymore. But we know that there exists various biological processes which operate in such unbiased non-equilibrium environments to accomplish a variety of chemical and mechanical tasks. The motion of bacterial flagella powers the movement of the bacteria at low Reynolds number. The various molecular motors in our bodies perform different tasks like transport of cellular cargo, protein synthesis and separating strands of DNA, all in a highly non-equilibrium cellular environment dominated by random thermal motion and high viscosity. Taking cue from these biological examples, there developed widespread research interest to understand how these molecular machines worked and whether one could design artificial physical devices or 'Brownian motors' which could replicate their action. Although the idea of using unbiased thermal fluctuations to realize useful work, also called the 'ratchet effect', has been known since the works by Smoluchowski and Feynman [1, 2], it was in the early 1990s that the idea of Brownian motors was brought into the limelight due to several notable theoretical and experimental discoveries in statistical and biological physics [3–10]. The essential ingredients in order to realize a ratchet effect with Brownian motors were soon agreed upon: (i) the system should be spatially

periodic, (ii) the average of all the forces with respect to space, time and statistical ensemble should vanish, (iii) there should be random forces (thermal, nonthermal or chaotic) present, (iv) the system should be out of equilibrium breaking the detailed balance symmetries and (v) some other spatial and/or temporal symmetries should be necessarily broken. Different types of ratchets were classified according to how these necessary conditions were realized. In this chapter, we would give a brief introduction to the mathematical formalism behind such ratchet transport and discuss the various types of ratchets which have been realized over the years classified on the basis of their regime of operation.

1.2 Setup and mathematical model

The most general model to study the ratchet phenomena in one dimensional (1D) systems is to consider a Brownian particle of mass m with position $x(t)$ at time t moving in a potential landscape $V(x,t)$ which can in general be time-dependent, such that the dynamics is governed by the inertial Langevin equation

$$m\ddot{x} + \frac{\partial V(x,t)}{\partial x} = -\gamma\dot{x} + \xi(t). \tag{1.1}$$

Here γ is the dissipation coefficient accounting for friction, viscosity etc. and $\xi(t)$ is a randomly fluctuating force which models the thermal noise present in the system. The left hand side of the Eq.(1.1) represents the deterministic component of the particle dynamics due to the underlying space and time dependent potential and the right hand side is the stochastic component accounting for the particle's interaction with its thermal environment. The potential is considered periodic in space and time such that $V(x,t) = V(x+L,t) = V(x,t+T) = V(x+L,t+T)$ with L and T being the spatial and temporal periodicities of the system respectively. The time dependence of the potential can be realized via an external driving force which keeps the system out of equilibrium. The fluctuating thermal noise is usually modeled by a Gaussian white noise of zero mean $\langle \xi(t) \rangle = 0$ satisfying the fluctuation-dissipation relation $\langle \xi(t)\xi(s) \rangle = 2\eta k_B \mathcal{T} \delta(t-s)$ where k_B is the Boltzmann's constant and $\mathcal{T}$ is the temperature. In order to satisfy the requirement that the particle should not experience an average net force bias, one requires

$$\int_0^L \int_0^T dx\, dt\, [g(x,t) + \xi(t)] = 0, \quad g(x,t) = -\frac{\partial V(x,t)}{\partial x} \tag{1.2}$$

The key quantity of interest is the time-dependent transport in the system which is defined in terms of the particle's velocity as

$$J(t) = \langle \dot{x} \rangle_\Gamma \tag{1.3}$$

where $\langle ... \rangle_\Gamma$ denotes the average over a statistical ensemble. The asymptotic transport is given by

$$J = \langle J(t) \rangle_t, \quad \langle ... \rangle_t \equiv \lim_{t \to \infty} \int_0^t dt' (...) \tag{1.4}$$

and if $J \neq 0$ then the system is said to exhibit directed transport due to the ratchet phenomena. One of the key ingredients required to obtain a non-zero value of J has been shown to be some sort of spatial or temporal asymmetry in the system incorporated through the potential $V(x,t)$. A standard method to introduce such an asymmetry is by using a spatially asymmetric potential landscape, typically referred to as the 'ratchet potential'. Another method is via an external time dependent perturbation (either stochastic or deterministic) which is asymmetric with respect to time. Depending on how this asymmetry is introduced in the system along with the presence or absence of the stochastic component in the equation of motion Eq.(1.1), ratchets can be classified into different types. Originally, the different ratchet models were put forward to explain the working principle of molecular motors and hence thermal noise and dissipation were an integral part of these models. Hence they are referred to as Brownian ratchets. Later on, directed transport has been realized in ratchet setups which operate completely in the deterministic regime and hence were classified as deterministic ratchets. Later it was also possible to obtain directed transport in deterministic Hamiltonian systems without any dissipation and these setups were classified as Hamiltonian ratchets. In the following sections, we provide an overview of how directed transport is realized in these different classes of ratchets.

1.3 Brownian ratchets

The earliest works on modern ratchet research started with the so called *'on-off'* *ratchets* [3, 11, 12] consisting of non-interacting Brownian particles subjected to a 1D periodic asymmetric potential $V(x)$ switched periodically on and off (see Fig.(1.1)). The considered systems were all overdamped and the effects of inertia was negligible, i.e. $m\ddot{x} \approx 0$ in Eq.(1.1). With this approximation, the dynamics of

5
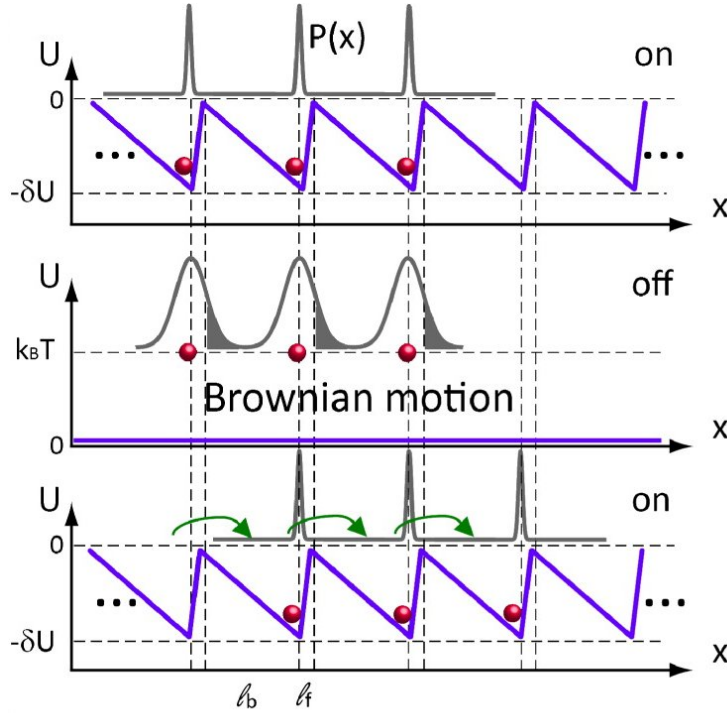
Figure 1.1: The distribution of particles in an on-off lattice. When the potential is switched on, the particles are distributed at the central minima of the potential. On switching the potential off, the particles diffuse symmetrically due to the unbiased white noise. However switching the potential on again leads to unequal particle distribution in the neighbouring left and right minima, thus leading to ratchet transport. Reprinted (adapted) with permission from [13]. Copyright 2016 by the American Chemical Society.

the Brownian particles in these 'on-off' ratchet setups could be modeled by

$$\gamma \dot{x} = -f(t)\frac{\partial V(x)}{\partial x} + \xi(t) \tag{1.5}$$

Essentially, this means that the background potential $V(x)$ could be turned 'on' and 'off' with the time dependent perturbations $f(t) = 1$ and $f(t) = 0$ respectively.

The working principle of such an on-off ratchet can be intuitively understood as follows: Consider an initial symmetric particle distribution located around the origin (see Fig.(1.1)). When the potential is switched on, the particles settle at the potential minimum at the origin and so that the distribution is peaked there. When the potential is switched off, the particles diffuse symmetrically both towards left and right due to the presence of unbiased thermal noise. However, on switching the potential back on again, the asymmetric shape of $V(x)$ forces more

number of particles to be trapped in the neighbouring right minimum than the neighbouring left minimum. As the whole process is repeated periodically over time, the particles on an average drift towards the right yielding a non-zero directed transport even though there is no average net force on the particles. There are three crucial ingredients required for the 'on-off' ratchet to function: (i) the left-right asymmetry of the potential $V(x)$, which breaks the symmetry of the particle distribution at later times, (ii) dissipation, which is responsible for the particles to relax back into the nearest particle minima during the 'off' phase and (iii) noise, due to which the particles can diffuse during the 'off' phase.

A second class of Brownian ratchets, which is now referred to as the *tilting ratchets*, has the general form

$$\gamma \dot{x} = -\frac{\partial V(x)}{\partial x} + f(t) + \xi(t) \tag{1.6}$$

where the background potential has $V(x)$ has a spatial asymmetry just like the on-off ratchet. However, in contrast to the on-off ratchet, the time-dependent perturbation $f(t)$ in the tilting ratchet is of additive nature rather than multiplicative. This unbiased perturbation can either be in the form of an external time-periodic driving force or a stochastic force of non-thermal origin. Depending on whether it is of stochastic or deterministic origin, the ratchet can be classified as *fluctuating* or *rocking ratchet* respectively. It has been shown that different types of noise profiles $f(t)$, both colored Gaussian or non-Gaussian, can yield a ratchet transport of particles [14, 15]. The rocking ratchet has also been realized in different physical setups like asymmetric superconducting quantum interference devices (SQUIDs), parallel arrays of Josephson junctions and vortex motion in superconductors [16–20]. One of the main difference of the tilting ratchet compared to the on-off ratchet is that the thermal noise $\xi(t)$ is not necessarily required to achieve a directed particle transport. This led to the relaxation of the requirement of stochastic forces in order to realize directed transport and gave birth to the completely new category of deterministic ratchets.

1.4 Deterministic ratchets

In the absence of stochastic forces or thermal fluctuations, the rectification mechanism of ratchets depends on the combination of non-linearity and symmetry

breaking of the underlying equation of motion. In [21], such a deterministic ratchet model was discussed for the first time where the inertial contribution was important. The equation of motion was of the form

$$m\ddot{x} + \gamma\dot{x} = -\frac{\partial V(x)}{\partial x} + f(t) \tag{1.7}$$

where the driving force was considered to be a unbiased periodic function of time $f(t) = d\sin t$, with d being the driving amplitude. The asymmetry was introduced through the asymmetric bi-harmonic ratchet potential $V(x) \propto \sin x + 0.25\sin 2x$. In the absence of the inertial term, the Eq.(1.7) allows only two types of particle dynamics: they are either trapped for small driving amplitude d or they move ballistically either to the left or the right with a fixed average velocity. However, the inertial term allow the particles additionally to exhibit diffusive chaotic dynamics. It was shown that by controlling the driving amplitude d and the mass m, the diffusive motion of the particles could be channelized either towards the left or the right, thus yielding directed transport. In an intriguing way, the authors found that the chaotic motion in such deterministic ratchets could play the role of stochastic component in the Brownian ratchets. Since then, a wide variety of deterministic ratchets have been explored [22–31]. It has been also shown that the necessary asymmetry can also be introduced in different ways. One of the popular methods is via 'harmonic mixing', where the driving force $f(t)$ is considered to be of bi-harmonic form [32]. Another method, commonly called 'gating', refers to the use of a multiplicative driving force (as in Eq.(1.5)) in conjunction with the additive driving $f(t)$, both having different frequencies [33–38].

1.5 Hamiltonian ratchets

With the advent of deterministic ratchets, it was clear that noise was not an indispensable requirement to achieve a ratchet like rectification of particle motion. The idea that chaos played somewhat analogous role of noise in these deterministic ratchet setups led to the question whether directed transport can also be observed in purely Hamiltonian setups without any dissipation, aided by the rich chaotic behavior that these systems exhibit. The answer was provided in the early 2000 by the paper [39], where the authors provided a minimal model of Hamiltonian
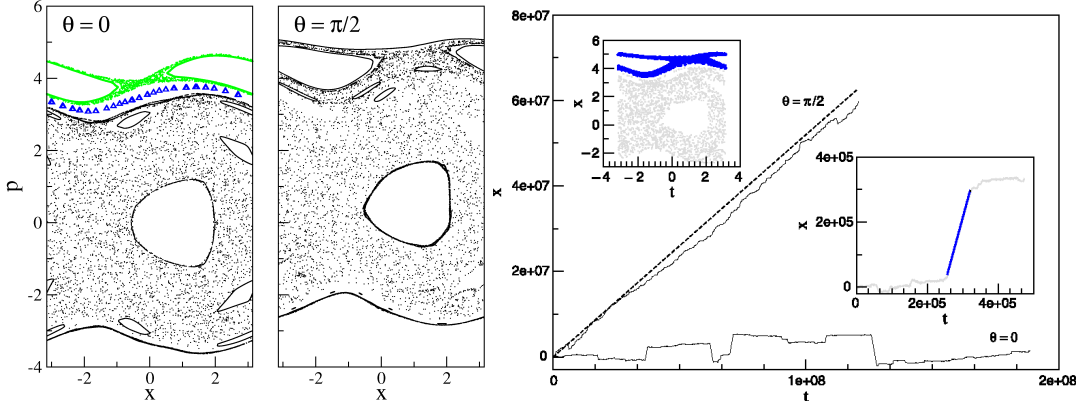
Figure 1.2: Poincaré surfaces of section for the Hamiltonian system corresponding to Eq(.1.8) for (left panel) $\theta = 0$ and (middle panel) $\theta = \frac{\pi}{2}$. The right panel shows directed transport for $\theta = \frac{\pi}{2}$ whereas no transport is observed for $\theta = 0$. Reprinted (adapted) with permission from [40]. Copyright 2014 by Elsevier.

ratchets:

$$m\ddot{x} = -\frac{\partial V(x)}{\partial x} + f(t) \tag{1.8}$$

with the underlying lattice potential $V(x) = \cos x$ and the bi-harmonic driving force $f(t) = E_1 \cos \omega t + E_2 \cos(2\omega t + \theta)$. They showed that for non-zero values of E_1 and E_2 along with $\theta \neq 0, \pi$, one could have directed transport of particles. For the very first time, this work also generalized the necessary symmetries that needs to be broken in order to expect a ratchet transport in both Hamiltonian and dissipative setups. We would discuss them in detail in the next section. Apart from he necessary symmetry breaking, they showed that another crucial requirement for directed transport to occur in Hamiltonian setups was the existence of a 'mixed' phase space describing the system. This can be explained in detail by constructing the Poincaré surfaces of sections (PSOS) of our setup in Eq.(1.8). For this, one plots the values of the particle coordinate x and momentum $p = m\dot{x}$ of different initial conditions stroboscopically at times $t = nT$ where $n = 1, 2, ...$ and T is the temporal period (see Fig.(1.2)). The PSOS shows the existence of both chaotic manifold, which describes diffusive motion of particles through the driven lattice and regular islands embedded in the chaotic manifold, describing either trapped or ballistic motion of the particles. Due to the existence of both these components, the system is said to posses a mixed phase space.

The principle behind the existence of directed transport can be explained in terms of the PSOS. A trajectory initiated in the chaotic layer would visit every point in the chaotic layer over long timescales due to the ergodic property of the

chaotic manifold. As a result, the asymptotic velocity of this trajectory can be shown to be equal to the average transport velocity of the chaotic manifold by a 'sum rule' [41, 42]. In presence of spatial parity and time-reversal symmetries (corresponding to $\theta = 0, \pi$), the PSOS has a reflection symmetry about $p = 0$ and this results in vanishing transport velocity of the chaotic manifold, hence no directed transport is observed (see Fig.(1.2)). On the other hand, for $\theta \neq 0, \pi$ the symmetries are broken which also breaks reflection symmetry of the PSOS and this ensures a non-zero transport velocity of particles. The Hamiltonian ratchets have been extensively realized using cold atoms in ac-driven optical lattices [43, 44]. Here the temperature of the atomic ensembles is in the micro-Kelvin regime and the classical description of the ratchets have been shown to accurately describe the transport properties [43, 44]. A more recent realization of Hamiltonian ratchets has been achieved by employing spatio-temporally driven lattices where a lattice of potential barriers can be individually driven with different driving laws [45, 46]. In addition to exhibiting directed transport, these setups have been shown to be useful in selective trapping of particles at specific lattice sites and in generating density wave like patterns [47, 48].

1.6 Symmetry breaking

One of major requirement for observing directed transport in all the different types of ratchets has been the breaking of certain symmetries of the setup. Although this was well known since the early days of ratchet research, the symmetries were strictly formalized only in the early 2000s in [39]. It was shown that in order to have a non-vanishing value of the average velocity J (see Eq.(1.4)) in an 1D driven system, one must break all the symmetries which keep the equation of motion Eq.(1.1) invariant, but change the sign of the particle velocity $\dot{x}$. In 1D, there are only two possible symmetry transformations which can change the sign of the particle velocity :

$$S_x : x \longrightarrow -x + \chi, \quad t \longrightarrow t + \tau \tag{1.9}$$

$$S_t : x \longrightarrow x + \chi, \quad t \longrightarrow -t + \tau \tag{1.10}$$

where χ and τ are arbitrary spatial and temporal shifts respectively. S_x and S_t are the most general form of spatial parity and time reversal symmetries in 1D

respectively. Hence, it was established that the equations of motion must break these symmetries. All the different methods to introduce asymmetry in the various ratchet setups, as discussed in the previous sections, can in fact be described in terms of these two symmetries alone.

For the Hamiltonian ratchets, the necessity to break these two symmetries can be intuitively explained as follows. If the system is invariant under at least one of the S_x and S_t symmetries, every trajectory can be mapped to another which has exactly similar dynamics as that of the former one but with opposite velocity. As a result, the average velocity of an ensemble of particles would always be zero at any time during the time evolution provided that the ensemble was initialized with a zero average velocity. Hence, such a system would not exhibit any directed transport. In terms of the underlying phase space, the existence of any of the two symmetries implies that the PSOS would be symmetric with respect to $p = 0$ (see Fig.(1.2)), resulting in zero transport velocity of the chaotic layer.

The situation is a bit different for the deterministic ratchets in presence of dissipation. Due to the presence of the inertial term in Eq.(1.7), the symmetry S_t is broken irrespective of the underlying potential and driving force. The asymptotic directed transport in these systems is completely determined by the properties of the dynamical attractors underlying its phase space. Each attractor $\mathcal{A}$ is characterized by its average velocity $v_{\mathcal{A}}$ and the set of all initial conditions in the phase space $\sum_{\mathcal{A}} = \{x, \dot{x}, t\}$ which asymptotically end up in $\mathcal{A}$ called the 'basin of attraction' of $\mathcal{A}$. If the system is invariant under S_x, an attractor is mapped either onto itself which imply $v_{\mathcal{A}} = 0$ or onto its symmetry related twin $\mathcal{A}'$ such that $v_{\mathcal{A}} = v_{\mathcal{A}'}$. Since the transformation S_x also maps the basins of attraction of $\mathcal{A}$ and $\mathcal{A}'$ onto each other, any distribution of initial conditions which occupies the same volume in both the basins will yield zero transport.

A detailed analysis of these symmetries along with different methods by which these symmetries can be broken in different systems can be found in [40]. It is important to note that even when these symmetries are broken, there might still be other specific mechanisms which prohibit a non-zero transport in a setup. Hence, the breaking of the symmetries is a necessary but not sufficient condition for observing a ratchet transport.

1.7 Higher dimensional ratchets

The phenomenon of directed transport is not limited to spatially 1D systems only, they can also occur in 2D and 3D systems. Conceptually, the new ingredient is the coupling between the spatial dimensions in the underlying potential. This allow us to realize not only particle motion along any arbitrary direction through the setup, but also rotational motion giving rise to vorticity. Analogous to their 1D counterpart, particles in a higher dimensional ratchet setup are modeled by the Langevin equation

$$m\ddot{\mathbf{r}} + \boldsymbol{\nabla}V(\mathbf{r},t) = -\gamma\dot{\mathbf{r}} + \boldsymbol{\xi}(t) \tag{1.11}$$

with the generalization of x in Eq.(1.1) to $\mathbf{r} \equiv (x,y,z)$. The requirement of zero net average force means that

$$\int_{\mathbf{0}}^{\mathbf{L}} \int_{0}^{T} d\mathbf{r}\, dt\, [\mathbf{g}(\mathbf{r},t) + \boldsymbol{\xi}(t)] = \mathbf{0}, \quad \mathbf{g}(\mathbf{r},t) = -\boldsymbol{\nabla}V(\mathbf{r},t) \tag{1.12}$$

1.7.1 Translational current

The time-dependent translational current in the system is characterized by the particle velocity averaged over a statistical ensemble Γ: $\mathbf{J}(t) = \langle\dot{\mathbf{r}}\rangle_\Gamma$. Hence, the asymptotic transport is given by

$$\mathbf{J} = \langle\mathbf{J}(t)\rangle_t, \quad \langle...\rangle_t \equiv \lim_{t\to\infty} \int_0^t dt'(...) \tag{1.13}$$

which now is a vector corresponding to transport along different directions x, y and z. The symmetries that need to be broken to realize directed transport in 2D and 3D systems were first discussed only in 2008 [49]. Analogous to 1D, the symmetries which keep Eq.(1.11) invariant but changes the sign of the velocity vector were identified to be

$$S_{\mathbf{r}} : \mathbf{r} \longrightarrow -\mathbf{r} + \boldsymbol{\chi}, \quad t \longrightarrow t + \tau \tag{1.14}$$

$$S_t : \mathbf{r} \longrightarrow \mathbf{r} + \boldsymbol{\chi}, \quad t \longrightarrow -t + \tau \tag{1.15}$$

which are the most general form of the spatial inversion symmetry and time-reversal symmetry respectively. Note that in a 2D system, the spatial inversion operation can be further decomposed into $S_{\mathbf{r}} \equiv P_x P_y + \boldsymbol{\Lambda} + \eta$ i.e. consecutive reflections $P_x : x \longrightarrow -x$ and $P_y : y \longrightarrow -y$ along x and y (or any two orthog-
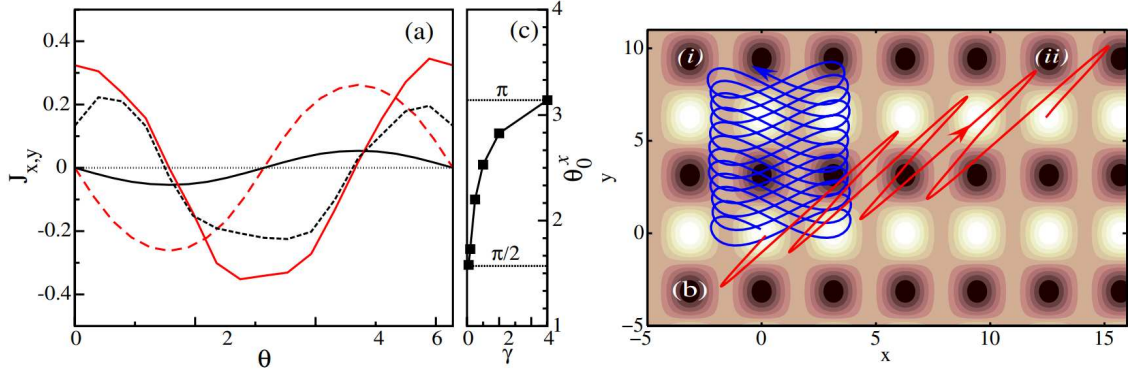
Figure 1.3: (left) Dependence of the translational current components, J_x (solid line) and J_y (dashed line) on $\theta_{x,y} = \theta$ for the system described by Eq.(1.16). The thick (thin) lines correspond to overdamped (underdamped) dynamics for $m = 0, \gamma = 1$ ($m = 1, \gamma = 0.1$). The dependence can be captured by a sinusoidal function of θ, with the phase depending upon γ as shown in the middle panel. (right) Two typical trajectories in the setup for two different parameter regimes showing the control of the transport direction. The blue trajectory exhibits directed transport only along y-direction due to the presence of P_x symmetry whereas the red trajectory is transported along both x and y directions since both P_x and P_y symmetries are broken. For detailed parameters, refer to [49]. Reprinted (adapted) with permission from [49]. Copyright 2008 by the American Physical Society.

onal) axes respectively followed by any arbitrary space and time translations $\mathbf{\Lambda}$ and η. This offers further control over the directed current $\mathbf{J}$ which is not possible in 1D. For e.g., one can constrain the directed transport to occur only along the x-direction by designing a setup which breaks the P_x symmetry but preserves the P_y symmetry. In [49], a 2D rocking ratchet model was presented which can be described by the model

$$m\ddot{\mathbf{r}} + \gamma\dot{\mathbf{r}} = -\mathbf{\nabla}V(\mathbf{r}) + \mathbf{f}(t) + \boldsymbol{\xi}(t) \qquad (1.16)$$

with the potential given by $V(x,y) = \cos x(1 + \cos(2y))$ and the driving force of the bi-harmonic form $f_{x,y}(t) = E_{x,y}^{(1)} \sin t + E_{x,y}^{(2)} \sin(2t + \theta_{x,y})$. The symmetries $S_{\mathbf{r}}$ and S_t can be broken for non-zero values of $E_{x,y}^{(1)}, E_{x,y}^{(2)}$. By controlling the phase $\theta_{x,y}$ of the driving force, one can control the strength and direction of the directed current (see Fig.(1.3)).

1.7.2 Vortical current

The possibility to realize rotational motion of particles is a completely new phenomenon in higher dimensional ratchet setups. In order to distinguish unbiased
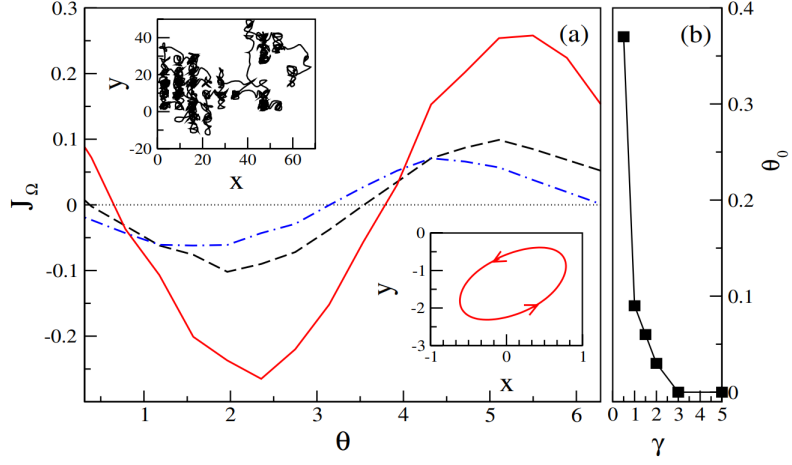
Figure 1.4: Dependence of the rotational current $\mathbf{J}_\Omega$ on the phase of driving θ for different values of dissipation strength $\gamma = 0.2$ (solid line), $\gamma = 0.05$ (dashed line) and $\gamma = 2$ (dashed–dotted line). The trajectory and the corresponding attractor solution are shown in the left and right insets for $\gamma = 0.2$ and $\theta = \pi/2$. The dependence of $\mathbf{J}_\Omega$ on θ can be captured by a sinusoidal function, with the phase depending upon γ as shown in the middle panel. For detailed parameters, refer to [49]. Reprinted (adapted) with permission from [49]. Copyright 2008 by the American Physical Society.

diffusive motion of particles from the rotational motion, a slightly different measure of angular velocity was introduced in [49]:

$$\mathbf{\Omega}(t) = \left[\dot{\mathbf{r}}(t) \times \ddot{\mathbf{r}}(t) \right] / \dot{\mathbf{r}}^2(t) \qquad (1.17)$$

which is equivalent to the definition of curvature of planar curves measuring the speed of rotation of the velocity vector of a particle about its origin. The average angular angular velocity is hence given by $\mathbf{J}_\Omega = \langle \mathbf{\Omega}(t) \rangle_t$. Just like the translational currents, one can deduce the necessary conditions which the Eq.(1.11) has to break in order to allow rotational currents by analyzing the symmetries. For a 2D potential, the symmetries which change the sign of the angular velocity $\mathbf{\Omega}(t)$ but keep the equation of motion invariant are

$$S_t \; : \; t \longrightarrow -t + \tau, \quad \mathbf{r} \longrightarrow \pm \mathbf{r} + \boldsymbol{\chi} \qquad (1.18)$$

$$S_p \; : \; \mathbf{r} \longrightarrow \mathcal{R}\left(\mathcal{P}\mathbf{r}\right) + \boldsymbol{\chi}, \quad t \longrightarrow t + \tau. \qquad (1.19)$$

S_t is the time reversal symmetry together with optional an spatial inversion and arbitrary space-time translations. Whereas, S_p is the most general form of reflection $\mathcal{P}$ about any plane perpendicular to the xy plane with optional spatial rotation $\mathcal{R}$ in the xy plane. In [49], it was shown that the potential $V(x,y) =$

14

$[-3(\cos x + \cos y) + \cos x \cos y]/2$ with an elliptical driving force $f_x(t) = E_x^{(1)} \cos t$, $f_y(t) = E_y^{(1)} \cos(t + \theta)$ can break these symmetries and induce vortex motion of particles (see Fig.(1.4)). Interestingly, this setup does not break the spatial inversion symmetry $S_\mathbf{r}$. Hence, the translational current $\mathbf{J} = \mathbf{0}$. By careful design of the setup with relevant symmetries, one can thus control both translational and rotational currents simultaneously in such 2D systems. A detailed discussion of the symmetry breaking governing these currents can be found in [40].

1.8 Experimental setups and applications

Since the inception of ratchet transport in the early 1990s, there has been numerous research on this topic and directed transport has since been realized in a variety of different physical systems. In this section, we would provide very brief accounts of two physical systems where the ratchet physics has been extensively studied. Alongside, we would highlight some of the practical applications of ratchet transport in some other physical systems too.

Colloidal ratchets: Since all the early ratchet models were developed keeping the Brownian regime in mind, unsurprisingly colloidal systems provided the foremost testbed for realization of the ratchet effect. In 1994, the flashing ratchet was demonstrated for the first time using polystyrene colloidal micro-spheres in a background potential which was switched on and off with time [11]. Directed transport of these spheres was observed as predicted by the theoretical model. A similar on-off ratchet transport was also realized using fragments of DNA in water using a micromachined silicon-chip device [50]. The possibility to use laser beams to trap and move colloidal particles in optical tweezers provided a very flexible setup to test the predictions of the Brownian ratchet models. Some of the first ratchet experiments with colloidal particles using optical tweezers yielded good quantitative agreements with the theoretical models [12, 51]. In the 2000s, due to the development of holographic optical traps which allowed the micro-manipulation of colloidal particles of sizes in the orders nanometers to microns [52–54], there has been considerable experimental thrusts to design colloidal ratchet devices. The first ratchet experiment using a lattice of holographic optical traps was successfully conducted using silica based micro-spheres in 2005 [55]. The asymmetry in the setup was realized by a three-step driving protocol. Since

then, holographic optical tweezers have been used to control directed transport of colloidal particles in both one and two dimensions with the driving force realized by the use of piezo-modulators [22, 56].

Cold atom ratchets: Cold atoms in driven optical lattices form an ideal system to explore ratchet physics. The main advantage over the aforementioned colloidal system is that the level of dissipation in cold atom ratchets can be flexibly controlled allowing both Hamiltonian and dissipative ratchets to be realized. The optical lattices are created by the interference of two or more laser fields. Far-detuned laser fields produces purely conservative potentials which are ideal for modeling Hamiltonian systems. In contrast, the near-resonant fields with appropriate Sisyphus cooling mechanism lead to a dissipative optical lattice. The first ratchet experiment using cold atoms was performed in 1999 by using an undriven dark optical lattice [57]. The experiments with driven optical lattices started in 2003 and here the driving mechanism was achieved by phase modulating the laser beams via acousto-optical modulators (AOM) [58]. In this work, the authors demonstrated a rocking ratchet using ^{85}Rb atoms where the direction of transport could be controlled by varying the driving phase. The experiment was performed in the regime of strong damping and small dissipation which allowed them to well approximate the Hamiltonian regime [59]. Experimental realization of dissipative ratchets with cold atoms has also been realized [60, 61]. Due to the flexibility in tuning the optical lattice systems, a host of cold atom ratchet setups have been studied experimentally [59, 62–68]. A detailed review of these different cold atom ratchets can be found in [43, 69].

Applications: Over the years, the ratchet effect has found numerous applications in various other disciplines as well. One of the most frequent application lies in particle separation based on 'internal' particle properties like mass, size and mobility. The central idea is that the particles having different physical properties would move in different directions under the ratchet effect, allowing them to be separated. Based on this, particle filters have been designed to separate two component mixtures with potential biomedical applications [70–72]. Other ratchet based segregation schemes include electrophoretic mobility based sorting [73], size-sorting of superparamagnetic particles using periodically switching magnetic fields [74], sorting active and passive particles in soft matter systems [75, 76], separating cell mixtures in microfluids [77] and separation of granular

16

particles [78]. Ratchet effect in superlattices also allow us to separate ballistic and diffusive particles from each other and filter them according to their velocities [47, 48]. Apart from particle separation, the ratchet effect has been shown to effectively induce voltage rectification in superconducting quantum interference devices (SQUIDs) [16, 79, 80], transportation of fluxons in Josephson junctions arrays [17, 81], and movement of trapped vortices in superconductors [19, 82–84] among others.

1.9 Control of directed transport

Due to the many applications of directed transport across disciplines, it is not surprising that much of the theoretical research has focused on how to control the strength and direction of the transport. It is important to note that although a symmetry analysis of the system as described in Sec.(1.6) can predict the existence of directed transport, it can not provide any information about its strength and direction. In fact, the direction of transport can be completely reversed following an appropriate change in the system parameter. This phenomenon is called current reversal and was first discussed in [7–9, 85] in the context of Brownian ratchets in presence of noise. It was shown that varying the profiles and strength of noise or by the amplitude of the external driving force, the direction of transport can be reversed in 1D. Since then, the origin and control of current reversals has become an important research direction in ratchet physics [22, 63, 67, 79, 86–92]. Most of the existing mechanisms to generate current reversals focus on changing the direction of asymptotic particle transport due to a change of system parameter [24, 82, 93, 94]. This serves as the basic principle behind particle separation based on different physical properties. Recent research has focused on setups where the current reversal can occur dynamically in time too [22, 95–97]. Such a dynamical reversal is caused either due to a time-dependent change of a system parameters or due to other effects like interaction between the particles, dimensional coupling in the background potential etc. Different 1D setups exhibiting multiple current reversals have also been explored [21, 24, 82, 87, 90, 98–102].

Two-dimensional ratchet setups allow richer degree of transport control because the particles can now be transported in different directions, not necessarily confined to the left or right. Followed by the identification of the symmetry conditions for the existence of directed transport in 2D [49], cold atom experiments

using a three-beam dissipative optical lattice demonstrated ratchet transport due to bi-harmonic driving forces in x and y-directions [66]. Some progress on 2D ratchets has been achieved in the context of vortex motion of superconductors, although the directed motion here is due to the long range interaction of the vortices and not a single particle effect [78, 83, 84, 103–107]. A new type of rectification has been shown in such systems due to which directed transport is achieved by applying a dc-force perpendicular to the ac-driving force. Very recently, a colloidal ratchet was realized in 2D holographic optical lattices due to which directed transport could be observed in arbitrary direction [56].

Although the control of ratchet transport has been quite well studied in 1D, there has not been comparable progress in 2D systems. This is in spite of the fact that 2D systems offer much richer phenomenology in terms of both translational and rotational transport of particles. Additionally, most of the 2D setups where the ratchet phenomena has been studied are overdamped. Although the understanding of directed transport in the Hamiltonian and underdamped regime is crucial for the development of miniature ratchet devices where the effect of noise and dissipation can be ignored, further research is still required in this domain. With the advancement of experimental technologies in designing 2D driven lattices, especially due to holographic optical trapping of colloids and cold atoms, it is a natural next step to explore the diverse phenomena that directed transport offers in 2D. In the next chapters, we would explain the progress achieved in that direction in the scope of this thesis.

2

Overview of scientific contributions

In this chapter, we provide a brief overview of each scientific contribution presented in this dissertation. More detailed explanations may be found in the actual manuscripts provided in the next chapter.

2.1 Directed transport of underdamped particles at arbitrary angles

As already mentioned in the previous chapter, the large body of literature on directed particle transport using externally driven two-dimensional periodic potentials has focused on the demonstration and controllability of transport along certain specific directions. It has been shown that in presence of a combination of both ac and dc drives, particle transport can be achieved opposite to the direction of the dc-force (absolute negative mobility) or completely orthogonal to it (absolute transverse mobility) [104, 108]. In the absence of a dc drive, it has been also shown that particles can be transported oblique to the axis of the ac driving force in the overdamped regime [56]. In all of these cases, either one or more of these three ingredients were necessary for directed transport: (i) overdamped particles, (ii) presence of a dc bias force, (iii) square lattice geometry. This leads to some important questions in the context of directed transport of particles in 2D driven lattices. How to predict the direction of transport in the systems which are underdamped? Is a dc drive necessary in addition to the ac drive in order to realize transport? What role does different lattice geometry play in controlling the transport direction? In this section of the dissertation, we try to address these questions.

2.1.1 Simultaneous control of multi-species 2D transport

In this paper $[A1]$ (see Sec.(3.1) for details), we consider an ensemble of under-damped particles moving in an 'egg-shell' 2D potential $V(x, y) = V \cos k_x x (1 + \cos k_y y)$ which is driven via external bi-harmonic driving forces of the form $f_{x,y}(t) = d_{x,y}(\cos \omega t + 0.25 \cos(2\omega t + \pi/2))$ acting in both x and y directions. Due to the bi-harmonic form of the driving law, both the spatial inversion $S_{\mathbf{r}}$ and time reversal S_t symmetries are broken, thus allowing directed transport. The ensemble consists of a mixture of particles, modeled as spherical particles of radius r, having different masses $m \propto r^3$ and Stokes' friction coefficient $\gamma \propto r$. We observe that upon initializing the mixture within a small region of the lattice with very low velocities, the particles travel at different angles which is characterized by their radii r. By analyzing the bifurcation diagrams of the particle velocities as a function of their radii, we show that particles with different radii r move with velocities corresponding to different ballistic attractors of the system. As a result, groups of particles having similar radii travels through the lattice along a specific direction with a specific speed. The direction of transport of particles having a specific radius can be further controlled by changing any other system parameter, for e.g., the lattice height V. This provides a systematic approach to separate particles having a specific radius, say $r = r_0$, from a mixture of particles having different sizes by constructing a 'two parameter bifurcation diagram' of the attractor velocities as functions of V and r. From such a diagram, one can choose a value $V = V_0$ which allows particles with radius $r = r_0$ to travel at an angle $\sim \theta_0$ ballistically and hence can be separated from the remaining particles having different radii. In summary, we demonstrated that it is possible to induce a directed ballistic transport of underdamped particles at any angle relative to the direction of the ac driving force without the aid of any additional dc bias in a species-selective way.

2.1.2 Effect of lattice geometry on 2D directed transport

In this work $[A2]$ (see Sec.(3.2) for details), instead of a sinusoidal optical lattice potential, we consider a lattice formed by 2D Gaussian barriers centered at positions $\mathbf{r}_{mn} = (m, n)$ with $m, n \in \mathbb{Z}$ and having site-dependent potential heights V_{mn}. This yields the potential $V(x, y) = \sum_{m,n=-\infty}^{+\infty} V_{mn} e^{-\beta(\mathbf{r}-\mathbf{r}_{mn})^2}$. The set of all the Gaussian barriers arranged periodically in space with a specific value of barrier

height V_{mn} forms a sublattice of our system. Our setup is hence a superlattice formed by the superposition of all these different sublattices. Additionally, we choose an oscillating driving force $\mathbf{F}(t) = d \cos t \, (\cos \theta_d, \sin \theta_d)$, where θ_d denotes the angle of the driving force with respect to the x-axis. Unlike the often used bi-harmonic driving law, our driving force being a single-harmonic function of time can not break the spatial inversion symmetry $S_\mathbf{r}$ of the setup. Each sub-lattice formed by the Gaussian barriers is also inversion symmetric. However, by superposing at least three such sublattices we could design a potential landscape $V(x, y)$ such that it breaks the $S_\mathbf{r}$ symmetry. The other major advantage of constructing the lattice out of individual Gaussian barriers is that it allows us to design Bravais lattices of arbitrary geometry: square, rectangular, oblique etc. As a result, we can probe into the role lattice geometry plays in determining the transport direction. One of the important results is that the geometry of the lattice along with the orientation θ_d of the driving force determines the average veloci-ties of the underlying non-linear dynamical attractors. This allows us to induce directed transport of underdamped particles along designated directions through the lattice. The particles exhibit axial, lateral or even oblique transport with re-spect to the orientation of the oscillating drive for different lattice geometries. Most importantly, we show that it is possible to direct the transport along one of the lattice vectors even in setups without any line of reflection symmetry, such as the oblique lattice. The standard symmetry arguments for directed transport preclude any prediction of the transport direction a priori for such setups. Yet we can explain the transport direction in terms of the attractors controlling the asymptotic dynamics of our non-linear dynamical system.

2.2 Time-dependent control of directed transport in Hamiltonian setups

In spite of the significant progress achieved in the control of ratchet based transport in the dissipative systems, similar control over the Hamiltonian systems has been limited. This is partly due to the structure of the underlying phase space of the higher dimensional Hamiltonian systems. The phase space of driven Hamiltonian systems in one spatial dimension is characterized by a bounded chaotic manifold, which means that the kinetic energies of the particles in such a setup is also bounded. However, this is no longer true for driven Hamiltonian setups in more than one spatial dimensions. Due to the unbounded chaotic sea, particles can undergo very slow diffusion in the momentum space and this prohibits the calculation of transport velocities of particles by direct numerical integration of their equations of motion due to convergence issues. In this section, we try to address this problem by developing a technique to understand the directed transport of a particle ensemble in terms of the dynamical population of the particles in the underlying phase space. This allows us to control the transport velocity of particles in both 1D and 2D Hamiltonian setups in a time-dependent manner.

2.2.1 Real-time control of 1D directed transport

In this work [A3] (see Sec.(3.3) for details), we consider an ensemble of particles in an 1D periodic potential $V(x,t) = V_S(x,t) + V_C(x,t)$ created by the superposition of two driven optical lattices: the 'substrate lattice' V_S and the 'carrier lattice' V_C with

$$\begin{aligned}
V_S(x,t) &= V_S \cos^2[k(x + d\cos(\omega t))] \\
V_C(x,t) &= V_C \cos^2[k(x + 2d\cos(2\omega t + \phi)) + \delta].
\end{aligned} \qquad (2.1)$$

Both the lattices have the same spatial period but are driven with different frequencies. This allows us to break the overall S_x and S_t symmetries of our setup thus allowing directed transport, even though the individual lattices preserve these symmetries. It is found that by switching the carrier lattice on and off in a time dependent manner, one can control the transport in real-time. Specifically on choosing $V_C = 0$, the transport velocity can be frozen to a constant value which can then be subsequently accelerated again by choosing a $V_C \neq 0$. Further-

more, by changing the sign of the driving phase ϕ, one can even decelerate the transport. Such a time dependent freezing, accelerating and slowing down of the transport velocity can be repeated multiple times up to timescales in the order of 10^5 driving periods. The mechanism behind our transport control protocol hinges on the structure of the underlying phase space of our non-linear dynamical system. The systems has a three dimensional phase space characterized by $(x, \dot{x}, t)$, which can be easily viewed in 2D by considering stroboscopic Poincáre surfaces of sections (PSOS). We analyzed the ensemble transport by superimposing time resolved snapshots of the ensemble dynamics over the PSOS. The PSOS reveals that the phase space has a mixed structure, i.e. it has both chaotic and regular manifolds. Most importantly, there exists a cantori in the chaotic manifold which controls the diffusion of particles from lower to higher kinetic energies. When the carrier lattice is switched off, the cantori forms an impenetrable barrier and prevents the particles from attaining higher speeds, hence the transport is frozen. On switching it back on, the particles can slowly diffuse through the chaotic sea into regions of higher kinetic energies and hence the transport can be accelerated again. On changing the sign of ϕ, we could show that the PSOS is inverted about $\dot{x} = 0$ which ultimately leads to a deceleration of transport. Our setup thus provides a flexible protocol to control the directed transport in 1D Hamiltonian systems in a time dependent manner by controlling the structure of the underlying phase space.

2.2.2 Dynamical current reversal in 2D induced by dimensional coupling

As discussed earlier, the special advantage of driven Hamiltonian systems in one spatial dimensions is that the phase space can be easily visualized in terms of the 2D Poincáre surfaces of sections (PSOS) characterized by the particles' position and momentum coordinates. The advantage is lost for 2D driven Hamiltonian setups since the PSOS, which is four dimensional, can not be visualized so easily. The aim of this project (see Sec.(3.4) for details) is to explain the particle dynamics in such a 2D driven Hamiltonian setup in terms of their dynamics in a well understood 1D system. We consider non-interacting classical particles in a 2D lattice of elliptic Gaussian barriers located at positions (m, n) yielding the potential landscape of the form $V(x,y) = \sum_{m,n=-\infty}^{+\infty} V e^{-\alpha\left[(x-m-f(t))^2 + \beta(y-n)^2\right]}$ $[A4]$. The barri-

ers are laterally driven along the x-direction via an external bi-harmonic driving force of the form $f(t) = d_x(\sin t + 0.25 \sin(2t + \pi/2))$. In the limit $\beta \to 0$, we have a quasi-1D lattice with a periodic potential along the x-direction but without any potential variation along the perpendicular y-direction. This uncouples the x and y degrees of freedom in the equation of motion of particles and hence we refer to the parameter β as the dimensional coupling strength. We showed that our driving law breaks the symmetries S_x and S_t and so the quasi-1D lattice ($\beta = 0$) shows a net transport along the negative x-direction. However for a non-zero value of β, although the particles are initially transported in the negative x-direction, the direction of transport gets reversed dynamically. The reversal timescale decreases with an increasing value of the dimensional coupling strength β. We explained the mechanism behind this current reversal by analyzing the time resolved snapshots of the ensemble dynamics in the 2D system ($\beta \neq 0$) superimposed over the PSOS of the quasi-1D system ($\beta = 0$). Additionally, the reversal timescale is also shown to depend linearly on the average time τ_β required by a particle to cross one lattice unitcell along the y-direction via statistical analysis. As β is increased, the variation of the potential landscape in the y-direction becomes more pronounced which decreases the value of τ_β and the current reversal timescale. Unlike most of the existing ratchet setups, our setup provides a method to dynamically control the ratchet current without any time dependent switch of parameters.

2.2.3 Multiple current reversals using superimposed driven lattices

In this project (see Sec.(3.5) for details) too, we consider a 2D driven Hamiltonian system and demonstrate that a spatial potential which is coupled in the x and y dimensions can lead to current reversals. However, unlike the previous setup in section 2.2.2, the underlying potential here consists of superimposed 2D lattices [A5]. One of the lattices forms the 'background lattice' represented by a separable potential in x and y: $V_B(\mathbf{r}) = U_B(\cos^2 \pi x + \cos^2 \pi y)$. The system is additionally driven in the x-direction by a bi-harmonic driving force. Due to the separable nature of the potential, the particle dynamics in the background lattice can be decoupled in both x and y directions. This means that any transport along the x-direction can be explained in terms of the 2D PSOS characterized by $(x, \dot{x})$. On top of the lattice V_B, we superimpose two lattices V_{G1} and V_{G2} consisting of 2D Gaussian barriers localized in different regions of space. The potential due to the

Gaussian barriers is coupled in x and y dimensions and hence is non-separable. In the absence of the lattices of Gaussian barriers, the background lattice exhibits a transport in the positive x-direction since the setup breaks the parity and time reversal symmetries. However, we show that by superimposing the lattices V_{G1} and V_{G2} at different locations in space, one can flip the direction of transport multiple times in a time dependent manner. The analysis is carried out by superimposing the time resolved snapshots of the ensemble dynamics in our 2D setup over the 2D PSOS corresponding to the background lattice. The underlying principle behind the current reversals is identified to be the conversion of particle dynamics from diffusive to ballistic and vice-versa when they encounter the lattices V_{G1} and V_{G2}. By controlling the spatial locations of the lattices V_{G1} and V_{G2}, one can control the timescales of such conversion processes and hence control the timescales of current reversals.

2.3 Controlling rotational currents in 2D driven superlattices

The unique feature of 2D ratchet setups is that alongside translational currents, it also allows us to generate an overall rotational current for an ensemble of particles. This is especially interesting since it provides a way to generate rotational motion of neutral particles by placing them in a driven periodic potential but without any explicit rotation of potential landscape being involved. The necessary symmetries one has to break in order to achieve this has been demonstrated for particles in an optical lattice in presence of an external oscillating driving field [49]. However, unlike the control of translational currents, there has not been much progress in controlling the rotational currents. The few existing setups either lead to a diffusive rotational motion over an extended space [49] or requires specific ingredients such as specially designed potentials [109, 110] and temporally correlated colored noise [111, 112]. In this work [A6] (see Sec.(3.6) for details), we demonstrate how the rotational motion of neutral classical particles can be controlled using driven superlattices. Our setup consists of a lattice of 2D Gaussian wells centered at positions $\mathbf{R}_{mn} = (m, n)$ with $m, n \in \mathbb{Z}$ giving rise to a potential $V(\mathbf{r}, t) = \sum_{m,n=-\infty}^{+\infty} U_{mn}(t) e^{-\beta(\mathbf{r}-\mathbf{R}_{mn})^2}$. The depths of the wells are modulated periodically with time by the driving law $U_{mn}(t) = V_{mn}(\cos(t + \phi_{mn}) - 1)$, which depends on the spatial location of the wells. The set of all wells arranged

periodically in space with a specific value of the driving phase ϕ_{mn} and amplitude V_{mn} forms a sublattice of our system. Hence our setup can be considered to be a driven superlattice formed by the superposition of these different sublattices. We showed that specific spatial arrangements of the wells driven with different driving phases ϕ_{mn} breaks the reflection symmetries in the setup and allows particle to rotate with non-zero angular momenta. Through an analysis of the underlying attractors, we could show that the angular momentum of the particles can be controlled by changing the driving amplitude V_{mn}. This allowed us to create spatially periodic patterns of particles rotating with different angular momenta, a phenomenon which is not possible in the existing 2D ratchet setups.

3

Publications and Manuscripts

3.1 Simultaneous control of multispecies particle transport and segregation in driven lattices

Simultaneous Control of Multispecies Particle Transport and Segregation in Driven Lattices

Aritra K. Mukhopadhyay,[1,*] Benno Liebchen,[2,3,†] and Peter Schmelcher[1,4,‡]

[1]*Zentrum für Optische Quantentechnologien, Universität Hamburg, Luruper Chaussee 149, 22761 Hamburg, Germany*
[2]*SUPA, School of Physics and Astronomy, University of Edinburgh, Peter Guthrie Tait Road, Edinburgh, EH9 3FD, United Kingdom*
[3]*Institute for Theoretical Physics II: Soft Matter, Heinrich-Heine Universität Düsseldorf,*
Universitätsstrasse 1, 40225 Düsseldorf, Germany
[4]*The Hamburg Centre for Ultrafast Imaging, Universität Hamburg, Luruper Chaussee 149, 22761 Hamburg, Germany*

We provide a generic scheme to separate the particles of a mixture by their physical properties like mass, friction, or size. The scheme employs a periodically shaken two-dimensional dissipative lattice and hinges on a simultaneous transport of particles in species-specific directions. This selective transport is achieved by controlling the late-time nonlinear particle dynamics, via the attractors embedded in the phase space and their bifurcations. To illustrate the spectrum of possible applications of the scheme, we exemplarily demonstrate the separation of polydisperse colloids and mixtures of cold thermal alkali atoms in optical lattices.

Introduction.—The controlled separation, or spatial sorting, of particle mixtures based on their physical properties like mass, size, shape, or mobility presents major challenges cutting across disciplines from biomedical problems such as the separating of malignant circulating tumor cells from leucocytes in the bloodstream [1] to technological problems on colloidal and granular scales [2]. Following these challenges, much effort has been devised to develop innovative separation schemes complementing traditional techniques such as the filtration, distillation, or evaporation of mixtures. For example, to separate heterogeneous granular particle mixtures in geological and biological systems, it has been shown that vibrating a substrate [3–5] allows us to separate two species by size. To separate particles on colloidal scales which are significantly affected by Brownian noise, it has been shown that techniques like vector chromatography [6], deterministic lateral displacement [7], or suitable external forcing may be sufficient to separate mixtures [2,8–10].

One important class of innovative separation schemes employs so-called Brownian ratchets, in which thermal Brownian motion combined with external time-dependent driving generates directed particle motion [2,11–15]. Based on an appropriate design of such ratchets, the direction of the emerging particle current may depend on "internal" particle properties such as mass, radius, or mobility. This dependence can be exploited to simultaneously transport two different particle species in opposite directions, i.e., for separating them [Fig. 1(a), upper panel]. Based on this idea, it has been possible to establish a rich set of schemes to separate two component particle mixtures, including a massively parallel particle filter [16] serving as an artificial microsieve with potential biomedical applications [2] and schemes allowing us to separate mixtures of cellular membrane associated molecules that differ in electrophoretic mobility and diffusion coefficient [17]. Further examples of ratchet-based separation devices allow for the size sorting of superparamagnetic particles using periodically switching magnetic fields [18], of active and passive particles using active ratchet systems [19,20], and of heterogeneous cell mixtures using microfluidic funnel ratchets [21]. Finally, we note that ratchets in superlattices also allow us to separate particles by the type of their motion (ballistic or chaotic) and allow us to sort (or filter) them by velocity [22,23].

These examples illustrate the rich versatility of ratchet-based separation schemes which, in the following respects, seems to be somewhat advantageous over traditional techniques like sieving or filtrating: (i) They may operate on many technologically relevant scales ranging from granular and colloidal sizes down to the nanoregime [2] and even to the size of single atoms [24], (ii) the particle current underlying the particle separation can be controlled with an external field [25], even in real time [26,27], and (iii) they allow us to separate particles with respect to all kinds of physical properties from size and mass to charge and mobility. However, these advantageous, ratchet-based schemes seem to have one striking disadvantage: Unlike sieves, which can be easily stacked to sort many-component mixtures by size, most (if not all) ratchet-based schemes are restricted to the separation of only two species, based on forward transport of one species and reverse transport of the other one. Since combinations of several ratchets, each separating two species, would be
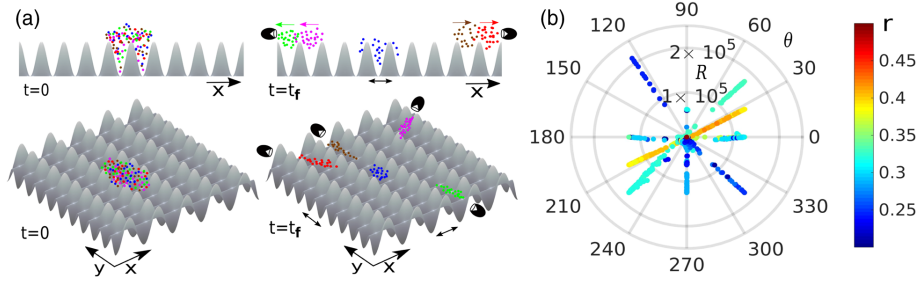
FIG. 1. (a) Upper panel: Cartoon of a standard particle segregation scheme based on 1D ratchets allowing for the separation of a mixture of particles (left) with different mass, mobility, or radius (color) into two components (right). Lower panel: The present scheme allows for a controlled angular-specific transport of many species which can be applied to sort multispecies mixtures. (b) Snapshot of particle positions (in radial R and angular θ coordinates) in a mixture of particles with different radii r (shown in the color bar) at $t = 5 \times 10^4$ T. Particles in at least four different radii (r) intervals can be separated at different angles (θ; position of the detector) using this setup: The pairs of the radii intervals and angles are $(0.32 \lesssim r \lesssim 0.33, \ \theta \approx 45°, 225°)$, $(0.38 \lesssim r \lesssim 0.40, \ \theta \approx 30°, \ 210°)$, $(0.26 \lesssim r \lesssim 0.27, \ \theta \approx 120°)$, and $(0.29 \lesssim r \lesssim 0.30, \ \theta \approx 270°)$. The remaining parameters are $V = 0.17$, $\eta = 0.01$, $d_x = d_y = 1$, $\omega = 1$, and $2k_x = k_y = 2$. The other particles remain confined near the origin, and one can repeat the process with a different value of V in order to segregate them (discussed later).

rather sophisticated to design and produce, it would be desirable to know a mechanism allowing for a simultaneous separation of many species.

Here we propose such a mechanism unifying the above advantages of ratchet-based separation schemes with the ability to efficiently separate multispecies mixtures [Fig. 1(a)] based on their physical properties like mass, friction, or size. To develop this scheme, we use a periodically shaken two-dimensional dissipative lattice and demonstrate that it is possible to induce ballistic-directed transport of individual species simultaneously at different angles. Here, we exploit the strongly nonlinear character of driven lattices to control the late-time particle dynamics species-selectively on the phase space level. Initializing mixtures of particles, we show that each species travels in an individual direction through the lattice, allowing for their collection with an angular detector (or a reservoir). To illustrate possible applications of this general scheme, we demonstrate the segregation of a mixture of polydisperse colloids differing in radius and a mixture of cold alkali atoms with different masses. The segregation scheme should apply generally to particles on atomic and nanoscales up to colloids and granular particles. In particular, contrasting many other ratchet-based separation schemes, the present one does not hinge on Brownian noise (but is robust against it) and should hence apply for granular particles which are too large to experience a significant effect from Brownian noise and, in principle, also for the extreme case of a mixture of cold thermal atoms with different masses in purely optical setups [24], where a noise-providing medium is practically absent.

Setup.—We consider a mixture of N noninteracting classical particles in a two-dimensional lattice defined by a periodic potential $V(x, y) = V \cos k_x x (1 + \cos k_y y)$ which is driven via external biharmonic driving forces $f_{x,y}(t) = d_{x,y}[\cos \omega t + 0.25 \cos(2\omega t + \pi/2)]$ acting in both

the x and y directions and breaking parity $\mathbf{x} \to -\mathbf{x} + \boldsymbol{\chi}$ and time-reversal $t \to -t + \tau$ symmetry, with additional constant spatial and temporal shifts, to allow for a directed particle transport [25,28]. Here, d_x and d_y denote the respective driving amplitudes in the two directions, k_x and k_y the respective wave numbers, and ω the frequency of the external driving force. The system thus has spatial and temporal periodicities of $L_{x,y} = 2\pi/k_{x,y}$ and $T = 2\pi/\omega$. Such a two-dimensional lattice potential can be created, for example, in cold atom setups by using two sets of counter-propagating laser beams of nonorthogonal polarizations between mirrors, and the driving can be implemented with standard techniques like acousto-optical modulators and radio frequency generators, leading to a lateral oscillation of the mirrors and hence of the lattice [29]. Here, the damping can be realized using optical molasses [30]. For colloids, such potential landscapes can be designed by interfering multiple laser beams [31], creating a 2D intensity pattern exerting optical forces on the particles [32,33]. The driving can be implemented using a velocity modulated piezo stage [33].

Introducing dimensionless variables $x' = k_x x$, $y' = k_y y$, and $t' = \omega t$ and dropping the primes for simplicity, the equation of motion for a single particle of mass m located at position $\mathbf{x}$ with momentum $\mathbf{p}$ in such a setup reads

$$\ddot{\mathbf{x}} = U_x \sin x (1 + \cos y) \mathbf{e}_x + U_y \cos x \sin y \mathbf{e}_y$$
$$+ [\cos t + 0.25 \cos(2t + \pi/2)] \mathbf{F} - \Gamma \dot{\mathbf{x}} + \boldsymbol{\xi}(t), \quad (1)$$

where $\mathbf{e}_x = (1, 0)$ and $\mathbf{e}_y = (0, 1)$. The parameter space of this model has five essential dimensions with $U_{x,y} = (Vk_{x,y}^2/m\omega^2)$ comparing the velocity of a particle in a static lattice with the velocity of the oscillating lattice, $\mathbf{F} = [(k_x d_x/m\omega^2), (k_y d_y/m\omega^2)]$ being a reduced driving amplitude, and $\Gamma = (\gamma/m\omega)$ comparing the relaxation time due to dissipation (in the underlying static lattice) with the timescale of the lattice oscillation. $\boldsymbol{\xi}(t) = (\xi_x, \xi_y)$ denotes

thermal fluctuations modeled by Gaussian white noise of zero mean with the property $\langle \xi_\alpha(t)\xi_\beta(t')\rangle = 2D\delta_{\alpha\beta}\delta(t-t')$, where $\alpha, \beta \in x, y$ and D is the dimensionless noise strength. Here we focus on the underdamped regime where dissipation is weak but important and neglect Brownian noise corresponding to low temperatures (cold atoms) or large masses (granular particles). Our main results are robust against typical noise, as discussed later.

Simultaneous control of directed transport and particle segregation.—We now illustrate the scheme for a poly-disperse mixture of $N = 2 \times 10^4$ underdamped colloids with uniformly distributed radii $r \in [0.2, 0.5]$. Here, we account for the impact of the radius on the colloidal mass ($m = \frac{4}{3}\pi\rho r^3$) and the dissipation coefficient ($\gamma = 6\pi\eta r$) but treat colloids as pointlike regarding their interactions with the lattice potential (for a CO_2 laser, $L_{x,y} \sim 10r$–$10^3 r$).

We initialize the particles randomly within a square region $L_x \times L_y$ of the lattice and give them small random velocities. To mimic potential experimental scenarios, we first allow the colloids to equilibrate in a static lattice for a time $1000T$ [Fig. 1(a), lower panel, left]. Now switching on the driving and waiting until $\sim 5 \times 10^4 T$, we observe ballistic particle jets ("rays"), radially moving away from their initial positions at different angles [Fig. 1(b)]. Strikingly, most of these rays have an almost uniform color [Fig. 1(b)], meaning that they involve only colloids with very similar radii and separate them from the rest of the mixture. The figure shows the simultaneous separation of four "species" by radius, while the rays at 0° and 180°, as well as the particle cloud around the origin, still contain a mixture of particles with different radii which may be considered as "losses." When analyzing the general working principle of our scheme below, it will become clear that the presented segregation is not at all limited to the four specific radii intervals separated so far but that it is tunable and can be applied to separate particles with a desired set of radii from the mixtures.

Discussion.—We now analyze the mechanism underlying the particle separation on the level of the five-dimensional phase space (x, y, p_x, p_y, t) of the system. We analyze the attractors determining the asymptotic $t \to \infty$ dynamics of all particles, which can be periodic (limit cycle attractors) or chaotic (chaotic attractors) and basins of attraction.

The idea is to tune the set of attractors via system parameters such that the late-time dynamics of particles with different properties is governed by species-dependent limit cycles which transport particles to species-specific directions. The limit cycle attractors represent trajectories which are synchronized with the lattice motion. As a result, they transport particles in well-defined directions with characteristic (quasi)periodic average velocity $\bar{\mathbf{v}} \equiv (\bar{v}_x, \bar{v}_y) = [(n_x L_x/m_x T), (n_y L_y/m_y T)]$, where n_x, m_x, n_y, m_y are attractor-specific integers [34]. Hence, at a large distance from the center of the square region $L_x \times L_y$, where the particles were initialized (which we henceforth refer to as the

"origin"), particles following the dynamics of a limit cycle attractor can be collected by placing a suitable collector (detector or reservoir) at an angle $\theta = \tan^{-1}(\bar{v}_y/\bar{v}_x) = \tan^{-1}(m_x n_y L_y/m_y n_x L_x)$. Thus, if we manage to tune the limit cycle attractors and their basins of attraction in the phase space such that particles with, e.g., different radii end up in different limit cycle attractors, they will be automatically separated [Fig. 1(b)]. The size of the detectors would depend on the angular spreading $\triangle\theta$ of the particle "jets," which for this setup [Fig. 1(b)] was found to be of the order of 0.01°. Hence, if one places the detectors at a radial distance of $R = 10^5$ from the origin, their required sizes would be determined by the arc length $R\triangle\theta \sim 4L_x$. Such a detection and tracking of colloidal particles are routinely done using high-resolution optical tracking and holographic microscopy [35,36]. The chaotic particles, owing to their diffusive nature, stay much closer to the origin and as a result do not interfere with the segregation process.

In order to predict whether a particle would end up in a chaotic attractor or a limit cycle, we compute the "bifurcation diagram" [Figs. 2(a) and 2(b)] associated with the
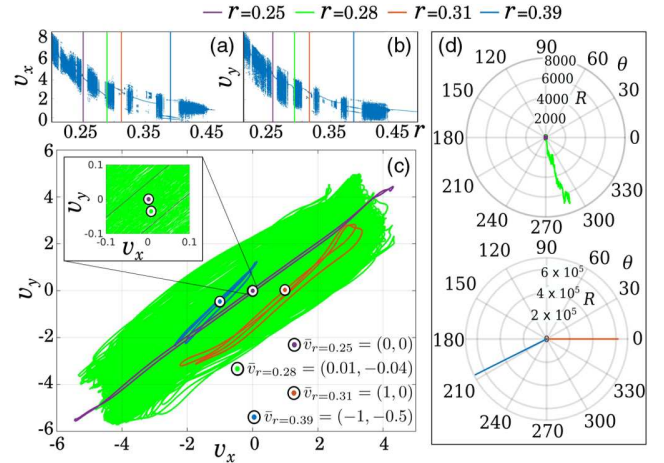

FIG. 2. (a), (b) Radius-dependent bifurcation diagram of the particle velocity (initialized at the potential minima $x = y = \pi$ with $\mathbf{v} = 0$). Regions with broad velocity fluctuations (e.g., $0.41 \lesssim r \lesssim 0.45$) represent chaotic attractors; single velocity values (see $r = 0.25$) denote period 1 limit cycles; others represent multiperiodic limit cycles (e.g., $r = 0.39$). (c) Asymptotic dynamics (in the v_x-v_y plane) and the mean velocities $\bar{v}_r$ of four exemplary particles having radii $r = 0.25, 0.28, 0.31$, and 0.39 (in magenta, green, red, and blue, respectively). The particles with $r = 0.25, 0.31$, and 0.39 belong to limit cycle attractors, whereas the one with $r = 0.28$ is attracted to a chaotic attractor. (d) Spatial trajectories of the four particles in polar coordinates between $t = 0$ and $t = 10^5 T$. The particle with $r = 0.25$ is trapped near the origin due to its vanishing mean velocity, whereas the one with $r = 0.28$ exhibits diffusive behavior (upper panel). The particles with radii $r = 0.31$ and 0.39 move ballistically through the lattice at angles governed by their mean velocities (lower panel). Note the difference in spatial length scales between the upper and lower panels. Remaining parameters: see Fig. 1(b).

particle velocity as a function of its radius by initializing particles of different radii and stroboscopically monitoring their late-time velocity (at multiples of T). This determines the attractors (chaotic, period one, or multiperiodic limit cycle) to which a particle of a given radius would be attracted and the resulting angles of transport [Figs. 2(c) and 2(d)]. For a detailed illustration of the dynamical processes underlying the segregation mechanism, see Supplemental Material [37].

To make the segregation scheme more flexible and separate particles of a varying range of sizes, we use the lattice potential height V as a control parameter. Using a similar concept as above, one can construct a two-parameter bifurcation diagram of the particle velocity $v_\theta = \tan^{-1}(v_y/v_x)$ (in the angular coordinates) showing whether a particle of radius r ends up in a limit cycle attractor or a chaotic attractor for a given lattice potential height V [Fig. 3(a)]. For our segregation scheme, we choose those values of V and r for which the particle dynamics is asymptotically governed by the limit cycle attractors. Depending on the average velocity $\bar{\mathbf{v}}$ of these limit cycles, particles of a given radius might be trapped ($\bar{\mathbf{v}} = 0$) in the lattice or fly out ballistically at certain angles ($\bar{\mathbf{v}} \neq 0$). The

asymptotic direction of flight $\theta = \tan^{-1}(\bar{v}_y/\bar{v}_x)$ for these ballistic particles as a function of V and r [Fig. 3(b)] predicts *a priori* at which angle a particle of a given radius would travel for a chosen lattice height V. At this stage, the segregation protocol becomes very simple: Given a set of particles with different radii, the task is to simply choose a value of V from Fig. 3(b) for which the different species travel ballistically at different angles. One can, in principle, repeat this process with a different value of V in order to also separate the cloud of "lost" particles, which, owing to their diffusive motion, remain close to the origin.

The segregation scheme mentioned here works not just for colloidal particles with a continuous size distribution but, for example, also for a mixture of particles differing only in mass. We now demonstrate this using a mixture of three cold thermal alkali atoms which can be treated classically in the regime of microkelvin temperatures [24,38]. Such a scheme can be tested, of course, also with two species only and also applies to isotopic mixtures of the same atom (see [39,40] for details on simultaneous trapping). In Fig. 4, we show how our scheme can be adapted to simultaneously separate three species of commonly used alkali atoms of different masses from a mixture. It shows that, after $t = 5 \times 10^4 T$, particle rays containing mostly one species emerge at different angles. A detector positioned, e.g., at $\theta \approx 320°$ would collect only Na atoms, whereas a detector at $\theta \approx 270°$ would see mostly Cs atoms. Such a scheme may be realized using state of the art cold atom experimental setups with optical lattices driven by phase modulation of the laser beams using acousto-optical modulators and radio frequency generators [24,41–43].

Contrary to most ratchet-based segregation schemes, the present one does not depend on noise, allowing its application also, e.g., to heavy and underdamped granular particles. For a noise strength of $D \lesssim 10^{-3}$ typical for cold
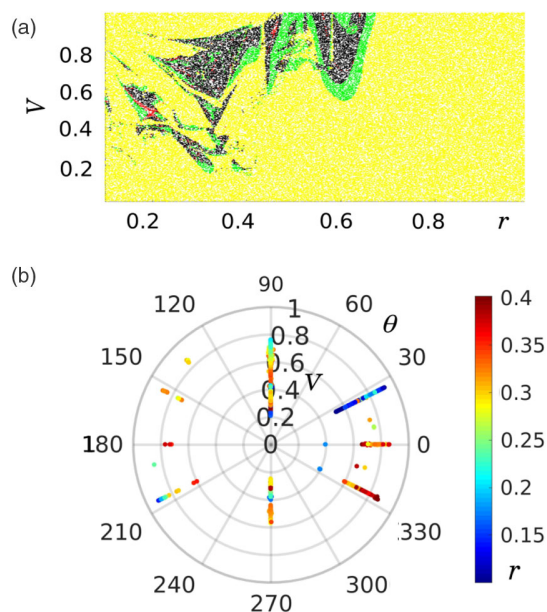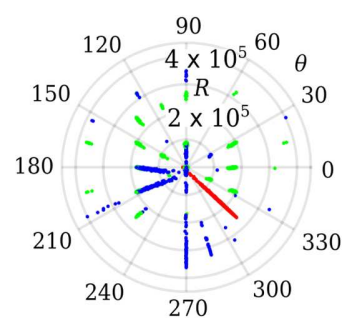

FIG. 3. (a) Bifurcation diagram of v_θ (color) as a function of lattice potential height V and particle radius r. The yellow, green, red, and black regions represent limit cycles with periodicities 1, 2, 3, and higher, respectively. (b) Asymptotic flight direction θ (angular coordinates) of ballistic particles with average velocity $\bar{\mathbf{v}} \neq 0$ for different V (radial coordinates) and r (color bar). Thus, a lattice of, e.g., $V = 0.6$ separates particles with radii in the intervals $0.26 \lesssim r \lesssim 0.3$ to $\theta \approx 90°$ and analogously $0.12 \lesssim r \lesssim 0.16$ to $\theta \approx 27°$ and $0.36 \lesssim r \lesssim 0.33$ to $\theta \approx 227°, 333°$. The remaining parameters are $\eta = 0.05$, $d_x = d_y = 1$, $\omega = 1$, and $2k_x = k_y = 2$.

FIG. 4. Snapshot of particle positions at $t = 5 \times 10^4 T$ (in radial R and angular θ coordinates) showing the segregation of three different masses 0.23 (red), 0.87 (green), and 1.33 (blue) corresponding to atoms Na, Rb, and Cs with masses 23, 87, and 133 a.m.u., respectively. The remaining parameters are $\gamma = 0.01$, $d_x = d_y = 3$, $\omega = 1$, $2k_x = k_y = 2$, and $V = 0.1679$. Since the dimensionless parameters depend on (V/m), $(d_{x,y}/m)$, and (γ/m), the parameters V, $d_{x,y}$, and γ can be scaled according to the atomic mass to correspond to relevant experimental setups.

atoms and underdamped colloids [2,44], we observe only minor fluctuations around the average velocity of the limit cycle attractor, which does not affect the functionality of the segregation mechanism. Weak long-range interactions, in turn, should mainly induce chaotic-to-ballistic transitions [26], possibly improving the segregation efficiency.

Conclusions.—We have presented a scheme allowing us to separate particles from a mixture based on different selection criteria like radius-dependent frictional forces or particle mass. This scheme exploits the strong nonlinearity of driven lattices to control the late-time particle dynamics species selectively on the phase space level. This contrasts standard segregation schemes based on overdamped ratchet setups and allows us to overcome their key limitation of segregating more than two species. Owing to its deterministic character, our new control mechanism can be applied to particle mixtures on an unusually broad range of scales from atoms to granular particles. The segregation scheme can be tested, for example, using polydisperse colloids or mixtures of cold thermal alkali atoms using ac-driven optical lattices. As a perspective, further studies may account for localized perturbations of the ideal periodic potential employed, which may allow us to transfer the scheme to overdamped or even to the pure Hamiltonian regime based on, e.g., a mass-selective accumulation of particles in the regular structures of the Hamiltonian phase space [45]. Interaction effects may add to the species-selective directed transport [46,47].

———

[*]Aritra.Mukhopadhyay@physnet.uni-hamburg.de
[†]liebchen@hhu.de
[‡]Peter.Schmelcher@physnet.uni-hamburg.de

[1] C. Jin, S. M. McFaul, S. P. Duffy, X. Deng, P. Tavassoli, P. C. Black, and H. Ma, Technologies for label-free separation of circulating tumor cells: From historical foundations to recent developments, Lab Chip **14**, 32 (2014).

[2] P. Hänggi and F. Marchesoni, Artificial Brownian motors: Controlling transport on the nanoscale, Rev. Mod. Phys. **81**, 387 (2009).

[3] T. Mullin, Coarsening of Self-Organized Clusters in Binary Mixtures of Particles, Phys. Rev. Lett. **84**, 4741 (2000).

[4] T. Shinbrot and F. J. Muzzio, Reverse Buoyancy in Shaken Granular Beds, Phys. Rev. Lett. **81**, 4365 (1998).

[5] D. C. Hong, P. V. Quinn, and S. Luding, Reverse Brazil Nut Problem: Competition between Percolation and Condensation, Phys. Rev. Lett. **86**, 3423 (2001).

[6] K. D. Dorfman and H. Brenner, Vector chromatography: Modeling micropatterned separation devices, J. Colloid Interface Sci. **238**, 390 (2001).

[7] S. C. Kim, B. H. Wunsch, H. Hu, J. T. Smith, R. H. Austin, and G. Stolovitzky, Broken flow symmetry explains the dynamics of small particles in deterministic lateral displacement arrays, Proc. Natl. Acad. Sci. U.S.A. **114**, E5034 (2017).

[8] S. Bouzat, Inertial effects, mass separation and rectification power in Lévy ratchets, Physica (Amsterdam) **389A**, 3933 (2010).

[9] C. Zeng, A. Gong, and Y. Tian, Current reversal and mass separation of inertial Brownian motors in a two-noise ratchet, Physica A (Amsterdam) **389**, 1971 (2010).

[10] F. Marchesoni, Conceptual design of a molecular shuttle, Phys. Lett. A **237**, 126 (1998).

[11] R. D. Astumian and P. Hänggi, Brownian motors, Phys. Today **55**, No. 11, 33 (2002).

[12] P. Hänggi, F. Marchesoni, and F. Nori, Brownian motors, Ann. Phys. (Amsterdam) **14**, 51 (2005).

[13] C. Reichhardt and C. J. Olson Reichhardt, Absolute transverse mobility and ratchet effect on periodic two-dimensional symmetric substrates, Phys. Rev. E **68**, 046102 (2003).

[14] D. Speer, R. Eichhorn, and P. Reimann, Directing Brownian Motion on a Periodic Surface, Phys. Rev. Lett. **102**, 124101 (2009).

[15] A. Soba, P. Tierno, T. M. Fischer, and F. Saguès, Dynamics of a paramagnetic colloidal particle driven on a magnetic-bubble lattice, Phys. Rev. E **77**, 060401 (2008).

[16] S. Matthias and F. Müller, Asymmetric pores in a silicon membrane acting as massively parallel Brownian ratchets, Nature (London) **424**, 53 (2003).

[17] A. van Oudenaarden, Brownian ratchets: Molecular separations in lipid bilayers supported on patterned arrays, Science **285**, 1046 (1999).

[18] F. Liu, L. Jiang, H. M. Tan, A. Yadav, P. Biswas, J. R. C. van der Maarel, C. A. Nijhuis, and J. A. van Kan, Separation of superparamagnetic particles through ratcheted Brownian motion and periodically switching magnetic fields, Biomicrofluidics **10**, 064105 (2016).

[19] C. J. O. Reichhardt and C. Reichhardt, Ratchet effects in active matter systems, Annu. Rev. Condens. Matter Phys. **8**, 51 (2017).

[20] B. Ai, Ratchet transport powered by chiral active particles, Sci. Rep. **6**, 18740 (2016).

[21] S. M. McFaul, B. K. Lin, and H. Ma, Cell separation based on size and deformability using microfluidic funnel ratchets, Lab Chip **12**, 2369 (2012).

[22] C. Petri, F. Lenz, B. Liebchen, F. Diakonos, and P. Schmelcher, Formation of density waves via interface conversion of ballistic and diffusive motion, Europhys. Lett. **95**, 30005 (2011).

[23] T. Wulf, C. Petri, B. Liebchen, and P. Schmelcher, Analysis of interface conversion processes of ballistic and diffusive motion in driven superlattices, Phys. Rev. E **86**, 016201 (2012).

[24] F. Renzoni, Driven Ratchets for Cold Atoms, in *Advances in Atomic Molecular and Optical Physics* (Academic, New York, 2009), Vol. 57.

[25] P. Reimann, Brownian motors: Noisy transport far from equilibrium, Phys. Rep. **361,** 57 (2002).

[26] B. Liebchen, F. K. Diakonos, and P. Schmelcher, Interaction-induced current-reversals in driven lattices, New J. Phys. **14,** 103032 (2012).

[27] A. K. Mukhopadhyay, B. Liebchen, T. Wulf, and P. Schmelcher, Freezing, accelerating, and slowing directed currents in real time with superimposed driven lattices, Phys. Rev. E **93,** 052219 (2016).

[28] S. Flach, O. Yevtushenko, and Y. Zolotaryuk, Directed Current due to Broken Time-Space Symmetry, Phys. Rev. Lett. **84,** 2358 (2000).

[29] J. Struck, M. Weinberg, C. Ölschläger, P. Windpassinger, J. Simonet, K. Sengstock, R. Höppner, P. Hauke, A. Eckardt, M. Lewenstein, and L. Mathey, Engineering Ising-XY spin-models in a triangular lattice using tunable artificial gauge fields, Nat. Phys. **9,** 738 (2013).

[30] G. Grynberg and C. Robilliard, Cold atoms in dissipative optical lattices, Phys. Rep. **355,** 335 (2001).

[31] M. Brunner and C. Bechinger, Phase Behavior of Colloidal Molecular Crystals on Triangular Light Lattices, Phys. Rev. Lett. **88,** 248302 (2002).

[32] P. Jákl, A. V. Arzola, M. Šiler, L. Chvátal, K. Volke-Sepúlveda, and P. Zemánek, Optical sorting of nonspherical and living microobjects in moving interference structures, Opt. Express **22,** 29746 (2014).

[33] A. V. Arzola, K. Volke-Sepúlveda, and J. L. Mateos, Experimental Control of Transport and Current Reversals in a Deterministic Optical Rocking Ratchet, Phys. Rev. Lett. **106,** 168104 (2011).

[34] M. Tabor, *Chaos and Integrability in Nonlinear Dynamics: An Introduction* (Wiley, New York, 1989), p. 364.

[35] N. Garbow, J. Muller, K. Schätzel, and T. Palberg, High-resolution particle sizing by optical tracking of single colloidal particles, Physica (Amsterdam) **235A,** 291 (1997).

[36] S. Lee, Y. Roichman, G. Yi, S. Kim, S. Yang, A. van Blaaderen, P. van Oostrum, and D. G. Grier, Characterizing and tracking single colloidal particles with video holographic microscopy, Opt. Express **15,** 18275 (2007).

[37] See Supplemental Material at http://link.aps.org/supplemental/10.1103/PhysRevLett.120.218002 for a detailed discussion of the trajectories associated with different regions of the bifurcation diagram.

[38] M. Brown and F. Renzoni, Ratchet effect in an optical lattice with biharmonic driving: A numerical analysis, Phys. Rev. A **77,** 033405 (2008).

[39] T. Best, S. Will, U. Schneider, L. Hackermüller, D. van Oosten, I. Bloch, and D. S. Lühmann, Role of Interactions in Rb87-K40 Bose-Fermi Mixtures in a 3D Optical Lattice, Phys. Rev. Lett. **102,** 030408 (2009).

[40] L. J. LeBlanc and J. H. Thywissen, Species-specific optical lattices, Phys. Rev. A **75,** 053612 (2007).

[41] R. Gommers, S. Bergamini, and F. Renzoni, Dissipation-Induced Symmetry Breaking in a Driven Optical Lattice, Phys. Rev. Lett. **95,** 073003 (2005).

[42] V. Lebedev and F. Renzoni, Two-dimensional rocking ratchet for cold atoms, Phys. Rev. A **80,** 023422 (2009).

[43] A. Eckardt, Colloquium: Atomic quantum gases in periodically driven optical lattices, Rev. Mod. Phys. **89,** 011004 (2017).

[44] D. Cubero, V. Lebedev, and F. Renzoni, Current reversals in a rocking ratchet: Dynamical versus symmetry-breaking mechanisms, Phys. Rev. E **82,** 041116 (2010).

[45] T. Wulf, B. Liebchen, and P. Schmelcher, Disorder Induced Regular Dynamics in Oscillating Lattices, Phys. Rev. Lett. **112,** 034101 (2014).

[46] B. Liebchen and P. Schmelcher, Interaction induced directed transport in ac-driven periodic potentials, New J. Phys. **17,** 083011 (2015).

[47] D. McDermott, C. J. O. Reichhardt, and C. Reichhardt, Collective ratchet effects and reversals for active matter particles on quasi-one-dimensional asymmetric substrates, Soft Matter **12,** 8606 (2016).

Simultaneous control of multi-species particle transport and segregation in driven lattices

Aritra K. Mukhopadhyay,[1, *] Benno Liebchen,[2, 3, †] and Peter Schmelcher[1, 4, ‡]

[1]*Zentrum für Optische Quantentechnologien, Universität Hamburg,*
Luruper Chaussee 149, 22761 Hamburg, Germany
[2]*SUPA, School of Physics and Astronomy, University of Edinburgh,*
Peter Guthrie Tait Road, Edinburgh, EH9 3FD, UK
[3]*Institute for Theoretical Physics II: Soft Matter, Heinrich-Heine University Düsseldorf,*
Universitätsstrasse 1, 40225, Düsseldorf, Germany
[4]*The Hamburg Centre for Ultrafast Imaging, Universität Hamburg,*
Luruper Chaussee 149, 22761 Hamburg, Germany
(Dated: February 14, 2018)

SUPPLEMENTAL MATERIAL

Here we discuss the trajectories associated with different regions of the bifurcation diagram in detail. We consider four different particles having radii $r = 0.25, 0.28, 0.31$ and 0.39 respectively in the same setup underlying the Figure 2 of the main text and illustrate their asymptotic dynamics in Fig. 1 below. The bifurcation diagrams in Fig. 1a and 1b show the radii intervals and types of attractors these four particles belong to, the Fig. 1c depicts the asymptotic velocities of these four particles for a time duration of $10^3 T$ and the Fig. 1d shows their spatial trajectories during $t = 0$ and $t = 10^5 T$.

The particle with radius $r = 0.25$ (magenta) is attracted to a limit cycle attractor of period 1 (Fig. 1a and 1b) and hence exhibits regular dynamics characterized by a periodic orbit (Fig. 1c, magenta-colored orbit). But since it has a vanishing mean velocity $\bar{v}_{(r=0.25)} = 0$, it is trapped near the origin (Fig. 1d). The particles with radii $r = 0.31$ and 0.39 (red and blue) are also attracted to limit cycle attractors (but with higher periodicity) and hence have regular orbits (Fig. 1c, in red and blue respectively). But since they have non-zero mean velocities $\bar{v}_{(r=0.31)} = (1, 0)$ and $\bar{v}_{(r=0.39)} = (-1, -0.5)$, they travel *ballistically* at angles $\theta = \tan^{-1}(\frac{0}{1}) = 0°$ and $\theta = \tan^{-1}(\frac{-0.5}{-1.0}) \simeq 206°$ respectively through the two dimensional lattice (Fig. 1d). In contrast, the particle with radius $r = 0.28$ belongs to a chaotic attractor and

hence exhibits a diffusive behaviour characterized by a broad (but bounded) velocity distribution (Fig. 1c, in green). Since it has a non-zero mean velocity $\bar{v}_{(r=0.28)} = (0.01, -0.04)$, it moves *diffusively* and irregularly through the lattice at an angle $\theta = \tan^{-1}(\frac{-0.04}{0.01}) \simeq 284°$ (Fig. 1d).

Hence the particles with radii $r = 0.31$ and 0.39 can be separated from a mixture of particles with these four radii by placing two detectors at angles $\theta \simeq 0°$ and $\theta \simeq 206°$ respectively at a radial distance of, for e.g., $R = 4 \times 10^5$. The particles with radius $r = 0.28$, owing to their diffusive dynamics, are much slower and stay closer to the origin (note the difference in spatial length scales between the upper and lower panels of Fig. 1d); hence they do not affect the segregation process. Note that the four specific radii have been exemplarily chosen such that they represent complete intervals of radii corresponding to different chaotic and limit cycle attractors in the bifurcation diagram. Hence the dynamics of these particles embodies the dynamics of all the particles with radii belonging to these radii intervals.

* Aritra.Mukhopadhyay@physnet.uni-hamburg.de
† liebchen@hhu.de
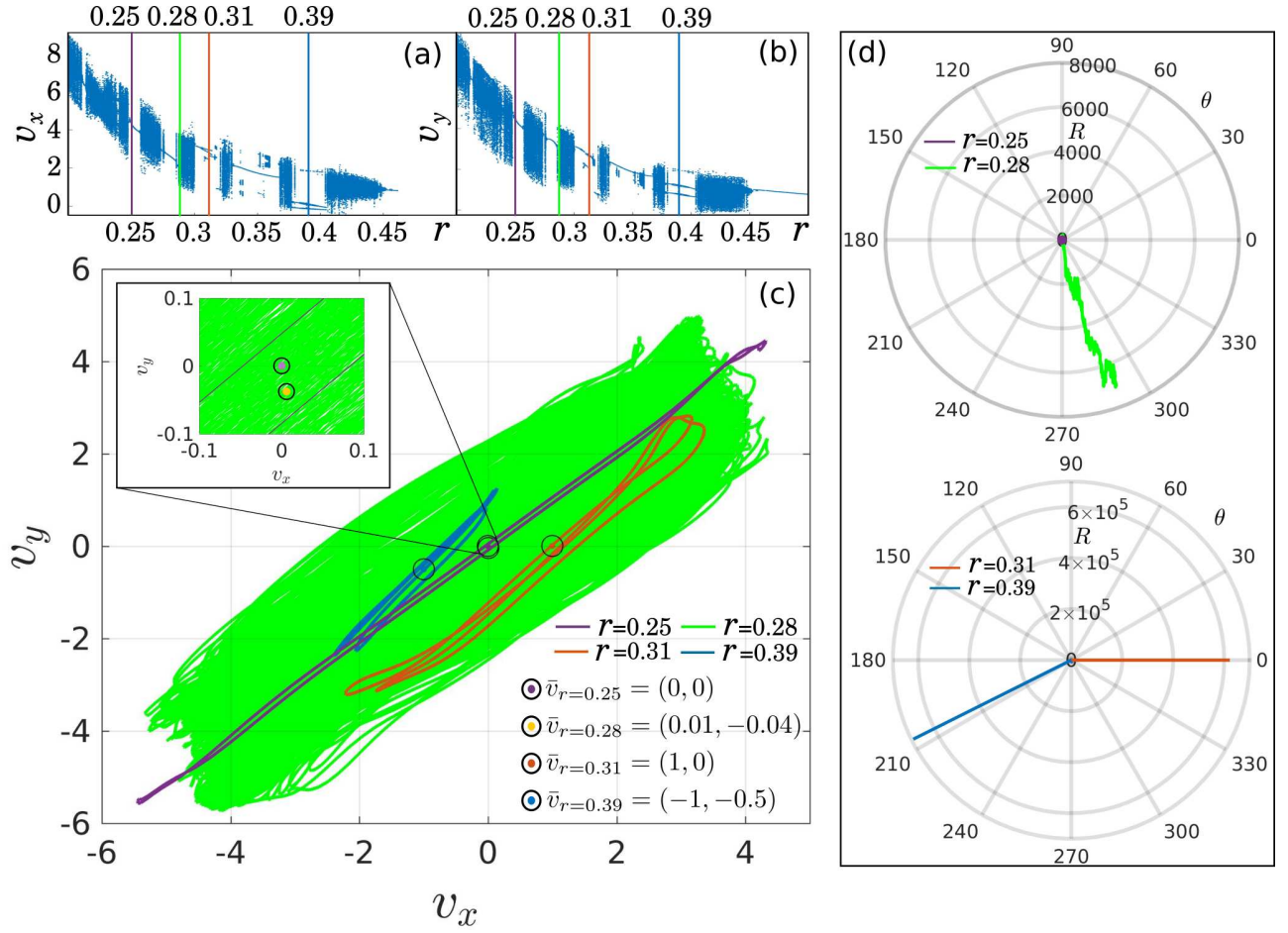‡ Peter.Schmelcher@physnet.uni-hamburg.de

Figure 1. (a) and (b) Radius dependent bifurcation diagram of the particle velocity. (c) Asymptotic dynamics and mean velocity $\bar{v}_r$ of particles having different radii r in the $v_x - v_y$ plane. (d) Spatial trajectories of particles having different radii in polar coordinates.

3.2 Controlling transport of underdamped particles in two-dimensional driven Bravais lattices

Controlling transport of underdamped particles in two-dimensional driven Bravais lattices

Aritra K. Mukhopadhyay [1,*] and Peter Schmelcher[1,2,†]

[1]*Zentrum für Optische Quantentechnologien, Fachbereich Physik, Universität Hamburg, Luruper Chaussee 149, 22761 Hamburg, Germany*
[2]*The Hamburg Centre for Ultrafast Imaging, Universität Hamburg, Luruper Chaussee 149, 22761 Hamburg, Germany*

We demonstrate the directed transport of underdamped particles in two-dimensional lattices of arbitrary geometry driven by an unbiased AC driving force. The direction of transport can be controlled via the lattice geometry as well as the strength and orientation of the oscillating drive. The breaking of the spatial inversion symmetry, which is necessary for the emergence of directed transport, is achieved solely due to the structure and geometry of the lattice. The most important criterion determining the transport direction is shown to be the ballistic attractors underlying the phase space of our weakly dissipative nonlinear dynamical system. This allows the prediction of transport direction even for setups like driven oblique lattices where the standard symmetry arguments of transport control fail. Our results can be experimentally realized using holographic optical-lattice-based setups with colloids or cold atoms.

I. INTRODUCTION

The interplay between nonlinearity and symmetry breaking in an unbiased nonequilibrium environment has been shown to rectify random particle motion into unidirectional particle transport, a phenomenon usually referred to as the ratchet effect [1–8]. It was initially conceived as a working principle to describe the performance of various biological motors [9,10]. However, today the ratchet effect attracts widespread interest and has found applications across various disciplines such as biological, atomic, and condensed matter physics [4,11–14]. Different schemes based on this mechanism have been implemented to, for example, control the topological soliton dynamics in ionic crystals [15], design electron transport in organic semiconductors [16] and organic bulk heterojunctions [17], control diffusion of driven magnetic nanoparticle [18], realize unidirectional motion of active matter [14,19], rectify voltage in superconducting quantum interference devices [20,21], and induce transport of fluxons in Josephson junction arrays [22,23] or vortices in conformal crystal arrays [24,25].

Due to such a widespread applicability of ratchet-based transport, unsurprisingly, a vast body of literature has been devoted to controlling the strength and direction of the ratchet current. While the ratchet setups in one spatial dimensional address only forward or backward transport of particles [3,4,26–32], two-dimensional (2D) setups allow for transport at arbitrary angles. It has been shown that particles driven via external time periodic forces on a spatially periodic 2D lattice allow directed transport not only parallel to the drive but also at an angle relative to the driving law [33,34] or even completely orthogonal to it [35]. Although there has been major technical advancement in experimental realization of such 2D ratchets involving different systems like cold atoms and colloids, there are certain common drawbacks in most of them. First, most of these ratchet-based setups in two dimensions operate in the overdamped regime where the inertial effects can be neglected. However, there exists a large class of systems which do not operate in this overdamped regime, such as self-propelled vibrated particles [36], underdamped colloids and tracer particles [37,38], gold and polystyrene nanoparticles in optical systems [39], and granular particles. Although the control of directed transport would certainly be desirable in these systems, an understanding of the ratchet phenomenon in such underdamped 2D setups is lacking. Second, a majority of these setups usually require an external static force as a bias in order to realize directed transport of particles. There are very few setups in two dimensions where the transport is achieved solely due to an unbiased AC driving force [33,34]. Finally, almost all of these setups have focused on directed transport in driven square lattices. Only recently has it been shown that lattices with other geometries, especially oblique lattices, also allow directed transport, although in the overdamped regime [33].

In this work we address the above three key limitations of the traditional 2D ratchet setups. Specifically, we show that it is possible to realize directed transport of underdamped particles along designated directions by externally driving 2D Bravais lattices of different geometries with an unbiased time-dependent driving force. The necessary breaking of the spatial inversion symmetry in our setup is achieved solely due to the lattice geometry. Any residual reflection symmetry can be optionally broken by a suitable orientation of the driving force. We show that the resulting direction of transport can be controlled and explained in terms of the ballistic attractors

---

*Aritra.Mukhopadhyay@physnet.uni-hamburg.de
†Peter.Schmelcher@physnet.uni-hamburg.de

underlying the phase space of our dissipative nonlinear dynamical system. It is important to stress that generally such a setup does not allow the prediction of the transport direction *a priori* due to the absence of any line of reflection symmetry. However, we show that it is possible to realize directed transport of particles along specific directions irrespective of the lattice geometry and orientation of the oscillating drive.

II. SETUP

We consider N noninteracting classical particles in a 2D dissipative potential landscape $V(x, y) = \sum_{m,n=-\infty}^{+\infty} V_{mn} e^{-\beta(\mathbf{r}-\mathbf{r}_{mn})^2}$ formed by a lattice of 2D Gaussian barriers centered at positions $\mathbf{r}_{mn} = (mL, nL)$, $m, n \in \mathbb{Z}$, having site-dependent potential heights V_{mn}. The lattice is driven by an external harmonic driving force $\mathbf{f}(t) = a \cos \omega t (\cos \theta_d, \sin \theta_d)$. Here a and ω are the amplitude and the frequency of the driving, respectively, and θ_d denotes the angle of the driving force with respect to the x axis. Introducing dimensionless variables $x' = \frac{x}{L}$, $y' = \frac{y}{L}$, and $t' = \omega t$ and dropping the primes for simplicity, the equation of motion for a single particle at position $\mathbf{r} = (x, y)$ with velocity $\dot{\mathbf{r}} = (\dot{x}, \dot{y})$ reads

$$\ddot{\mathbf{r}} = -\gamma \dot{\mathbf{r}} + \mathbf{F}(t) + \boldsymbol{\xi}(t)$$
$$+ \sum_{m,n=-\infty}^{+\infty} U_{mn}(\mathbf{r} - \mathbf{R}_{mn}) e^{-\alpha(\mathbf{r}-\mathbf{R}_{mn})^2}, \quad (1)$$

where $\mathbf{F}(t) = d \cos t (\cos \theta_d, \sin \theta_d)$ is the effective site-dependent driving law and $\mathbf{R}_{mn} = (m, n)$ denotes the positions of the maxima of the Gaussian barriers. The different scaled parameters governing the system are the effective barrier heights $U_{mn} = \frac{2V_{mn}\beta}{m\omega^2}$, an effective driving amplitude $d = \frac{a}{m\omega^2 L}$, an effective dissipation coefficient $\gamma = \frac{\tilde{\gamma}}{m\omega}$, and the parameter $\alpha = \beta L^2$. In addition, $\boldsymbol{\xi}(t) = (\xi_x, \xi_y)$ denotes thermal fluctuations modeled by Gaussian white noise of zero mean with the property $\langle \xi_i(t)\xi_j(t') \rangle = 2D\delta_{ij}\delta(t - t')$, where $i, j \in x, y$ and $D = \frac{\tilde{\gamma} k_B \mathcal{T}}{m\omega^2 L^2}$ is the dimensionless noise strength, with $\mathcal{T}$ and k_B denoting the temperature and Boltzmann constant, respectively. The set of all Gaussian barriers arranged periodically in space with a specific value of barrier height U_{mn} forms a sublattice of our system. Our setup is hence a driven superlattice formed by the superposition of different sublattices, each consisting of barriers possessing distinct heights U_{mn}. The necessary condition for any setup to exhibit directed transport is to break both the generalized spatial inversion symmetry $S_\mathbf{r}$: $\mathbf{r} \to -\mathbf{r} + \boldsymbol{\delta}$ and $t \to t + \tau$, and the generalized time-reversal symmetry S_t: $t \to -t + \tau$ and $\mathbf{r} \to \mathbf{r} + \boldsymbol{\delta}$ (for any arbitrary constant translations $\boldsymbol{\delta}$ and τ of space and time, respectively) [4,40]. In our setup, each sublattice is individually symmetric with respect to the symmetry $S_\mathbf{r}$ and this symmetry can be broken by a superposition of at least three sublattices consisting of barriers with different heights (see Appendix A). Since our setup is dissipative, the symmetry S_t is also broken.

The setup can be experimentally realized, e.g., by using monodisperse colloidal particles in a 2D lattice obtained by reflecting a linearly polarized laser beam onto a spatial light modulator displaying a computer-generated hologram which

can then be driven using a piezomodulator [33]. A second highly controllable setup could be driven lattices based on holographic trapping of atoms [41–44] in the regime of microkelvin temperatures where a classical description of cold-atom ratchets is appropriate [12].

In order to explore the particle transport in our lattice characterized by the average velocity of the particle ensemble, we initialize $N = 10^4$ particles within a square region $x, y \in [-10, 10]$ with small random velocities $v_x, v_y \in [-0.1, 0.1]$ such that their initial kinetic energies are small compared to the potential height of the Gaussian barriers. Subsequently, we time evolve our ensemble up to time $t_f = 2 \times 10^4$ by numerical integration of Eq. (1). For all our setups, we consider noise strength $D > 0$ and the resulting asymptotic transport velocity is independent of the specific initial conditions of each particles. We demonstrate that it is possible to realize particle transport parallel to the driving force axis (axial transport), orthogonal to it (lateral transport), or even in an oblique direction for different lattice geometries using our setup.

III. RESULTS AND DISCUSSION

A. Axial transport in a rectangular lattice

In our first setup [Figs. 1(a) and 1(b)], we consider a rectangular superlattice constructed by superposing three rectangular lattices with lattice vectors $\mathbf{a} = (3, 0)$ and $\mathbf{b} = (0, 1)$.
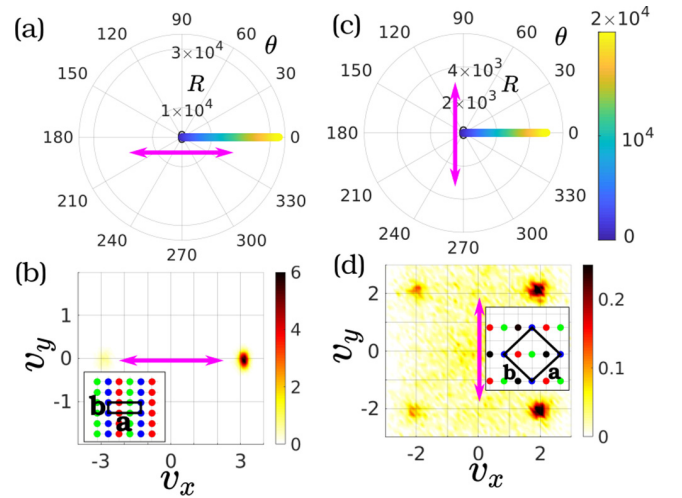

FIG. 1. Mean position of the particle ensemble (in radial R and angular θ coordinates) as a function of time t (in the colorbar) for the (a) rectangular lattice driven along $\theta_d = 0°$ with $d = 0.3$ and (c) square lattice driven along $\theta_d = 90°$ with $d = 0.5$. (b) and (d) Snapshots of the ensemble velocity distribution at $t = t_f$ for the setups in (a) and (c), respectively. The insets in (b) and (d) depict schematic representations of the two corresponding lattices along with the lattice vectors $\mathbf{a}$ and $\mathbf{b}$, with each colored circle denoting the position of an individual Gaussian barrier. The different colors denote different barrier heights $U_{mn} = 0.5$ (blue), 1.0 (red), and 1.5 (green) [inset in (b)] and $U_{mn} = 0.3$ (blue), 0.6 (red), 0.9 (green), and 1.2 (black) [inset in (d)]. The driving axis is denoted by the pink double arrowed lines. The other parameters are $\gamma = 10^{-2}$, $\alpha = 5$, and $D = 1.5 \times 10^{-4}$.

Although the setup breaks inversion symmetry $S_{\mathbf{r}}$, it is invariant under $P_y : y \rightarrow -y$, rendering any line parallel to the x axis as the line of reflection symmetry modulo a spatial translation along the y direction. The lattice is driven along this symmetry axis by choosing $\theta_d = 0°$. As expected from the symmetry argument, the particles exhibit no transport along the y direction and a net directed transport is observed along the positive x direction [Fig. 1(a)]. The direction of transport can be better understood by analyzing the asymptotic velocity distribution of the particles at the end of the simulation time, i.e., t_f, which shows that most particles travel along the x axis with a velocity of either $\mathbf{v} \approx (3, 0)$ or $(-3, 0)$ [Fig. 1(b)]. For the chosen parameter regime, these velocities correspond to the average velocities of the two ballistic attractors denoting synchronized motion of particles through the oscillating lattice traveling one unit cell per unit time either parallel or antiparallel to the lattice vector $\mathbf{a}$ in the deterministic limit $D \rightarrow 0$. Even for $D > 0$, the attractors are not completely destroyed and at longer timescales the particles move approximately with the same velocities as the average velocities of these attractors. Thus, these ballistic attractors correspond to almost straight distinct channels through the lattice corresponding to regular motion of the particles towards left and right with opposite velocities. The average transport velocity of the ensemble is simply the sum of the velocities of all the particles in both these channels. Due to the broken $P_x : x \rightarrow -x$ symmetry, the velocity distribution is asymmetric and significantly more particles travel to the right than to the left, resulting in an axial transport along the positive x direction.

B. Lateral transport in a square lattice

Lattices possessing a line of reflection symmetry can also exhibit directed transport along a direction orthogonal to the driving force. To illustrate this, we consider a square lattice formed by the superposition of four square lattices with lattice vectors $\mathbf{a} = (2, 2)$ and $\mathbf{b} = (-2, 2)$ [Figs. 1(c) and 1(d)]. This lattice too breaks both $S_{\mathbf{r}}$ and P_x symmetries but preserves the P_y symmetry. Upon driving the lattice along the y axis, which is orthogonal to the symmetry axis, a lateral current is observed along the positive x direction in accordance with the symmetry argument [Fig. 1(c)]. From the peaks of the asymptotic velocity distribution of the particles [Fig. 1(d)], it is evident that the underlying particle dynamics is governed mainly by the four ballistic attractors with average velocities $(2,2)$, $(2, -2)$, $(-2, 2)$, and $(-2, -2)$. These correspond to particles exhibiting regular motion, moving one unit cell per unit time along directions parallel and antiparallel to the two lattice vectors $\mathbf{a}$ and $\mathbf{b}$. The P_y symmetry is clearly reflected in the asymptotic velocity distribution due to which almost equal numbers of particles possess $v_y > 0$ and $v_y < 0$, thus prohibiting any average transport in the y direction [Fig. 1(d)]. However, due to the P_x symmetry breaking, the number of particles moving along the positive x direction is much higher and hence directed transport occurs along this direction.

C. Driving-induced breaking of the reflection symmetry

The residual reflection symmetry P_y in our rectangular or square lattice setups can be broken by driving the lattice
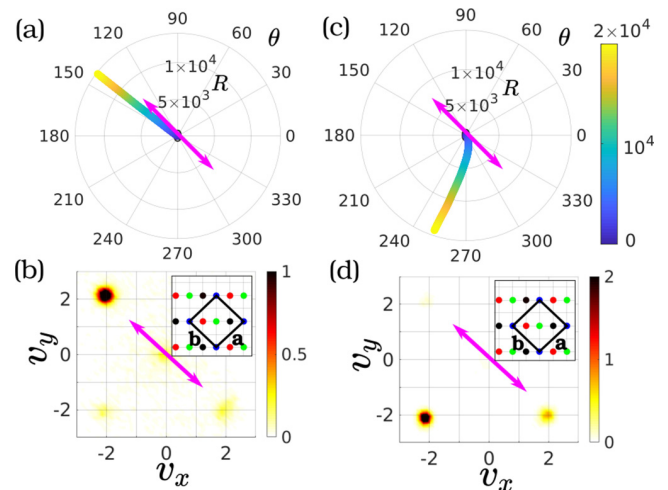

FIG. 2. Mean position of the particle ensemble (in radial R and angular θ coordinates) as a function of time t (in the colorbar) for the same square lattice setup as in Figs. 1(c) and 1(d) driven along $\theta_d = 135°$ (pink double arrowed lines) with (a) $d = 0.6$ and (c) $d = 1.0$. (b) and (d) Snapshots of the ensemble velocity distribution at $t = t_f$ for the setups in (a) and (c), respectively; the insets depict schematic representations of the corresponding lattice. The other parameters are the same as in Figs. 1(c) and 1(d).

oblique to the line of reflection symmetry. Since P_y transforms $\theta_d \rightarrow -\theta_d$, $\mathbf{F}(t) \rightarrow \tilde{\mathbf{F}}(t) = d \cos t (\cos \theta_d, -\sin \theta_d)$, which cannot be transformed back to $\mathbf{F}(t)$ by any additional time shift operation for $\theta_d \neq 0°$, $90°$, $180°$, or $270°$. To illustrate this, we consider the same square lattice as in Figs. 1(c) and 1(d) but now driven along the lattice vector $\mathbf{b}$ by choosing $\theta_d = 135°$ (Fig. 2). Although the broken $S_{\mathbf{r}}$ symmetry ensures the existence of directed transport, the direction of transport can no longer be predicted from symmetry considerations alone. However, we show that it is possible to control the underlying ballistic attractors and hence the transport direction by varying the amplitude of the driving force d. For $d = 0.6$, the ensemble is transported along $\theta \approx 140°$, almost parallel to the driving force along the lattice vector $\mathbf{b}$ [Fig. 2(a)]. The peak at $\mathbf{v} \approx (-2, 2)$ in the asymptotic particle velocity distribution shows that the asymptotic dynamics of the ensemble is governed primarily by a single ballistic attractor with average velocity $(-2, 2)$ [Fig. 2(b)] denoting synchronized particle motion parallel to $\mathbf{b}$. Therefore, directed transport appears along this direction. Upon driving the lattice along the same axis, but with a higher driving amplitude $d = 1.0$, the direction of transport can be rotated to an almost perpendicular direction $\theta \approx 250°$ [Fig. 2(c)]. The change in the driving strength changes the dominant attractor governing the transport, which now has an average velocity $(-2, -2)$, propelling a majority of the particles to move with this velocity in a direction antiparallel to the lattice vector $\mathbf{a}$ [Fig. 2(d)], hence explaining the transport. We note that for a broad range of value of d, the particle dynamics is governed by the four ballistic attractors with average velocities $(2,2)$, $(2, -2)$, $(-2, 2)$, and $(-2, -2)$ (see Appendix B). The transport direction is determined by the attractor with the highest asymptotic particle occupancy. Hence, for different values of d, directed
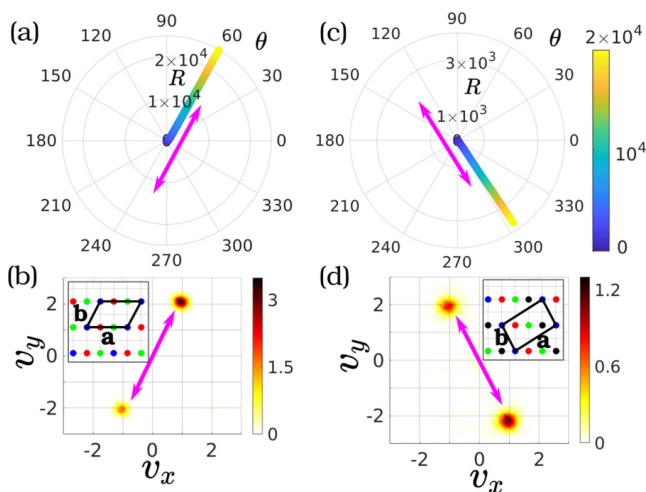
FIG. 3. Mean position of the particle ensemble (in radial R and angular θ coordinates) as a function of time t (in colorbar) for the two oblique lattices: (a) $O1$ driven along $\theta_d \approx 63°$ with $d = 0.75$ and (c) $O2$ driven along $\theta_d \approx 116°$ with $d = 0.6$. (b) and (d) Snapshots of the ensemble velocity distribution at $t = t_f$ for the setups in (a) and (c), respectively. The insets in (b) and (d) depict schematic representations of the two corresponding lattices with different colored circles denoting different barrier heights: $U_{mn} = 0.3$ (blue), 0.6 (red), 0.9 (green), and 1.2 (black). The driving axis is denoted by the pink double arrowed lines. The other parameters are $\gamma = 10^{-2}$, $\alpha = 5$, and $D = 2 \times 10^{-4}$.

transport occurs, to a good approximation, along one of these four directions.

D. Oblique lattice

In contrast to square and rectangular lattices, a 2D oblique lattice does not possess any lines of reflection symmetry and therefore has no obvious symmetry direction along which directed transport should occur. Even for such a setup we can realize directed transport of particles along a particular direction, specifically along the shortest lattice vector, by controlling the underlying ballistic attractors determining the transport. We illustrate this by considering an oblique lattice $O1$ composed of three superimposed oblique lattices with lattice vectors $\mathbf{a} = (3, 0)$ and $\mathbf{b} = (1, 2)$ ($|\mathbf{a}| > |\mathbf{b}|$) with an angle of approximately $63°$ between them. Upon driving the lattice along $\mathbf{b}$, an axial directed transport of particles is observed along $\theta \approx 63°$ parallel to $\mathbf{b}$ [Fig. 3(a)]. Most of the particles move asymptotically with $\mathbf{v} \approx (1, 2)$ or $(-1, -2)$, which denote the average velocities of the ballistic attractors corresponding to particles moving one unit cell per unit time parallel or antiparallel to the shortest lattice vector $\mathbf{b}$ [Fig. 3(b)]. The spatial asymmetry due to the breaking of $S_\mathbf{r}$ symmetry is responsible for a higher number of particles moving parallel to $\mathbf{b}$, resulting in the transport along this direction.

Next we demonstrate that it is possible to direct the particle transport either parallel or antiparallel to the shortest lattice vector of an oblique lattice irrespective of the direction of the driving force. To illustrate this, we consider a second oblique lattice setup $O2$ constructed by the superposition of
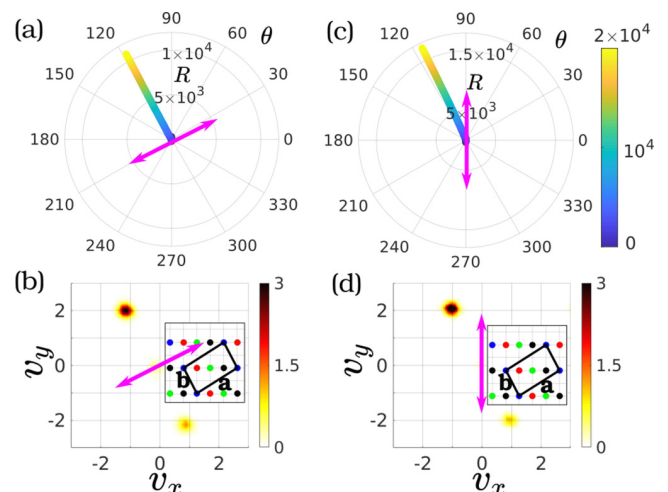
FIG. 4. Mean position of the particle ensemble (in radial R and angular θ coordinates) as a function of time t (in the colorbar) for the oblique lattice $O2$ [see Figs. 3(c) and 3(d)] driven along (pink double arrowed lines) (a) $\theta_d \approx 26°$ with $d = 1.0$ and (c) $\theta_d \approx 90°$ with $d = 1.6$. (b) and (d) Snapshots of the ensemble velocity distribution at $t = t_f$ for the setups in (a) and (c), respectively. The insets depict schematic representations of the corresponding lattices. The other parameters are the same as in Figs. 3(c) and 3(d).

four oblique lattices having lattice vectors $\mathbf{a} = (3, 2)$ and $\mathbf{b} = (-1, 2)$ (hence $|\mathbf{a}| > |\mathbf{b}|$) such that the angle between them is approximately $83°$. When the lattice is driven along the lattice vector $\mathbf{b}$ with $d = 0.6$, an axial directed transport is observed at $\theta \approx 300°$ antiparallel to $\mathbf{b}$ [Fig. 3(c)]. However, upon driving the lattice along an axis perpendicular to $\mathbf{b}$ with $d = 1$, a reversal of transport occurs and the ensemble moves along $\theta \approx 120°$, almost parallel to $\mathbf{b}$, thereby exhibiting lateral transport [Fig. 4(a)]. A directed transport along $\theta \approx 120°$ is also observed when the external drive is along the y axis and $d = 1.6$, thus allowing us to realize oblique transport with respect to the driving force [Fig. 4(c)]. The transport in all these three scenarios is governed by the two ballistic attractors having average velocities $(-1, 2)$ and $(1, -2)$ around which the asymptotic velocity distribution of the particles is localized [Figs. 3(d), 4(b), and 4(d)]. Similar to the setup $O1$, these velocities corresponds to synchronized motion of particles moving either parallel or antiparallel to the shortest lattice vector $\mathbf{b}$ and the transport direction is determined by the relative asymmetry in the number of particles moving along these two directions. Since the dominant ballistic attractors for both setups $O1$ and $O2$ remain the same as those in Figs. 3 and 4 upon varying d, the direction of transport also does not change considerably (see Appendix B).

IV. CONCLUSION

We have demonstrated the control of directed transport of underdamped particles along specific directions in different types of 2D Bravais lattices driven by unbiased external forces. Most importantly, we have shown that it is possible to direct the transport along one of the lattice vectors in setups without any line of reflection symmetry irrespective of the driving axis. These setups preclude any prediction of the

transport direction *a priori* based on the standard symmetry arguments. However, we have shown that the direction of transport can be well understood in terms of the attractors controlling the asymptotic dynamics of our nonlinear dynamical system. The observed directions of transport persists for noise strengths up to $D \lesssim 10^{-3}$, typical for cold atoms or underdamped colloids. The fact that different lattice geometries can be realized simply by varying the potential heights of the Gaussian barriers constituting the sublattices should also allow for time-dependent control of the transport direction using dynamic holographic optical tweezers [45] or dynamical digital hologram generation techniques [46,47]. Future perspectives include the investigation of the impact of the lattice geometry on the chaotic transport in very weakly dissipative and pure Hamiltonian regime and relevant technological applications such as the development of miniature devices helpful for colloidal sorting or targeted drug delivery.

ACKNOWLEDGMENTS

APPENDIX A: SYMMETRY ANALYSIS

In order to observe directed transport of a particle ensemble in any driven lattice setup, the necessary condition is to break both the generalized spatial inversion symmetry $S_{\mathbf{r}}$: $\mathbf{r} \rightarrow -\mathbf{r} + \delta$ and $t \rightarrow t + \tau$, and the generalized time-reversal symmetry S_t: $t \rightarrow -t + \tau$ and $\mathbf{r} \rightarrow \mathbf{r} + \delta$ (for any arbitrary constant translations δ and τ of space and time, respectively) of the setup [4,40]. In a 2D system, the spatial inversion operation can be further decomposed into $S_{\mathbf{r}} \equiv P_x P_y + \mathbf{\Lambda} + \eta$, i.e., consecutive reflections $P_x : x \rightarrow -x$ and $P_y : y \rightarrow -y$ along x and y (or any two orthogonal) axes, respectively, followed by any optional arbitrary space and time translations $\mathbf{\Lambda}$ and η. Since our setup is dissipative, S_t is always broken. The driving force $\mathbf{F}(t)$ being a single harmonic function of time does not break the $S_{\mathbf{r}}$ symmetry, in contrast to a biharmonic driving force [4,48]. Since any single Bravais lattice is symmetric with respect to spatial inversion operation, the sublattices in our setups are symmetric with respect to the symmetry operation $S_{\mathbf{r}}$. However, superposition of more than one sublattice breaks the $S_{\mathbf{r}}$ symmetry (Fig. 5) and leads to directed transport as discussed in the paper.

APPENDIX B: ROLE OF DRIVING STRENGTH IN DIRECTED TRANSPORT

Here we discuss the behavior of the attractors underlying the phase space of the different lattices described in the main text for different driving amplitudes d. As mentioned in the main text, the deterministic $D \rightarrow 0$ dynamics of our driven lattice setup is governed by the asymptotic attractors in the system, which can be either chaotic, denoting diffusive particle motion through the lattice, or ballistic, representing regular periodic motion of the particles. The attractors are characterized by their average velocities $\bar{\mathbf{v}}$, which for the ballistic attractors can be expressed as $\bar{\mathbf{v}} = \frac{1}{T}(\frac{m_a}{n_a}\mathbf{a} + \frac{m_b}{n_b}\mathbf{b})$,
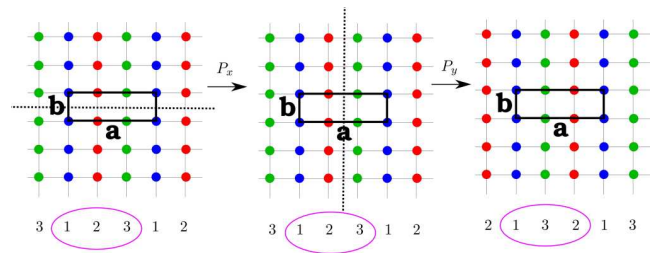

FIG. 5. Schematic diagram showing the breaking of the $S_{\mathbf{r}}$ symmetry in our rectangular lattice setup with lattice vectors $\mathbf{a}$ and $\mathbf{b}$. Each closed colored circles represent Gaussian barriers with different heights $U_{mn} = 0.5$ (blue), 1.0 (red), and 1.5 (green). The P_x transformation about the horizontal dotted line leaves the lattice invariant. However, the subsequent P_y transformation about the vertical dotted axis interchanges the positions of the green and red lattice points which cannot be restored and optional spatial translations or time shifts. The numbers 1, 2, and 3 below correspond to the blue, red, and green lattice points, respectively, and have been provided to allow a better visualization of the breaking of symmetry.

with $m_a, n_a, m_b, n_b \in \mathbb{Z}$, $\mathbf{a}$ and $\mathbf{b}$ being the two lattice vectors and T the temporal driving period, which for our case is unity. The ballistic attractors correspond to almost straight distinct channels through the lattice yielding regular motion of the particles synchronized with the external driving force. The average transport velocity of our particle ensemble is simply the vector sum of the velocities of the particles in all these channels.

Although all our setups are characterized by both the chaotic and ballistic attractors, we have focused on the directed transport governed solely by the ballistic attractors. In the following, we discuss the ballistic attractors corresponding to each of our setups for different values of the driving strength d. For this, we numerically propagate $N = 10^4$ particles within a square region $x, y \in [-10, 10]$ with small random velocities $v_x, v_y \in [-0.1, 0.1]$ for different values of d up to $t = 2 \times 10^4$. The asymptotic average velocities of each of these trajectories correspond to the average velocity $\bar{\mathbf{v}}$ of the different attractors underlying the setup. When $\bar{\mathbf{v}}$ is expressed in polar coordinates, the angular component $\bar{\theta}$ denotes the average direction of an attractor and the modulus $|\bar{\mathbf{v}}|$ denotes its average speed.

1. Rectangular lattice

First, we consider the rectangular lattice with spatial period (3,1) and lattice vectors $\mathbf{a} = (3, 0)$ and $\mathbf{b} = (0, 1)$ driven along the x axis [Fig. 6(a)] as described in the main text. For different values of the driving strength d, we note that the majority of the attractors are located along either $\bar{\theta} = 0°$ or $\bar{\theta} = 180°$ [Fig. 6(b)], with some isolated ones along $\theta = 30°, 90°, 210°, 270°$. Therefore, for almost any value of d, we would expect most of the particles in our setup to move along either the positive or negative x direction. The breaking of the spatial inversion symmetry induces an asymmetry in the number of particles moving in the two directions; therefore, directed transport emerges along any one of them as discussed in the main text. The reflection symmetry in the y direction forbids any transport along the y direction.
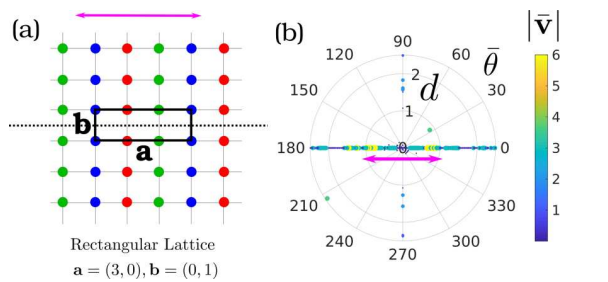
FIG. 6. (a) Schematic representation of our rectangular lattice setup with lattice vectors **a** and **b**. Each closed colored circles represent Gaussian barriers with different heights $U_{mn} = 0.5$ (blue), 1.0 (red), and 1.5 (green). The dotted line parallel to the x axis denotes the line of reflection symmetry. (b) Average direction of the attractors $\bar{\theta}$ (in angular coordinates) as a function of driving amplitude d (in radial coordinates) with the colorbar denoting their average speed $|\bar{\mathbf{v}}|$. The driving axis is denoted by the pink double arrowed lines in both the figures. The other parameters are $\gamma = 10^{-2}$, $\theta_d = 0°$, $\alpha = 5$, and $D = 1.5 \times 10^{-4}$.

2. Square lattice

For our square lattice setup with lattice vectors $\mathbf{a} = (2, 2)$ and $\mathbf{b} = (-2, 2)$ [Figs. 7(a) and 7(b)], there exist
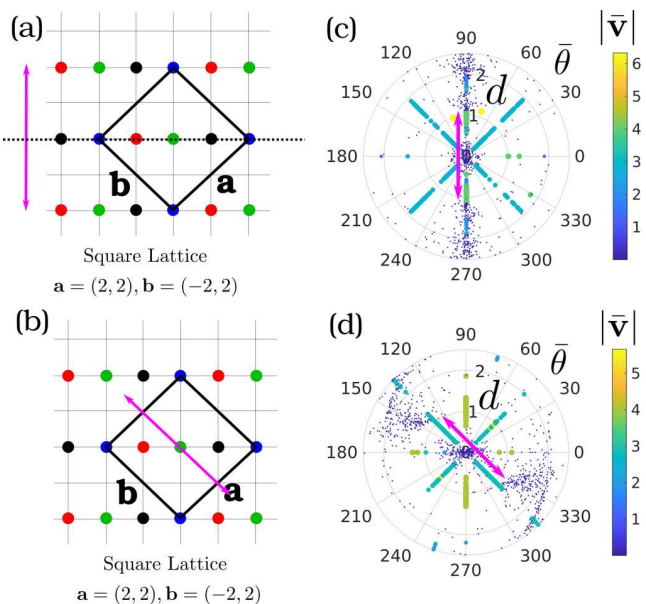

FIG. 7. Schematic representation of our square lattice setup with lattice vectors **a** and **b** driven along (a) the y axis with $\theta_d = 90°$ and (b) $\theta_d = 135°$. Closed colored circles represent Gaussian barriers with different heights $U_{mn} = 0.3$ (blue), 0.6 (red), 0.9 (green), and 1.2 (black). The dotted line in (a) denotes the line of reflection symmetry. (c) and (d) Average direction of the attractors $\bar{\theta}$ (in angular coordinates) as a function of driving amplitude d (in radial coordinates) with the colorbar denoting their average speed $|\bar{\mathbf{v}}|$ corresponding to (a) and (b), respectively. The blue colored smaller dots denote the chaotic attractors, whereas the larger closed circles of other colors denote the ballistic attractors. The driving axis is denoted by the pink double arrowed lines in all the figures. The other parameters are $\gamma = 10^{-2}$, $\alpha = 5$, and $D = 1.5 \times 10^{-4}$.
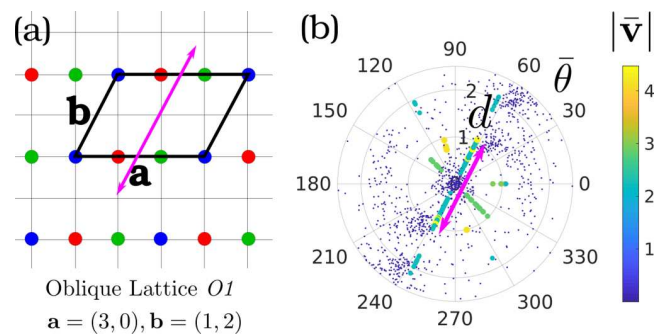

FIG. 8. (a) Schematic representation of our oblique lattice setup $O1$ with lattice vectors **a** and **b** driven parallel to **b**. Closed colored circles represent Gaussian barriers with different heights $U_{mn} = 0.3$ (blue), 0.6 (red), and 0.9 (green). (b) Average direction of the attractors $\bar{\theta}$ (in angular coordinates) as a function of driving amplitude d (in radial coordinates) with the colorbar denoting their average speed $|\bar{\mathbf{v}}|$. The blue colored smaller dots denote the chaotic attractors, whereas the larger closed circles of other colors denote the ballistic attractors. The driving axis is denoted by the pink double arrowed lines in both the figures. The other parameters are $\gamma = 10^{-2}$, $\theta_d \approx 63°$, $\alpha = 5$, and $D = 2 \times 10^{-4}$.

roughly six different directions corresponding to the ballistic attractors irrespective of the driving axis and driving strength. These are along 45°, 90°, 135°, 225°, 270°, and 315° [Figs. 7(c) and 7(d)]. However, in the presence of noise, the breaking of the spatial inversion symmetry induces asymmetric jumps of trajectories between different attractors such that only one or two ballistic attractors govern the particle dynamics asymptotically (see Figs. 1 and 2 in the main text).

When the lattice is driven along the y axis [Fig. 7(a)], the reflection symmetry about the x axis ensures that equal numbers of particles asymptotically end up in attractors with $0° < \bar{\theta} < 180°$ and $180° < \bar{\theta} < 360°$, thus prohibiting transport in the y direction. However, the spatial inversion symmetry ensures an imbalance between the number of particles whose dynamics is governed by the ballistic attractors with $\bar{\theta} = 45°, 315°$ and those with $\bar{\theta} = 135°, 225°$. This ensures a net transport along the positive or negative x direction as discussed in the main text.

For any other choice of the driving axis, e.g., as in Fig. 7(b), there exists no line of symmetry and usually only one of the six ballistic attractors controls the asymptotic particle dynamics. Hence, for different values of the driving strength d, directed transport is observed along one of these directions. In the main text we showed two such examples, where the transport is governed by the attractors with $\bar{\theta} = 135°$ and 225°, respectively, for the same orientation of the driving axis as in Fig. 7(b) but for two different driving strengths d.

3. Oblique lattice

For our oblique lattice setups ($O1$ and $O2$) with lattice vectors **a** and **b** ($|\mathbf{a}| > |\mathbf{b}|$), we find that there are always two ballistic attractors oriented parallel and antiparallel to the smallest lattice vector **b** irrespective of the orientation
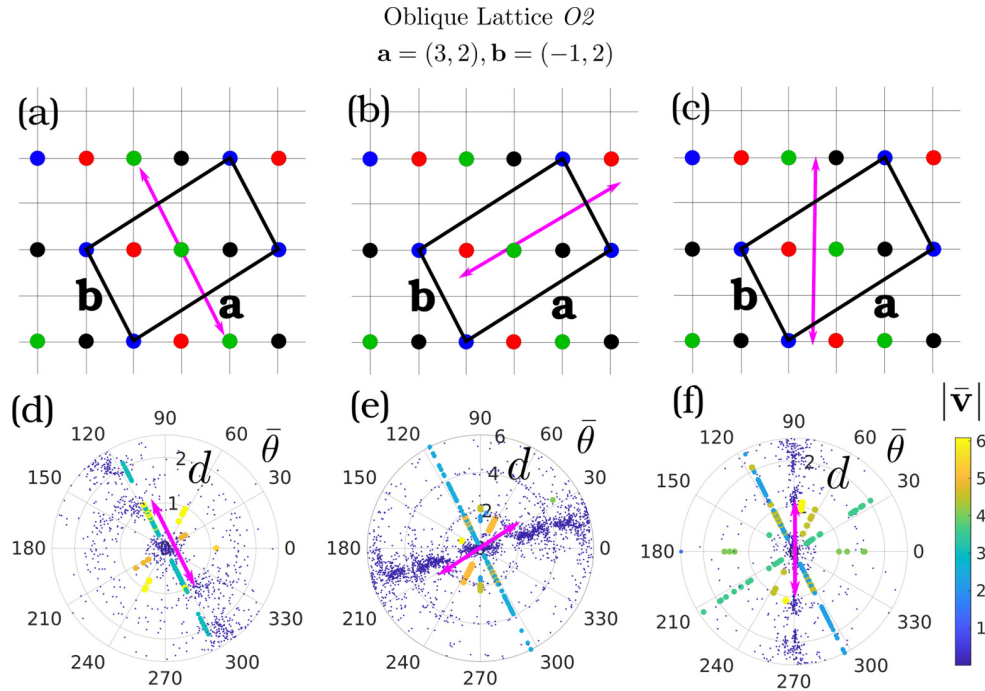
Oblique Lattice *O2*

$\mathbf{a} = (3, 2), \mathbf{b} = (-1, 2)$

FIG. 9. Schematic representation of our oblique lattice setup *O2* with lattice vectors **a** and **b** driven along (a) $\theta_d \approx 116°$, (b) $\theta_d \approx 26°$, and (c) $\theta_d = 90°$. Closed colored circles represent Gaussian barriers with different heights $U_{mn} = 0.3$ (blue), 0.6 (red), 0.9 (green), and 1.2 (black). (d)–(f) Average direction of the attractors $\bar{\theta}$ (in angular coordinates) as a function of driving amplitude d (in radial coordinates) with the colorbar denoting their average speed $|\bar{\mathbf{v}}|$ corresponding to (a)–(c), respectively. The blue colored smaller dots denote chaotic attractors, whereas the larger closed circles of other colors denote the ballistic attractors. The driving axis is denoted by the pink double arrowed lines in all the figures. The other parameters are $\gamma = 10^{-2}$, $\alpha = 5$, and $D = 2 \times 10^{-4}$.

and strength of the driving force (see Figs. 8 and 9). As a result, for most values of driving strength d and orientation θ_d, it is possible to realize directed transport of particles along any one of these directions, as we have discussed in the main text.

Hence, for all our setups, the underlying ballistic attractors are quite robust with respect to slight variations of the driving strength d. The particular values of d in the main text have been chosen in order to exemplify the directed transport at specific angles in each of these setups.

[1] R. D. Astumian, Science **276**, 917 (1997).

[2] F. Jülicher, A. Ajdari, and J. Prost, Rev. Mod. Phys. **69**, 1269 (1997).

[3] S. Flach, O. Yevtushenko, and Y. Zolotaryuk, Phys. Rev. Lett. **84**, 2358 (2000).

[4] S. Denisov, S. Flach, and P. Hänggi, Phys. Rep. **538**, 77 (2014).

[5] J. Prost, J. F. Chauwin, L. Peliti, and A. Ajdari, Phys. Rev. Lett. **72**, 2652 (1994).

[6] M. O. Magnasco, Phys. Rev. Lett. **71**, 1477 (1993).

[7] R. Bartussek, P. Hänggi, and J. G. Kissner, Europhys. Lett. **28**, 459 (1994).

[8] L. P. Faucheux, L. S. Bourdieu, P. D. Kaplan, and A. J. Libchaber, Phys. Rev. Lett. **74**, 1504 (1995).

[9] R. D. Astumian and P. Hänggi, Phys. Today **55** (11), 33 (2002).

[10] R. Ait-Haddou and W. Herzog, Cell Biochem. Biophys. **38**, 191 (2003).

[11] P. Hänggi, F. Marchesoni, and F. Nori, Ann. Phys. (Leipzig) **14**, 51 (2005).

[12] F. Renzoni, Adv. At. Mol. Opt. Phys. **57**, 1 (2009).

[13] D. Cubero and F. Renzoni, *Brownian Ratchets* (Cambridge University Press, Cambridge, 2016).

[14] C. J. O. Reichhardt and C. Reichhardt, Annu. Rev. Condens. Matter Phys. **8**, 51 (2017).

[15] J. Brox, P. Kiefer, M. Bujak, T. Schaetz, and H. Landa, Phys. Rev. Lett. **119**, 153602 (2017).

[16] E. M. Roeling, W. C. Germs, B. Smalbrugge, E. J. Geluk, T. de Vries, R. A. J. Janssen, and M. Kemerink, Nat. Mater. **10**, 51 (2011).

[17] O. Kedem, B. Lau, M. A. Ratner, and E. A. Weiss, Proc. Natl. Acad. Sci. USA **114**, 8698 (2017).

[18] R. L. Stoop, A. V. Straube, and P. Tierno, Nano Lett. **19**, 433 (2019).

[19] B. Q. Ai, Sci. Rep. **6**, 18740 (2016).

[20] I. Zapata, R. Bartussek, F. Sols, and P. Hänggi, Phys. Rev. Lett. **77**, 2292 (1996).

[21] J. Spiechowicz and J. Łuczka, New J. Phys. **17**, 023054 (2015).

[22] F. Falo, P. J. Martínez, J. J. Mazo, and S. Cilla, Europhys. Lett. **45**, 700 (1999).

[23] Y. Zolotaryuk, Phys. Rev. E **86**, 026604 (2012).

[24] C. Reichhardt and C. J. O. Reichhardt, Phys. Rev. B **93**, 064508 (2016).

[25] C. Reichhardt, D. Ray, and C. J. O. Reichhardt, Phys. Rev. B **91**, 184502 (2015).

[26] P. Reimann, Phys. Rep. **361**, 57 (2002).

[27] P. Hänggi and F. Marchesoni, Rev. Mod. Phys. **81**, 387 (2009).

[28] H. Schanz, M. F. Otto, R. Ketzmerick, and T. Dittrich, Phys. Rev. Lett. **87**, 070601 (2001).

[29] H. Schanz, T. Dittrich, and R. Ketzmerick, Phys. Rev. E **71**, 026228 (2005).

[30] T. Wulf, C. Petri, B. Liebchen, and P. Schmelcher, Phys. Rev. E **86**, 016201 (2012).

[31] B. Liebchen, F. K. Diakonos, and P. Schmelcher, New J. Phys. **14**, 103032 (2012).

[32] A. K. Mukhopadhyay, B. Liebchen, T. Wulf, and P. Schmelcher, Phys. Rev. E **93**, 052219 (2016).

[33] A. V. Arzola, M. Villasante-Barahona, K. Volke-Sepúlveda, P. Jákl, and P. Zemánek, Phys. Rev. Lett. **118**, 138002 (2017).

[34] A. K. Mukhopadhyay, B. Liebchen, and P. Schmelcher, Phys. Rev. Lett. **120**, 218002 (2018).

[35] C. Reichhardt and C. J. O. Reichhardt, Phys. Rev. E **68**, 046102 (2003).

[36] C. Scholz, S. Jahanshahi, A. Ldov, and H. Löwen, Nat. Commun. **9**, 5156 (2018).

[37] J. M. Sancho, Phys. Rev. E **92**, 062110 (2015).

[38] O. Bénichou, P. Illien, G. Oshanin, A. Sarracino, and R. Voituriez, J. Phys.: Condens. Matter **30**, 443001 (2018).

[39] Y. Shi, S. Xiong, L. K. Chin, J. Zhang, W. Ser, J. Wu, T. Chen, Z. Yang, Y. Hao, B. Liedberg, P. H. Yap, D. P. Tsai, C. W. Qiu, and A. Q. Liu, Sci. Adv. **4**, 0773 (2018).

[40] S. Denisov, Y. Zolotaryuk, S. Flach, and O. Yevtushenko, Phys. Rev. Lett. **100**, 224102 (2008).

[41] F. Nogrette, H. Labuhn, S. Ravets, D. Barredo, L. Béguin, A. Vernier, T. Lahaye, and A. Browaeys, Phys. Rev. X **4**, 021034 (2014).

[42] H. Kim, W. Lee, H. G. Lee, H. Jo, Y. Song, and J. Ahn, Nat. Commun. **7**, 13317 (2016).

[43] D. Barredo, S. de Léséleuc, V. Lienhard, T. Lahaye, and A. Browaeys, Science **354**, 1021 (2016).

[44] D. Stuart and A. Kuhn, New J. Phys. **20**, 023013 (2018).

[45] J. E. Curtis, B. A. Koss, and D. G. Grier, Opt. Commun. **207**, 169 (2002).

[46] M. Reicherter, S. Zwick, T. Haist, C. Kohler, H. Tiziani, and W. Osten, Appl. Opt. **45**, 888 (2006).

[47] P. M. P. Lanigan, I. Munro, E. J. Grace, D. R. Casey, J. Phillips, D. R. Klug, O. Ces, and M. A. A. Neil, Biomed. Opt. Express **3**, 1609 (2012).

[48] V. Lebedev and F. Renzoni, Phys. Rev. A **80**, 023422 (2009).

3.3 Freezing, accelerating and slowing directed currents in real time with superimposed driven lattices

Freezing, accelerating, and slowing directed currents in real time with superimposed driven lattices

Aritra K. Mukhopadhyay,[1,*] Benno Liebchen,[2,†] Thomas Wulf,[1,‡] and Peter Schmelcher[1,3,§]

[1]*Zentrum für Optische Quantentechnologien, Universität Hamburg, Luruper Chaussee 149, 22761 Hamburg, Germany*

[2]*SUPA, School of Physics and Astronomy, University of Edinburgh, Edinburgh EH9 3FD, United Kingdom*

[3]*The Hamburg Centre for Ultrafast Imaging, Universität Hamburg, Luruper Chaussee 149, 22761 Hamburg, Germany*

We provide a generic scheme offering real-time control of directed particle transport using superimposed driven lattices. This scheme allows one to accelerate, slow, and freeze the transport on demand by switching one of the lattices subsequently on and off. The underlying physical mechanism hinges on a systematic opening and closing of channels between transporting and nontransporting phase space structures upon switching and exploits cantori structures which generate memory effects in the population of these structures. Our results should allow for real-time control of cold thermal atomic ensembles in optical lattices but might also be useful as a design principle for targeted delivery of molecules or colloids in optical devices.

I. INTRODUCTION

Temporally driven lattice potentials have attracted considerable attention in recent years [1–8] as their experimental controllability allows for an insightful approach into the complex world of nonequilibrium physics. A phenomenon of particular interest in these systems is the ratchet effect. Here, the breaking of certain spatiotemporal symmetries of the system allows one to convert unbiased fluctuations into directed particle motion even in the absence of mean forces [9–12]. This can be seen as a working principle of a motor operating on smallest scales relevant to phenomena ranging from intracellular transport problems [13] and cancer cell metastasis [14] to the transport of colloidal particles [15,16] in optical lattices or vortices in Josephson junction arrays [17]. Novel ratchet experiments using atomic ensembles in ac-driven optical lattices [18,19] allow for an admirable controllability both in the ultracold quantum regime [1] and at microkelvin temperatures where a classical dynamics approach successfully describes experiments [3,20]. Naturally, in view of their widespread applications, the controllability of directed particle currents has been a focal point of research since the early days of ratchet physics. Here, owing to the absence of an obvious force bias, even the transport direction is sometimes difficult to predict and numerous cases of "current reversals" have been reported where the direction of the transport in the asymptotic time limit could be reversed by changing a control parameter even though the symmetries of the system remain unaffected [21–29]. A limitation of most of these schemes is that only the asymptotic transport direction can be controlled rather than allowing for real-time control of the current which would be certainly desirable in order to apply ratchets as nanomotors [6] and to problems like targeted drug delivery [30]. A recent exception is Ref. [22], which requires, however, dissipation and is restricted to "flipping" the directed current at fixed strength.

Here, we exemplify a generic route towards the real-time control of directed currents. This allows us not only to dynamically control both direction and strength of the transport, up to unusually high efficiencies, but also to freeze the transport velocity on demand. Using one nontransporting and symmetric oscillating lattice as a "substrate" for particles (Fig. 1, top), we subsequently switch a second oscillating lattice, called the "carrier" lattice, on and off. In particular, switching the carrier lattice on breaks the parity and time-reversal symmetries of our setup and induces a directed particle current (Fig. 1, middle) accelerating the transport in a direction which can be controlled by the phase difference between the carrier and the substrate lattice. Switching the carrier lattice off does not lead to a decay of the transport towards zero but "freezes" it at constant velocity (Fig. 1, bottom). This can be repeated many times and allows one to design transport in real time. As the underlying mechanism, we identify a systematic opening and closing of cantorus structures, acting as barriers between transporting and nontransporting phase space structures upon switching. Thereby, the time scale on which the current can be manipulated is set by the flux through the cantorus and we show that manipulations are, in fact, possible for up to $\sim 1 \times 10^5$ driving periods. Our scheme does not require noise, but is robust to it, and is designed for straightforward implementation with cold thermal atoms in superimposed driven optical lattices where state of the art technologies allow one to avoid interference terms between the two lattices. Here, our scheme can be applied to guide atomic ensembles through optical lattices on paths which can be designed in real time. The underlying working principle should be of more general relevance, for example, as a design principle for real-time controlled targeted delivery of molecules or colloids in optical lattices or, possibly, also on other vibrated substrates.

II. SETUP

We consider noninteracting classical particles of mass m located at position x and having momentum p, described by a single-particle Hamiltonian $H(x,p,t) = \frac{p^2}{2m} + V(x,t)$, in a periodic potential $V(x,t) = V_S(x,t) + V_C(x,t)$. Here, V_S

---

*aritra.mukhopadhyay@physnet.uni-hamburg.de

†benno.liebchen@ed.ac.uk

‡thomas.wulf@physnet.uni-hamburg.de

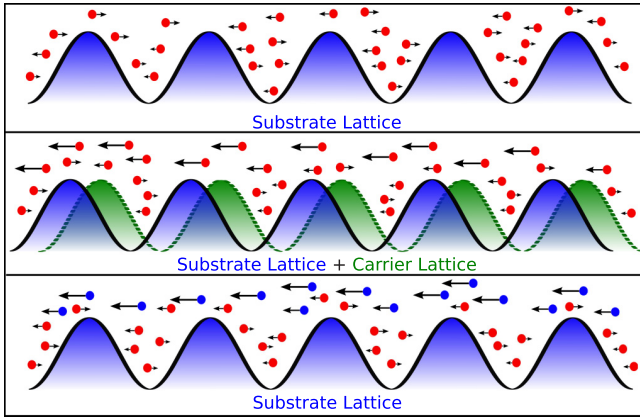§peter.schmelcher@physnet.uni-hamburg.de

FIG. 1. Schematic diagram of the setup and real-time control of directed transport. Top: Nontransporting state in the oscillating substrate lattice. Middle: Directed transport after switching on the carrier lattice. Bottom: Persistent transport after switching off the carrier lattice. Red particles perform diffusive motion whereas the blue ones are ballistic. The length and direction of the arrow indicate the speed and direction of the particle, respectively.

represents the substrate lattice and V_C the carrier lattice with

$$V_S(x,t) = V_S \cos^2\{k[x + d\cos(\omega t)]\}$$
$$V_C(x,t) = V_C \cos^2\{k[x + 2d\cos(2\omega t + \phi)] + \delta\}. \quad (1)$$

Both lattices have identical wave number k, but the oscillation amplitude d and frequency ω of the carrier lattice are twice as large as those for the substrate, which leads to spatial and temporal periodicities of $L = 2\pi/k$ and $T = 2\pi/\omega$ of H. Clearly, after averaging over time and space, this system is force free and hence unbiased. Our Hamiltonian may describe, for example, cold atoms in the classical regime of microkelvin temperatures [3,20] exposed to two counterpropagating laser beams of perpendicular polarization, preventing the occurrence of interference terms in Eq. (1). The lateral oscillation of both lattices can be achieved by phase modulating both laser beams using standard techniques like acousto-optical modulators and radio frequency generators (see, e.g., Refs. [18,31]).

To identify the relevant control parameters we introduce dimensionless variables $x' = 2kx$ and $t' = \omega t$. Using $\mu = \frac{m\omega^2}{2V_S k^2}$, $\nu = 2kd$, and $\gamma_V = \frac{V_C}{V_S}$, we get the equation of motion

$$\mu\ddot{x} = \sin(x + \nu\cos t) + \gamma_V \sin[x + 2\nu\cos(2t + \phi) + \delta], \quad (2)$$

where we omitted the primes on t' and x'.

III. RATCHET TRANSPORT AND LATTICE SWITCHES

In order to explore the transport properties of our setup, we propagate $N = 2\times10^4$ particles up to $t_{tot} = 4\times10^5 T$ by numerical integration of Eq. (2) using a Runge-Kutta Dormand-Prince integrator [32]. The initial velocities of the particles are chosen randomly within the low velocity regime such that their initial kinetic energies are small compared to the potential height of both the lattices. In this section, we present the main results and we discuss the underlying physical mechanisms in the following sections.
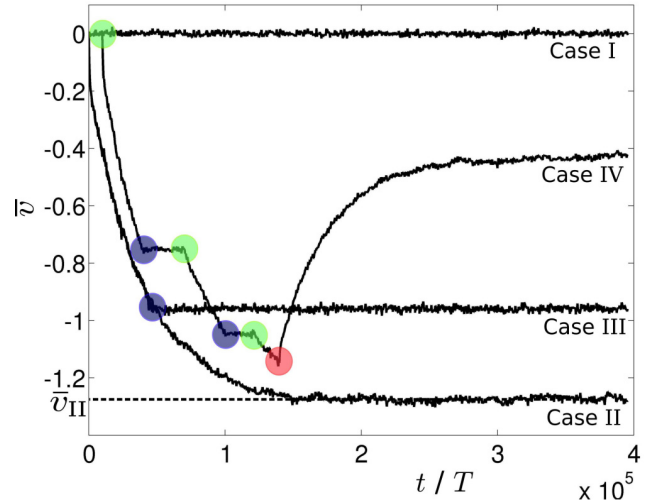

FIG. 2. Mean transport velocity $\bar{v}$ of a particle ensemble as a function of time for four different cases. Case I: in presence of only substrate lattice ($\gamma_V = 0$). Case II: in presence of both substrate and superimposed carrier lattice $\gamma_V = 1$. Case III: in presence of both lattices but carrier lattice switched off at $t = 0.11t_{tot}$ (blue dot) ($\gamma_V = 1$). Case IV: subsequent switches of the carrier lattice; blue dots show times ($t = 0.10t_{tot}$ and $t = 0.25t_{tot}$) where the carrier lattice is switched off, and green dots when it is switched on ($t = 0.025t_{tot}$, $t = 0.175t_{tot}$, and $t = 0.30t_{tot}$). At the final switch (red dot, $t = 0.35t_{tot}$), we switched also the relative driving phase ϕ from $\phi = \pi/2$ to $\phi = -\pi/2$. Remaining parameters: $\mu = 1.2665$, $\nu = \pi$, $\delta = \pi/2$, and $\phi = \pi/2$.

In the case of only the substrate lattice being present, we do not observe directed transport (case I in Fig. 2). This is to be expected, because the corresponding equation of motion [Eq. (2) with $\gamma_V = 0$] is invariant under time reversal, $t \to -t$, thus preventing directed particle motion in unbiased systems [11]. Applying the carrier lattice additionally [$\gamma_V = 1$ in Eq. (2)] and choosing appropriate "phase shifts" to the substrate ($\phi \neq 0, \pi$ and $\delta \neq 0, \pi$) allows one to break both time reversal and parity symmetry which leads indeed to directed transport (case II in Fig. 2). This transport slowly accelerates and finally saturates at $\bar{v}_{II} \simeq -1.25$ which is comparable to the spread of the velocity distribution of the particles. This constitutes an unusually high efficiency for a Hamiltonian ratchet, where the mean drift velocity is typically one or two orders of magnitude less than the standard deviation of the particle velocity distribution. We now consider the same situation, but switch off the carrier lattice, instantaneously, at $t = 0.11t_{tot}$ (blue dot; case III in Fig. 2). Interestingly, after switching off the carrier lattice the transport persists. Rather than decaying back towards zero, as one might expect for a symmetric setup, it does not decay but is frozen at its value at the time of the switch. That is, our atomic ensemble travels with constant average speed through the symmetrically oscillating lattice. Remarkably, this allows for an intriguingly simple real-time control of the transport velocity: Once the desired transport is achieved, one simply needs to switch off the carrier lattice.

We now consider a similar case, but switch the carrier lattice subsequently on and off (case IV in Fig. 2). Once the transport has been frozen for a while we can accelerate it by switching

on the carrier lattice again (second green dot on case IV curve). Switching it off, for a second time (second blue dot), freezes also this enhanced transport at a constant strength. Clearly, to achieve a highly flexible real-time control of the transport it would be desirable to be able to slow it down. This can in fact be achieved by switching on the carrier lattice again, but this time with a phase difference of $\phi = -\pi/2$ to the substrate (red dot). We see in Fig. 2 that this indeed slows the transport systematically down. Overall, we demonstrated a remarkably simple protocol allowing one to enhance, freeze, or slow the transport of atomic ensembles in two optical lattices on demand.

IV. DISCUSSIONS

A. Phase space analysis

It turns out that the physical mechanism underlying the real-time control of directed currents we just demonstrated crucially hinges on the mixed phase space structure of our two lattice system. Hence, to understand it we perform a systematic analysis of its microscopic composition and analyze its dynamical occupation by the considered particle ensemble. First, to understand the structure of the phase space itself, we take "stroboscopic" snapshots of particles with different initial conditions leading to Poincaré surfaces of sections (PSOS) which provide a representative overview of the structure of the complete three-dimensional (3D) phase space [33]. We also exploit the spatial periodicity of our setup and project the particle position back to the first unit cell $x \in [0, L)$ of the lattice. The PSOS of the substrate lattice (henceforth referred to as P1) is symmetric about $v = 0$ [Fig. 3(a), black dots] and contains a large central "chaotic sea" $\mathcal{C}_C^1$ between $v \simeq \pm 1.6$. On top of the PSOS, we show the snapshot of the particle coordinates, at a given time, used to determine $\bar{v}$ in case I of Fig. 2 [green dots in Fig. 3(a)], illustrating the uniform symmetric chaotic diffusion of particles through the lattice resulting in no transport. The chaotic sea is bounded by the first invariant spanning curves [FISCs; red lines in Fig. 3(a)], which prevents acceleration of our low velocity initial conditions beyond $|v| > 1.6$. Contrarily, a particle with initial condition on one of the regular invariant curves at $|v| \gtrsim 1.6$ [black lines in Fig. 3(a)] shows ballistic unidirectional motion through the lattice.

Let us now explore how the phase space structure changes in the presence of the carrier lattice. Most prominently, the two-lattice PSOS [black dots in Fig. 3(b)], henceforth referred to as P2, is not mirror symmetric about the $v = 0$ axis. Besides the chaotic sea $\mathcal{C}_C^2$ at small velocities, it exhibits two additional chaotic layers at higher velocities: the upper layer $\mathcal{C}_U^2$ at $v \gtrsim 2.2$ and the lower layer $\mathcal{C}_L^2$ at $v \lesssim -2.2$. The crucial point now is that the choice of an appropriate value for γ_V allows one to connect $\mathcal{C}_C^2$, asymmetrically, only with $\mathcal{C}_L^2$ through a "cantorus" structure [red dashed line in Fig. 3(b)], which is a hierarchical chain of stable and unstable fixed points, while it remains separated from $\mathcal{C}_U^2$ by a regular invariant curve [red solid line in Fig. 3(b)]. This allows particles to enter $\mathcal{C}_L^2$ but not $\mathcal{C}_U^2$. This can be easily seen from the fixed time snapshot of the particle distribution onto P2 corresponding to case III denoted by the green dots in Fig. 3(b). These particles in $\mathcal{C}_L^2$ still move irregularly but now only in one direction through the lattice, which is the origin of the transport we observed in Fig. 2. The fact that the transport velocity does not quickly
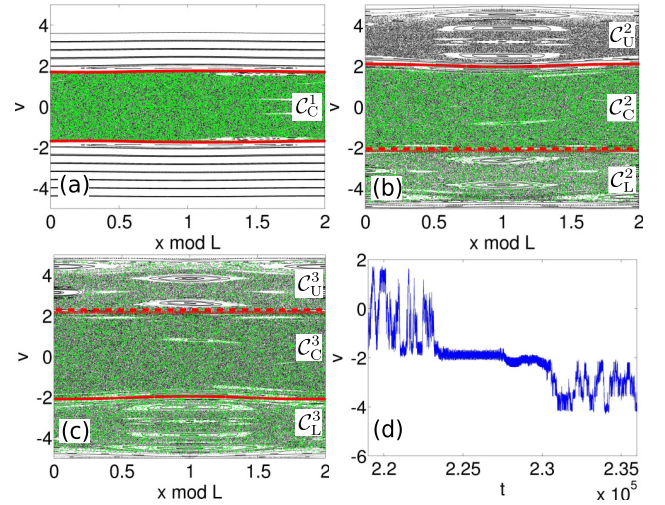

FIG. 3. The position (mod L) and velocity of all the N particles (green) at (a) $t = 0.04 t_{\text{tot}}$ in case I superposed on the PSOS P1 (black dots and lines) of the substrate lattice, (b) $t = 0.42 t_{\text{tot}}$ in case III superposed on the PSOS P2 (black dots) corresponding to both the substrate and the carrier lattices, and (c) $t = 0.95 t_{\text{tot}}$ in case IV superposed on the PSOS P3 (black dots) corresponding to both lattices but with $\phi = -\frac{\pi}{2}$. Red solid lines denote the position of the FISCs whereas the red dashed lines indicate the location of the cantorus (see text). $\mathcal{C}_{U,C,L}^i$, $i = 1, 2, 3$, denotes the upper, central, and lower chaotic layer of P1, P2, and P3, respectively. (d) A zoom into the typical trajectory of a particle initiated at low velocity in the central chaotic sea of the PSOS P2 in (b), showing the particle's stickiness to the cantorus.

converge to a constant velocity, but accelerates very slowly, on time scales of 1×10^5 driving periods towards its asymptotic value (case II in Fig. 2) is owed to the cantorus linking $\mathcal{C}_C^2$ and $\mathcal{C}_L^2$, which effectively acts as a semipermeable barrier to the particles approaching it and slows down the uniform filling of the accessible parts of the phase space.

B. Conversion between diffusive and ballistic motion

To understand how switching the carrier lattice subsequently on and off allows one to freeze, accelerate, and revert the directed transport, we now analyze the impact of lattice switches on the population of phase space structures [green dots in Figs. 3(a)–3(c)].

In Fig. 2, case III, when we froze the directed transport by switching off the carrier lattice, the phase space changed suddenly from P2 to P1. The crucial observation is now that particles located in $\mathcal{C}_L^2$ and some regions of $\mathcal{C}_C^2$ of P2 at the instant of the lattice switch [green dots below $v \sim -1.6$ in Fig. 3(b)] are located in the regular domain of spanning curves in P1 [see Fig. 3(a)] after the switch. As usual, particles which are located on regular spanning curves after the switch [black lines in Fig. 3(a)] are confined to these structures and travel with almost constant velocity through the lattice. Hence, also the ensemble averaged velocity, i.e., the directed transport, remains approximately constant or "frozen," which explains our observation in Fig. 2, case III (the particles in the chaotic sea $\mathcal{C}_C^1$ of P1 do not contribute to the transport as P1 is symmetric around $v = 0$). In conclusion, the instantaneous

switch of the dynamical system has caused a conversion from diffusive to regular motion for some particles, which is reminiscent of the conversion processes between regular and ballistic dynamics observed in driven superlattices [34,35].

It is now straightforward to see how switching the carrier lattice for a second time (case IV in Fig. 2) accelerates the transport again. This switch suddenly changes the underlying phase space from P1 to P2 and connects, again, $\mathcal{C}_C^2$ with $\mathcal{C}_L^2$. Hence, since the particle density in $\mathcal{C}_C^2$ is (still) higher than the density in $\mathcal{C}_L^2$ [Fig. 3(b)], particles continue penetrating through the cantorus into $\mathcal{C}_L^2$ which stops only for a uniform particle distribution over the entire chaotic sea. Furthermore, there is now a natural way to slow down the transport. Choosing an inverse phase difference of $\phi = -\pi/2$ (instead of $+\pi/2$) mirrors P2 around $v = 0$ and the particles now slowly redistribute from the central chaotic layer $\mathcal{C}_C^3$ into the upper chaotic layer $\mathcal{C}_U^3$ as shown in the PSOS P3 [black dots in Fig. 3(c)]. This creates a "counterweight" to the particles in $\mathcal{C}_L^3$ which slowly, but continuously, grows [for a snapshot see green dots in Fig. 3(c)], which explains the observed decrease of the directed transport.

How long can we proceed to accelerate, slow down, and revert the transport? The time scale is set by the uniform filling of the entire chaotic sea of P2. This limiting time scale depends crucially on the flux through the cantorus which in turn can be tuned by varying the relative strengths of both lattices, i.e., by changing γ_V. For $\gamma_V = 1$ (the value we used), at about $t \sim 4 \times 10^5 T$ the entire chaotic sea of the two-lattice setup (lower, central, and upper sea) is uniformly filled with particles. At this point, no further modulation of the transport is possible within our scheme.

V. EXPERIMENTAL REALIZATIONS

We believe that our dynamical control of directed currents can be realized in experimental setups using cold atoms in driven optical lattices where the periodic potential is generated by counterpropagating laser beams of perpendicular polarization [12,18,20,31]. The resulting lattice can be driven by phase modulation using acousto-optical modulators and radio frequency generators which also allow one to keep both lattices in phase and to implement a driving amplitude on length scales of the order of L [12,20]. Translating our parameters to experimentally relevant quantities for rubidium atoms, we obtain $V_S = V_C \sim 20 E_r$, $\omega \sim 10 \omega_r$, and the product $dk \sim \frac{\pi}{2}$, where E_r and ω_r are the recoil energy and recoil frequency of the atom, respectively. These experiments operate in the demonstrated classical regime of microkelvin temperature [20]. Even for colder temperatures, in the semiclassical regime, we expect tunneling through cantori [5], which should not alter our control scheme in general but only reduce the operational timescale. We note that our scheme can be refreshed by employing Sisyphus cooling, which can be used to localize our particle ensemble in the

central chaotic sea again. Notably in these experiments many particle effects are not important, but one can in principle tune parameters to probe the impact of weak interaction effects [36]. This can have important consequences for the transport [37], but it affects the particle distribution in phase space only on long time scales [37] and should therefore leave our scheme unaffected. In contrast to Brownian ratchets, our mechanism does not depend on noise and we explicitly checked that it is robust to noise of strengths in the regime typical for cold atom ratchet experiments [38]. Stronger noise would enhance the particle flux through the cantori and other regular structures, significantly decreasing both the maximally achievable transport velocity and the operational time scale of our scheme. Also, the thermal broadening of the atomic beam momentum distribution in this microkelvin temperature regime is small compared to the width of the central chaotic sea and thus would not contribute to the particle flux, hence keeping the efficiency of our scheme unaffected.

Another possible realization is provided by using a superconducting quantum interference device (SQUID) setup with Josephson junctions as in Ref. [39] operating in the underdamped classical regime of temperatures ~ 1 K (in which damping, noise, as well as quantum effects can be neglected safely) with a time dependent biharmonic external flux. Since this underdamped classical regime has already been realized experimentally, we believe that realizing our scheme using such setup is possible [40–43]. Finally, we note that our control scheme is not restricted to two-lattice systems but could be applied also to other Hamiltonian systems having mixed phase spaces and offering chaotic layers which can be systematically connected and disconnected.

VI. CONCLUSIONS

We provide a scheme offering the real-time control of directed currents in superimposed driven lattices. It can be straightforwardly implemented in ac-driven optical lattices and allows one to design directed currents of cold thermal atomic ensembles which can be consecutively accelerated, slowed, and reverted on demand. The mechanism underlying our scheme operates in phase space and depends only on large scale structures like the presence of different chaotic layers and cantori structures and should therefore be applicable more generally, e.g., as a design principle for targeted delivery of molecules or colloids in optical devices, or possibly on other vibrating substrates.

[1] T. Salger, S. Kling, T. Hecking, C. Geckeler, L. Morales-Molina, and M. Weitz, Science **326**, 1241 (2009).

[2] S. Denisov, S. Flach, and P. Hänggi, Europhys. Lett. **74**, 588 (2006).

[3] M. Brown and F. Renzoni, Phys. Rev. A **77**, 033405 (2008).

[4] R. Gommers, V. Lebedev, M. Brown, and F. Renzoni, Phys. Rev. Lett. **100**, 040603 (2008).

[5] P. Reimann, Phys. Rep. **361**, 57 (2002).

[6] P. Hänggi and F. Marchesoni, Rev. Mod. Phys. **81**, 387 (2009).

[7] T. Dittrich and F. L. Dubeibe, Phys. Rev. Lett. **114**, 094101 (2015).

[8] D. Cubero and F. Renzoni, Phys. Rev. Lett. **116**, 010602 (2016).

[9] S. Denisov, S. Flach, and P. Hänggi, Phys. Rep. **538**, 77 (2014).

[10] S. Denisov, Y. Zolotaryuk, S. Flach, and O. Yevtushenko, Phys. Rev. Lett. **100**, 224102 (2008).

[11] S. Flach, O. Yevtushenko, and Y. Zolotaryuk, Phys. Rev. Lett. **84**, 2358 (2000).

[12] R. Gommers, S. Bergamini, and F. Renzoni, Phys. Rev. Lett. **95**, 073003 (2005).

[13] F. Jülicher, A. Ajdari, and J. Prost, Rev. Mod. Phys. **69**, 1269 (1997).

[14] G. Mahmud, C. Campbell, K. Bishop, Y. Komarova, O. Chaga, S. Soh, S. Huda, K. Kandere-Grzybowska, and B. A. Grzybowski, Nat. Phys. **5**, 606 (2009).

[15] L. P. Faucheux, L. S. Bourdieu, P. D. Kaplan, and A. J. Libchaber, Phys. Rev. Lett. **74**, 1504 (1995).

[16] J. Rousselet, L. Salome, A. Ajdari, and J. Prost, Nature (London) **370**, 446 (1994).

[17] J. B. Majer, J. Peguiron, M. Grifoni, M. Tusveld, and J. E. Mooij, Phys. Rev. Lett. **90**, 056802 (2003).

[18] M. Schiavoni, L. Sanchez-Palencia, F. Renzoni, and G. Grynberg, Phys. Rev. Lett. **90**, 094101 (2003).

[19] V. Lebedev and F. Renzoni, Phys. Rev. A **80**, 023422 (2009).

[20] F. Renzoni, *Driven Ratchets in Cold Atoms* (Elsevier, Amsterdam, 2009).

[21] B. Dandogbessi, O. Akin-Ojo, and A. Kenfack, Phys. Scr. **90**, 055206 (2015).

[22] A. V. Arzola, K. Volke-Sepúlveda, and J. L. Mateos, Phys. Rev. Lett. **106**, 168104 (2011).

[23] S. Denisov, L. Morales-Molina, S. Flach, and P. Hänggi, Phys. Rev. A **75**, 063424 (2007).

[24] M. Schreier, P. Reimann, P. Hänggi, and E. Pollak, Europhys. Lett. **44**, 416 (1998).

[25] C. de Souza Silva, J. Van de Vondel, M. Morelle, and V. Moshchalkov, Nature (London) **440**, 651 (2006).

[26] V. I. Marconi, Phys. Rev. Lett. **98**, 047006 (2007).

[27] J. Spiechowicz and J. Łuczka, New J. Phys. **17**, 023054 (2015).

[28] D. Cubero and F. Renzoni, Phys. Rev. E **86**, 056201 (2012).

[29] B. Liebchen, F. Diakonos, and P. Schmelcher, New J. Phys. **14**, 103032 (2012).

[30] P. Hoffmann, *Life's Ratchet: How Molecular Machines Extract Order from Chaos* (Basic Books, New York, 2012).

[31] A. Wickenbrock, P. C. Holz, N. A. Abdul Wahab, P. Phoonthong, D. Cubero, and F. Renzoni, Phys. Rev. Lett. **108**, 020603 (2012).

[32] J. R. Dormand and P. J. Prince, J. Comput. Appl. Math. **6**, 19 (1980).

[33] M. Tabor, *Chaos and Integrability in Nonlinear Dynamics: An Introduction* (Wiley, New York, 1989).

[34] T. Wulf, C. Petri, B. Liebchen, and P. Schmelcher, Phys. Rev. E **86**, 016201 (2012).

[35] C. Petri, F. Lenz, B. Liebchen, F. Diakonos, and P. Schmelcher, Europhys. Lett. **95**, 30005 (2011).

[36] C. Chin, R. Grimm, P. Julienne, and E. Tiesinga, Rev. Mod. Phys. **82**, 1225 (2010).

[37] B. Liebchen and P. Schmelcher, New J. Phys. **17**, 083011 (2015).

[38] D. Cubero, V. Lebedev, and F. Renzoni, Phys. Rev. E **82**, 041116 (2010).

[39] J. Spiechowicz, P. Hänggi, and J. Łuczka, Phys. Rev. B **90**, 054520 (2014).

[40] J. M. Kivioja, T. E. Nieminen, J. Claudon, O. Buisson, F. W. J. Hekking, and J. P. Pekola, Phys. Rev. Lett. **94**, 247002 (2005).

[41] P. Silvestrini, O. Liengme, and K. E. Gray, Phys. Rev. B **37**, 1525 (1988).

[42] P. Silvestrini, V. G. Palmieri, B. Ruggiero, and M. Russo, Phys. Rev. Lett. **79**, 3046 (1997).

[43] B. Ruggiero, C. Granata, E. Esposito, M. Russo, and P. Silvestrini, Appl. Phys. Lett. **75**, 121 (1999).

3.4 Dimensional coupling-induced current reversal in two-dimensional driven lattices

Dimensional coupling-induced current reversal in two-dimensional driven lattices

Aritra K. Mukhopadhyay,[1,*] Tianting Xie,[1,2,†] Benno Liebchen,[3,4,‡] and Peter Schmelcher[1,5,§]

[1]*Zentrum für Optische Quantentechnologien, Universität Hamburg, Luruper Chaussee 149, 22761 Hamburg, Germany*
[2]*College of Mathematics, Sichuan University, Chengdu 610065, China*
[3]*SUPA, School of Physics and Astronomy, University of Edinburgh, Peter Guthrie Tait Road, Edinburgh, EH9 3FD, United Kingdom*
[4]*Institute for Theoretical Physics II: Soft Matter, Heinrich-Heine Universität Düsseldorf, Universitätsstrasse 1, 40225 Düsseldorf, Germany*
[5]*The Hamburg Centre for Ultrafast Imaging, Universität Hamburg, Luruper Chaussee 149, 22761 Hamburg, Germany*

We show that the direction of directed particle transport in a two-dimensional ac-driven lattice can be dynamically reversed by changing the structure of the lattice in the direction perpendicular to the applied driving force. These structural changes introduce dimensional coupling effects, the strength of which governs the timescale of the current reversals. The underlying mechanism is based on the fact that dimensional coupling allows the particles to explore regions of phase space which are inaccessible otherwise. The experimental realization for cold atoms in ac-driven optical lattices is discussed.

I. INTRODUCTION

The ratchet effect allows one to create a directed particle transport in an unbiased nonequilibrium environment and thus to extract mechanical work from a fluctuating bath [1–3]. Such a conversion is impossible for macroscopic equilibrium systems and makes the ratchet effect a fundamental nonequilibrium phenomenon. While originally conceived as proof-of-principle examples of rectification schemes producing work from fluctuations [4–7] and as possible explanations for the mechanism allowing molecular motors to show directed motion along cytoskeleton filaments [8,9], ratchets now form a widespread paradigm with a large realm of applications in atomic, condensed matter, and biophysics.

Specific applications range from the rectification of atomic [10], colloidal [11], and bacterial motion [12–15] to the transportation of fluxons in Josephson junction arrays [16,17] and vortices in conformal crystal arrays [18,19]. Very recently, it has been demonstrated that ratchets also allow one to control the dynamics of topological solitons in ionic crystals [20], enhance photocurrents in quantum wells [21], can rectify the chirality of magnetization in artificial spin ice [22], and create a light modulated electron transport across organic bulk heterojunctions [23].

While the fact that a specific setup creates a directed particle transport can typically be predicted based on symmetry properties [24,25], the strength and even the direction of the emerging currents are far less immediate. In fact, the current direction can often be reverted by changing the value of a certain control parameter or the properties of the rectified objects (e.g., their mass or mobility), without changing the

symmetry of the underlying equations. Achieving such current reversals is the key aim of many investigations, as they allow segregation of particle mixtures by transporting particles of, e.g., different mass or mobility in opposite directions, where they can be collected.

While most ratchets are still studied in one spatial dimension (1D) [3,26], particularly those operating in the Hamiltonian regime [24,25,27–30], recent experiments have significantly progressed regarding the construction of highly controllable two-dimensional (2D) ratchet devices. These include cold atoms in ac-driven optical lattices [31–33] and the very recent example of a fully configurable 2D ratchet based on colloids in holographic optical tweezers [34]. Conceptually, the key new ingredient in 2D ratchets is the coupling between the dimensions, which has been shown to allow, in the overdamped regime, for a directed transport at an angle relative to the driving law [34,35] and may also involve transportation completely orthogonal to the driving [36]. In the present work, we demonstrate that dimensional coupling can even lead to current reversals.

A 2D potential landscape having a periodic potential along, e.g., the x direction but without any potential variation along the perpendicular y direction (henceforth referred to as "quasi-1D lattice") allows for directed particle transport when driven by an appropriately chosen ac-driving force in the x direction [see Fig. 1(a), upper panel]. Keeping the driving unchanged but performing a structural change of the lattice along the y direction introduces dimensional coupling effects. We show that this coupling does not affect the directed particle current for short timescales, but reverts its direction at longer timescales as compared to the quasi-1D lattice [see Fig. 1(a), lower panel]. These dimensional coupling-induced current reversals (DCIR) occur dynamically in time [30], as opposed to the standard scenario of asymptotic current reversals due to a change of system parameter where the direction of current is time independent [37–39]. We show that the reversal timescale can be varied by thousands of driving periods by varying the

───────────

*Aritra.Mukhopadhyay@physnet.uni-hamburg.de
†xietianting@hotmail.com
‡liebchen@hhu.de
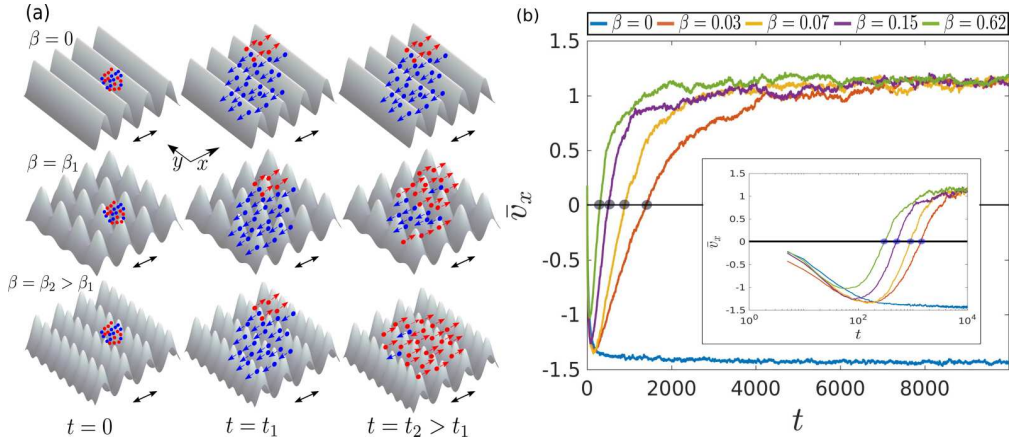§Peter.Schmelcher@physnet.uni-hamburg.de

FIG. 1. (a) Schematic diagram of the setup demonstrating the phenomenon of dimensional coupling-induced current reversal. The filled dots denote particles and the colors (red/blue) indicate the sign of the x component of their velocities (right/left). In a driven quasi-1D lattice (upper panel), most particles travel in the negative x direction resulting in an average transport in this direction. However, in the driven 2D lattice (middle and lower panels) having nonzero dimensional coupling β, most particles initially travel toward the negative x direction but at later times revert their movement, resulting in a dynamical current reversal. Larger values of the coupling β reduces the timescale of the current reversal (lower panel). (b) Mean transport velocity of the ensemble along the x direction as a function of time for different values of β for a linear and logarithmic (inset) timescale. The gray circles correspond to the reversal timescales $t_{r,\beta}$ for different values of β. Remaining parameters: $U = 0.88$, $a = 0.48$, $\alpha = 9.61$, and $\gamma = 0.62$. There is no directed transport of particles along the y direction.

structure of the lattice perpendicular to the driving direction [see Fig. 1(a), middle panel]. The underlying mechanism of these current reversals uses the fact that changing the structure of the lattice along the second dimension allows the particles to explore different regions of phase space which are inaccessible in the quasi-1D lattice.

II. SETUP

We consider N noninteracting classical particles in a 2D lattice of elliptic Gaussian barriers laterally driven along the x direction via an external biharmonic driving force $f(t) = d_x[\sin \omega t + 0.25 \sin(2\omega t + \pi/2)]$. Here, d_x and ω are the amplitude and the frequency of the driving, thereby introducing a temporal periodicity of $T = 2\pi/\omega$. The system is described by the Hamiltonian:

$$H = \frac{p_x^2}{2m} + \frac{p_y^2}{2m} + \sum_{i,j=-\infty}^{+\infty} V e^{-\{\beta_x[x-f(t)-(i+\frac{1}{2})L_x]^2 + \beta_y[y-(j+\frac{1}{2})L_y]^2\}}, \quad (1)$$

where the potential barriers have a height V and the equilibrium distances between them along x and y are given by L_x and L_y, respectively. This potential breaks both the parity $x \rightarrow -x + \chi$ symmetry along the x direction and the time-reversal $t \rightarrow -t + \tau$ symmetry (for all possible constants χ and τ), while preserving parity symmetry along the y direction. Possible realizations of this setup include cold atoms in optical lattices, at microkelvin temperatures, where a classical description is appropriate [33] and which to a good approximation represents a Hamiltonian setup.

Introducing dimensionless variables $x' = \frac{x}{L_x}$, $y' = \frac{y}{L_y}$, and $t' = \omega t$ and dropping the primes for simplicity, the equation of motion for a single particle at position $\mathbf{r}$ with momentum $\mathbf{p}$ reads

$$\ddot{\mathbf{r}} = \sum_{m,n=-\infty}^{+\infty} \mathcal{U}[\mathbf{r} - F(t)\mathbf{e_x} - \mathbf{R}_{m,n}]e^{-\mathcal{G}[\mathbf{r}-F(t)\mathbf{e_x}-\mathbf{R}_{m,n}]}, \quad (2)$$

where $F(t) = [a \sin t + 0.25a \sin(2t + \pi/2), 0]$ is the effective driving law, $\mathbf{e_x} = (1,0)$, $\mathbf{R}_{m,n} = (m,n)$ denotes the positions of the maxima of the Gaussian barriers where $(m - \frac{1}{2}), (n - \frac{1}{2}) \in \mathbb{Z}$ and $\mathcal{U}(\mathbf{r}) = (Ux, \beta Uy)$, $\mathcal{G}(\mathbf{r}) = \alpha(x^2 + \gamma y^2)$. The parameter space of our system is therefore essentially five dimensional, where the dimensionless parameters are given by a reduced barrier height $U = \frac{2V\beta_x}{m\omega^2}$, an effective driving amplitude $a = \frac{d_x}{L_x}$, as well as the two parameters, $\alpha = \beta_x L_x^2$ and $\gamma = \frac{\beta_y L_y^2}{\beta_x L_x^2}$, characterizing the localization of the Gaussian barriers along the x and y directions. A final key control parameter is $\beta = \frac{\beta_y}{\beta_x}$ which measures the coupling between the two dimensions. The limits $\beta \rightarrow 0$ and $\beta \rightarrow \infty$ both correspond to quasi-one-dimensional lattices.

III. RESULTS

To explore the transport properties of our setup, we initialize $N = 10^4$ particles with small random velocities $v_x, v_y \in [-0.1, 0.1]$ such that their initial kinetic energies are small compared to the potential height of the lattice. In order to mimic a localized loading of particles into the lattice, we initialize the particles within the square regions $[-0.1, 0.1] \times [-0.1, 0.1]$ centered around the potential minima of the lattice. Subsequently, we time evolve our ensemble up to $t = 10^4$ by numerical integration of Eq. (2) using a Runge-Kutta Dormand Prince integrator.

For $\beta = 0$, the lattice is quasi-1D [upper panels in Fig. 1(a)] and produces a nonzero mean velocity pointing in the negative x direction [Fig. 1(b)]. This behavior is expected since the system breaks both the parity and time-reversal symmetry

along the x direction, thus satisfying the necessary criteria for a nonzero directed transport [24,27,28]. Since there is no driving in the y direction, the symmetries are preserved and hence there is no directed transport along this direction. The transport in the x direction accelerates until it finally saturates at $\bar{v}_x \simeq -1.4$.

We now vary β to explore the impact of dimensional coupling effects on the directed transport. As shown in Fig. 1(b), for $\beta = 0.03$, the early time transport velocity is negative and approaches a similar speed of $\bar{v}_x \simeq -1.35$, as in the quasi-1D case at around $t \simeq 1.5 \times 10^2$. Remarkably, thereafter the transport begins to slow down and vanishes at $t = t_{r,\beta=0.03} \simeq 1.5 \times 10^3$. Further on, it changes sign which leads to a current reversal. Finally, it approaches an asymptotic constant value of $\bar{v}_x \simeq 1.2$. Therefore, the structural change of the lattice in the direction orthogonal to the driving force reverts the transport direction.

To study this dimensionality-induced current reversal in more detail, we perform our simulations for a stronger dimensional coupling $\beta = 0.15$ and $\beta = 0.62$, which leads to a qualitatively similar behavior [see Fig. 1(b)]. However, we find that the timescale at which the reversal occurs strongly depends on the strength of the dimensional coupling coefficient β. Specifically for $\beta = 0.62$, we obtain $t_r \simeq 3 \times 10^2$ showing that the reversal timescale can be tuned by at least a factor of 5. We have performed longer simulations up to $t = 10^5$ and found that the transport velocity does not reverse again during this timescale.

IV. DISCUSSION

The underlying mechanism of the DCIR effect depends on two generic ingredients: (i) the existence of a mixed phase space (containing regular and at least two disconnected chaotic components) in the underlying quasi-1D lattice and (ii) the diffusional spreading dynamics in the 2D lattice along the orthogonal direction. We now discuss the occurrence of negative transport in the quasi-1D lattice ($\beta = 0$) and will then analyze how the dimensional coupling effect can revert the transport direction.

Due to the absence of forces acting along the y direction, the dynamics in the quasi-1D lattice [Fig. 1(a)] can be decomposed into a constant drift in the y direction and a motion in a 1D lattice driven along the x axis. The latter case is described by a three-dimensional (3D) phase space illustrated by taking stroboscopic snapshots of $x(t), v_x(t)$ at $t = n(n \in \mathbb{N})$ of particles with different initial conditions. This leads to Poincáre surfaces of section (PSOS) as shown in Fig. 2(a) where the reflection symmetry about $v_x = 0$ is broken. This PSOS is characterized by two prominent chaotic components or "seas": the upper sea $\mathcal{C}_U$ between $0.75 \lesssim v_x \lesssim 6.0$ and the lower sea $\mathcal{C}_L$ between $-3.5 \lesssim v_x \lesssim 0.2$. These chaotic seas are separated from each other by regular invariant spanning curves at $v_x \simeq 0.2$ preventing particles from traveling between the chaotic components. Hence, particles initialized with low initial energies $v_x \in [-0.1, 0.1]$ and occupying $\mathcal{C}_L$, matching the initial conditions used in our simulations, undergo chaotic diffusion through the lattice with negative velocities along the x direction until they are uniformly distributed over $\mathcal{C}_L$. As a result, we observe a negative directed transport of the
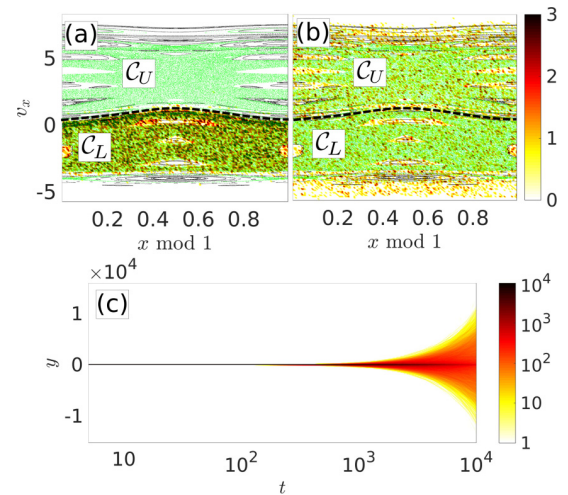

FIG. 2. The particle distribution as a function of position x mod 1 and v_x (in colormap) of all the $N = 10^4$ particles propagating in the 2D lattice with $\beta = 0.03$ superimposed on the PSOS of the quasi-1D driven lattice (regular islands in black and chaotic seas in green) at (a) $t = 50$ and (b) $t = 10^4$. The region of invariant spanning curves separating the two chaotic seas has been highlighted by the thick black dashed line. (c) The particle distribution as a function of y and t showing the spreading of the ensemble along the y direction with time.

ensemble. The magnitude of the transport velocity for the quasi-1D lattice can also be estimated using the "sum rule" involving the location and size of the regular islands embedded in $\mathcal{C}_L$ [27,28].

Let us now explore the mechanism allowing dimensional coupling ($\beta > 0$) to revert the transport direction: In this case, the phase space is five-dimensional (5D) characterized by (x, v_x, y, v_y, t) which complicates both the illustration and analysis of the transport based on the phase-space structures. However, up to a certain timescale, the dynamics of the particles even in this higher dimensional phase space can be effectively understood in terms of the dynamic occupation of the ensemble in the quasi-1D PSOS. To show this, we superpose the snapshots of the ensemble particle coordinates (x, v_x) for $\beta = 0.03$ on the quasi-1D PSOS at two different times $t = 50$ and $t = 10^4$ (Fig. 2). At $t = 50$, well before the reversal timescale $t_{r,\beta=0.03} = 1.5 \times 10^3$, the ensemble population is confined to $\mathcal{C}_L$ in a similar way as we have observed for $\beta = 0$ [Fig. 2(a)]. Physically, this results from the fact that at shorter timescales the particles experience comparatively strong driving forces which allow them to quickly move along the x direction while in the y direction they move only very slowly with a velocity largely dictated by the initial conditions. Therefore, for a long time, they stay close to the potential valleys at $y = 0$ [Fig. 2(c)] where they hardly experience the 2D landscape of the potential.

As time evolves, particles experience more and more of the 2D character of the potential which effectively transfers motion in the x direction into motion along the y direction leading to a symmetric spreading of the ensemble along the y direction [Fig. 2(c)]. Particles are therefore no longer dictated by the structure of the 3D phase space but can
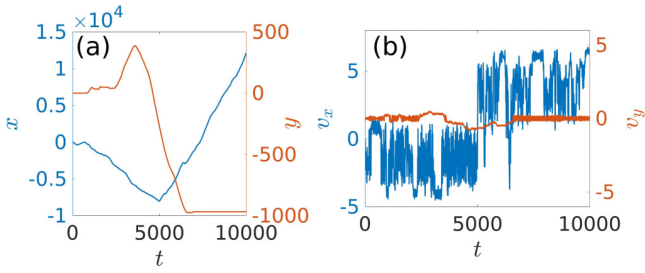
FIG. 3. The time dependence of (a) position and (b) velocity of a typical particle in the 2D lattice with $\beta = 0.03$ initialized in the lower chaotic sea $\mathcal{C}_L$ [Fig. 2(a)] demonstrating the crossover to the upper chaotic sea $\mathcal{C}_U$ [Fig. 2(b)]. Remaining parameters are the same as in Fig. 1(b). Note that for this particular trajectory, the crossover happens at $t \simeq 5 \times 10^3$, which is larger than the average reversal timescale $t_{r,\beta=0.03} = 1.5 \times 10^3$ of the ensemble.

FIG. 4. (a) The probability density $P(t)$ of the FCT t required by a particle to cross one lattice site along the y direction for the first time. (b) The mean FCT τ_β (in blue) and the reversal timescale $t_{r,\beta}$ (in red) as functions of β with corresponding inverse power-law fits. The inset shows the linear relationship between $t_{r,\beta}$ and τ_β.

explore the entire 5D phase space. They can, in particular, now freely cross the invariant spanning curves at $v_x \simeq 0.2$ of the 3D phase space to attain significant positive velocities [Fig. 2(b)]. During the phase of temporal evolution when the particles can cross the invariant curve, the directed current slows down and reduces to zero. It finally becomes positive, since the asymptotic average velocity of the particles along the positive x direction is higher than that along the negative x direction. A typical trajectory demonstrating the crossover from $\mathcal{C}_L$ to $\mathcal{C}_U$ is shown in Fig. 3. We checked that the current reversal and the underlying phase-space structures (especially the invariant spanning curves separating the chaotic layers) is robust against moderate variations of the setup parameters, hence no parameter fine-tuning is necessary to observe the phenomena.

V. CONTROL OF THE CURRENT REVERSAL

Let us finally discuss the dependence of the current reversal time $t_{r,\beta}$ on the parameter β. Following the above-outlined physical picture, the current reversal occurs at time scales comparable to the time a particle needs to experience a significant deviation from the neighborhood of the minimum of the lattice potential along the y direction. For a particular value of β and a given set of initial conditions, one can thus expect the reversal timescale $t_{r,\beta}$ to depend linearly on the average time τ_β the particles need to cross one lattice site along the y direction for the very first time. In order to estimate τ_β for different values of β, we simulate ensembles of 10^4 particles each with initial conditions identical to that used in our setup (Fig. 1), but for different β values and calculate the corresponding probability density $P(t)$ of the first crossing time (FCT) t required by a particle to cross one lattice site along the y direction [Fig. 4(a)]. As β increases, the particles are likely to have shorter FCT and hence can experience the 2D landscape of the potential much earlier. This can be clearly seen in Fig. 4(b) (blue) which shows that the mean FCT τ_β decreases with increasing β following a $\tau_\beta \sim \beta^{-0.6}$ power law. Confirming our expectation, a linear fit is shown to describe the relation between $t_{r,\beta}$ and τ_β to a good approximation [see Fig. 4(b) (inset)] and hence $t_{r,\beta}$ follows a similar inverse power law $t_{r,\beta} \sim \beta^{-0.55}$ [Fig. 4(b), red]. The reversal timescale depends also (weakly) on the initial
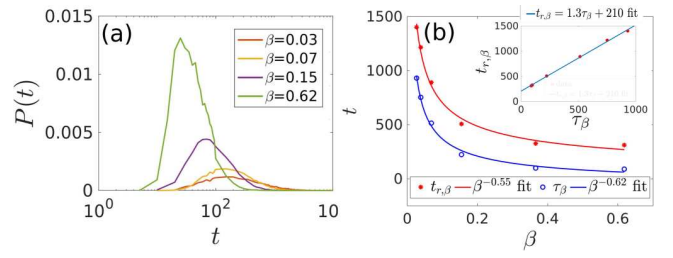
velocities of the particles and we verified that a decrease of the initial velocity by a factor of 0.01 increases the reversal timescale approximately by a factor of 1.34.

VI. EXPERIMENTAL REALIZATION

A setup to experimentally observe dimensional coupling-induced current reversals are cold atoms in optical lattices generated by laser beams in the regime of microkelvin temperatures where a classical description is appropriate [33]. Setups based on holographic trapping of atoms [40–43] might also provide an interesting and highly controllable alternative. The resulting lattice can be driven by phase modulation using acousto-optical modulators and radio-frequency generators. Translating our parameters to experimentally relevant quantities for an optical lattice setup with cold rubidium (Rb^{87}) atoms and 780 nm lasers, we obtain the lattice height $V \sim 22 E_r$, the width $\frac{1}{\sqrt{\beta_x}} \sim 252$ nm, the driving frequency $\omega \sim 10\omega_r$, and the driving amplitude $d_x \sim 390$ nm, where E_r and ω_r are the recoil energy and recoil frequency of the atom, respectively. Interaction, disorder, and noise effects would probably lead to a slow accumulation of particles within the regular portions of the phase space [30,44,45], which may also aid them in crossing the regular barrier confining the initial conditions in the quasi-2D case to negative and only weakly positive velocities and may therefore lead to a slight decrease of the reversal time.

VII. CONCLUDING REMARKS

Dimensional coupling effects in two-dimensional lattices create another route to produce current reversals. Conversely to most other cases, the current reversal occurs dynamically here with a characteristic timescale that can be controlled by the strength of the coupling. The underlying mechanism is generic, in the sense that it depends only on the mixed phase-space structure of the underlying uncoupled quasi-1D lattice and may therefore apply to a variety of physical systems. Possible future perspectives include an extensive characterization and visualization of the *four-dimensional* PSOS [46,47] in order to analyze the effect of the dimensional coupling on the underlying invariant manifolds and directed transport.

[1] P. Hänggi, F. Marchesoni, and F. Nori, Ann. Phys. (NY) **14**, 51 (2005).

[2] R. D. Astumian and P. Hänggi, Phys. Today **55**(11), 33 (2002).

[3] P. Hänggi and F. Marchesoni, Rev. Mod. Phys. **81**, 387 (2009).

[4] J. Prost, J.-F. Chauwin, L. Peliti, and A. Ajdari, Phys. Rev. Lett. **72**, 2652 (1994).

[5] M. O. Magnasco, Phys. Rev. Lett. **71**, 1477 (1993).

[6] R. Bartussek, P. Hänggi, and J. G. Kissner, Europhys. Lett. **28**, 459 (1994).

[7] L. P. Faucheux, L. S. Bourdieu, P. D. Kaplan, and A. J. Libchaber, Phys. Rev. Lett. **74**, 1504 (1995).

[8] R. D. Astumian, Science **276**, 917 (1997).

[9] F. Jülicher, A. Ajdari, and J. Prost, Rev. Mod. Phys. **69**, 1269 (1997).

[10] M. Schiavoni, L. Sanchez-Palencia, F. Renzoni, and G. Grynberg, Phys. Rev. Lett. **90**, 094101 (2003).

[11] J. Rousselet, L. Salome, A. Ajdari, and J. Prost, Nature (London) **370**, 446 (1994).

[12] R. Di Leonardo, L. Angelani, D. Dell'Arciprete, G. Ruocco, V. Iebba, S. Schippa, M. P. Conte, F. Mecarini, F. De Angelis, and E. Di Fabrizio, Proc. Natl. Acad. Sci. USA **107**, 9541 (2010).

[13] N. Koumakis, A. Lepore, C. Maggi, and R. Di Leonardo, Nat. Commun. **4**, 2588 (2013).

[14] C. J. O. Reichhardt and C. Reichhardt, Annu. Rev. Condens. Matter Phys. **8**, 51 (2017).

[15] G. Vizsnyiczai, G. Frangipane, C. Maggi, F. Saglimbeni, S. Bianchi, and R. Di Leonardo, Nat. Commun. **8**, 15974 (2017).

[16] F. Falo, P. J. Martínez, J. J. Mazo, and S. Cilla, Europhys. Lett. **45**, 700 (1999).

[17] Y. Zolotaryuk, Phys. Rev. E **86**, 026604 (2012).

[18] C. Reichhardt and C. J. Olson Reichhardt, Phys. Rev. B **93**, 064508 (2016).

[19] C. Reichhardt, D. Ray, and C. J. Olson Reichhardt, Phys. Rev. B **91**, 184502 (2015).

[20] J. Brox, P. Kiefer, M. Bujak, T. Schaetz, and H. Landa, Phys. Rev. Lett. **119**, 153602 (2017).

[21] P. Faltermeier, G. V. Budkin, J. Unverzagt, S. Hubmann, A. Pfaller, V. V. Bel'kov, L. E. Golub, E. L. Ivchenko, Z. Adamus, G. Karczewski, T. Wojtowicz, V. V. Popov, D. V. Fateev, D. A. Kozlov, D. Weiss, and S. D. Ganichev, Phys. Rev. B **95**, 155442 (2017).

[22] S. Gliga, G. Hrkac, C. Donnelly, J. Büchi, A. Kleibert, J. Cui, A. Farhan, E. Kirk, R. V. Chopdekar, Y. Masaki, N. S. Bingham, A. Scholl, R. L. Stamps, and L. J. Heyderman, Nat. Mater. **16**, 1106 (2017).

[23] O. Kedem, B. Lau, M. A. Ratner, and E. A. Weiss, Proc. Natl. Acad. Sci. USA **114**, 8698 (2017).

[24] S. Flach, O. Yevtushenko, and Y. Zolotaryuk, Phys. Rev. Lett. **84**, 2358 (2000).

[25] S. Denisov, S. Flach, and P. Hänggi, Phys. Rep. **538**, 77 (2014).

[26] P. Reimann, Phys. Rep. **361**, 57 (2002).

[27] H. Schanz, M.-F. Otto, R. Ketzmerick, and T. Dittrich, Phys. Rev. Lett. **87**, 070601 (2001).

[28] H. Schanz, T. Dittrich, and R. Ketzmerick, Phys. Rev. E **71**, 026228 (2005).

[29] T. Wulf, C. Petri, B. Liebchen, and P. Schmelcher, Phys. Rev. E **86**, 016201 (2012).

[30] B. Liebchen, F. K. Diakonos, and P. Schmelcher, New J. Phys. **14**, 103032 (2012).

[31] V. Lebedev and F. Renzoni, Phys. Rev. A **80**, 023422 (2009).

[32] D. Cubero and F. Renzoni, Phys. Rev. E **86**, 056201 (2012).

[33] F. Renzoni, *Advances in Atomic Molecular and Optical Physics* (Elsevier, New York, 2009), Vol. 57, pp. 1–32.

[34] A. V. Arzola, M. Villasante-Barahona, K. Volke-Sepúlveda, P. Jákl, and P. Zemánek, Phys. Rev. Lett. **118**, 138002 (2017).

[35] A. K. Mukhopadhyay, B. Liebchen, and P. Schmelcher, Phys. Rev. Lett. **120**, 218002 (2018).

[36] C. Reichhardt and C. J. Olson Reichhardt, Phys. Rev. E **68**, 046102 (2003).

[37] V. I. Marconi, Phys. Rev. Lett. **98**, 047006 (2007).

[38] J. L. Mateos, Phys. Rev. Lett. **84**, 258 (2000).

[39] C. C. de Souza Silva, J. Van de Vondel, M. Morelle, and V. V. Moshchalkov, Nature (London) **440**, 651 (2006).

[40] F. Nogrette, H. Labuhn, S. Ravets, D. Barredo, L. Béguin, A. Vernier, T. Lahaye, and A. Browaeys, Phys. Rev. X **4**, 021034 (2014).

[41] H. Kim, W. Lee, H.-g. Lee, H. Jo, Y. Song, and J. Ahn, Nat. Commun. **7**, 13317 (2016).

[42] D. Barredo, S. de Léséleuc, V. Lienhard, T. Lahaye, and A. Browaeys, Science **354**, 1021 (2016).

[43] D. Stuart and A. Kuhn, New J. Phys. **20**, 023013 (2018).

[44] B. Liebchen and P. Schmelcher, New J. Phys. **17**, 083011 (2015).

[45] T. Wulf, B. Liebchen, and P. Schmelcher, Phys. Rev. Lett. **112**, 034101 (2014).

[46] M. Richter, S. Lange, A. Bäcker, and R. Ketzmerick, Phys. Rev. E **89**, 022902 (2014).

[47] S. Lange, M. Richter, F. Onken, A. Bäcker, and R. Ketzmerick, Chaos **24**, 024409 (2014).

3.5 Multiple current reversals using superimposed driven lattices

Multiple Current Reversals Using Superimposed Driven Lattices

Aritra K. Mukhopadhyay [1] [ID] **and Peter Schmelcher** [1,2,*]

1 Zentrum für Optische Quantentechnologien, Fachbereich Physik, Universität Hamburg,
   Luruper Chaussee 149, 22761 Hamburg, Germany; Aritra.Mukhopadhyay@physnet.uni-hamburg.de
2 The Hamburg Centre for Ultrafast Imaging, Universität Hamburg, Luruper Chaussee 149,
   22761 Hamburg, Germany
* Correspondence: Peter.Schmelcher@physnet.uni-hamburg.de

Abstract: We demonstrate that directed transport of particles in a two dimensional driven lattice can be dynamically reversed multiple times by superimposing additional spatially localized lattices on top of a background lattice. The timescales of such current reversals can be flexibly controlled by adjusting the spatial locations of the superimposed lattices. The key principle behind the current reversals is the conversion of the particle dynamics from chaotic to ballistic, which allow the particles to explore regions of the underlying phase space which are inaccessible otherwise. Our results can be experimentally realized using cold atoms in driven optical lattices and allow for the control of transport of atomic ensembles in such setups.

1. Introduction

Originally conceived as a proof of principle behind the working of biological motors [1–4], the phenomenon of 'ratchet' transport of particles, i.e., the emergence of unidirectional particle transport in an unbiased non-equilibrium environment, has gained widespread applications across various disciplines [2,5–14]. The necessary ingredients required for such a rectification of random particle motion into directed transport has been shown to be non-equilibrium, non-linearity and the breaking of certain spatio-temporal symmetries [7,15,16]. Since then the ratchet effect has found numerous applications including particle separation based on physical properties [17–19], design of efficient velocity filters [20,21], transportation of fluxons in Josephson junctions arrays [22,23], unidirectional motion of active matter [13,24], voltage rectification in superconducting quantum interference devices (SQUID) [25–27], and enhancement of photocurrents in quantum wells [28].

Due to novel experimental progress in atom trapping techniques, directed transport of atomic ensembles has been realized in ac-driven optical lattices [29,30] both in the ultracold quantum regime [31] and at micro kelvin temperatures where a classical dynamics approach successfully describes the experiments [14,32]. Apart from the vast majority of ratchet-based setups in one spatial dimension (1D) [7,15,16,33,34], recent experiments have significantly progressed the realization of highly controllable two dimensional (2D) setups using ac-driven optical lattices [14,29,35,36] and holographic optical tweezers [37]. Due to such widespread applications of directed particle transport, the different mechanisms to control the transport have been a topic of ongoing research. One such mechanism is 'current reversal' where the direction of the particle transport can be reversed by suitably changing one or more system parameters [25,35,38–46]. Indeed, most of the existing schemes to generate current reversals focus on reverting the direction of asymptotic particle transport

due to a change of system parameter [47–50]. Only recently has research focused on setups where the current reversal occurs dynamically in time either due to a time-dependent switching of system parameters or due to the presence of interactions and dimensional coupling [33,38,51,52].

Here, we present a scheme to dynamically generate multiple current reversals due to superimposed driven lattices in two dimensions. The setup employs a 'background lattice' driven by an external bi-harmonic oscillating driving force, whose underlying potential is separable in terms of the spatial coordinates. This allows directed transport of particles along the direction of the driving force and trapped motion in the orthogonal direction. Superimposing a second lattice in a finite region of space along the direction of transport leads to a reflection behavior and hence generates a current reversal. Subsequently, the superposition of a third identical lattice can reflect the transport direction once again yielding a second reversal of transport. The timescales of the current reversals can be controlled by the spatial locations of the superimposed lattices. The underlying principle behind the current reversals lie in the conversion of the particle dynamics from chaotic to ballistic in the setup involving multiple lattices, a phenomenon which is forbidden in the background lattice alone. Our paper is structured as follows. In Section 2, we describe the underlying setup in detail and discuss its relevant symmetries followed by the main results in Section 3. We discuss the cause of the current reversals in terms of the underlying phase space in Section 4. Finally, in Section 5, we provide a possible experimental realization of our setup and conclude our findings in Section 6.

2. Setup, Equations of Motion and Symmetries

We consider N non-interacting classical particles of mass m in a two dimensional (2D) periodic potential $V(\mathbf{r}) = V_B(\mathbf{r}) + V_G(\mathbf{r})$. The separable potential due to the 'background lattice' is represented by $V_B(\mathbf{r}) = \tilde{V}_B(\cos^2 \frac{\pi x}{l} + \cos^2 \frac{\pi y}{l})$ with potential height $\tilde{V}_B$ and spatial period l in both x and y directions. On top of the lattice V_B, we superimpose two finite lattices of 2D Gaussian barriers V_{G1} and V_{G2} localized in different regions which can be described by the potential $V_G(\mathbf{r}) = \sum_{m,n=-\infty}^{+\infty} \tilde{U}_G(\mathbf{r}_{mn}) e^{-\alpha(\mathbf{r}-\mathbf{r}_{mn})^2}$ with the barriers centered at positions $\mathbf{r}_{mn} = (ml, nl)$ where $m, n \in \mathbb{Z}$ (see Figure 1a). These two lattices also have spatial period l along both x and y directions. $\tilde{U}_G(\mathbf{r}_{mn})$ denote the potential height of the barrier located at $\mathbf{r}_{mn}$ and α is a measure of the widths of the barriers. In addition, the lattices are driven by an external bi-harmonic periodic driving force $\mathbf{f_D}(t) = a(\cos \omega t + 0.5 \cos 2\omega t, 0)$ along the x-direction with driving amplitude a and frequency ω. This force is spatially independent. Introducing dimensionless variables $x' = \frac{x}{l}, y' = \frac{y}{l}$ and $t' = \omega t$ and dropping the primes for simplicity, the equation of motion for a single particle at position $\mathbf{r} = (x, y)$ with velocity $\dot{\mathbf{r}} = (\dot{x}, \dot{y})$ reads

$$
\begin{aligned}
\ddot{\mathbf{r}} &= \mathbf{F_B}(\mathbf{r}) + \mathbf{F_G}(\mathbf{r}) + \mathbf{F_D}(t) \\
&= U_B \pi (\sin 2\pi x, \sin 2\pi y) + 2\beta \sum_{m,n=-\infty}^{+\infty} U_G(\mathbf{R}_{mn}) (\mathbf{r} - \mathbf{R}_{mn}) e^{-\beta(\mathbf{r}-\mathbf{R}_{mn})^2} + d(\cos t + 0.5 \cos 2t, 0)
\end{aligned}
\tag{1}
$$

where $\mathbf{F_B}(\mathbf{r})$, $\mathbf{F_G}(\mathbf{r})$ and $\mathbf{F_D}(t)$ denote the forces due to the background lattice, superimposed lattices of Gaussian barriers and external driving respectively. The system is described by the four dimensionless parameters: $U_B = \frac{\tilde{V}_B}{ml^2\omega^2}$ denoting the effective potential height of the lattice V_B, $U_G(\mathbf{R}_{mn}) = \frac{\tilde{U}_G(\mathbf{r}_{mn})}{ml^2\omega^2}$ denoting the effective potential heights of the Gaussian barriers, $\beta = \alpha l^2$ and the effective driving amplitude $d = \frac{a}{ml\omega^2}$. $\mathbf{R}_{mn} = (m, n)$ denote the positions of the maxima of the Gaussian barriers which coincides with the positions of the potential maxima of the background lattice V_B. In this dimensionless form, the system has a spatial period $L = 1$ in both x and y directions and a temporal period $T = 2\pi$.

Our setup breaks the generalized time reversal symmetry S_t: $t \longrightarrow -t + \tau$, $\mathbf{r} \longrightarrow \mathbf{r} + \boldsymbol{\delta}$ (for arbitrary constant translations $\boldsymbol{\delta}$ and τ of space and time respectively) and the generalized parity symmetry P_x: $x \longrightarrow -x + \delta$, $t \longrightarrow t + \tau$ in the x-direction. As a result, directed transport of a particle ensemble is expected along the x-direction [7]. Since the setup preserves the generalized parity symmetry along the y-direction: P_y: $y \longrightarrow -y + \delta$, $t \longrightarrow t + \tau$, directed transport is not possible along this direction. Throughout the following discussions, by 'transport' we would always refer to the directed transport along the x-direction.
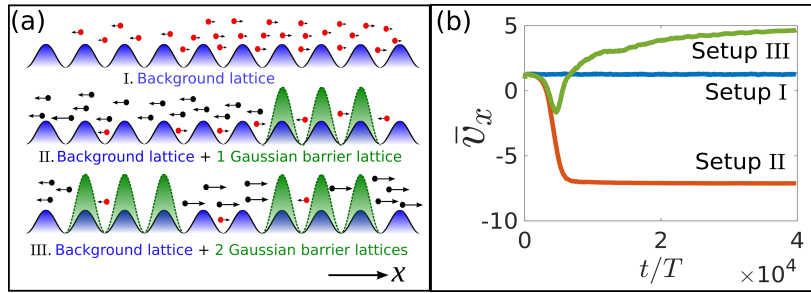
Figure 1. (**a**) Schematic representation of a slice of our 2D setup along the x-direction and viewed along the y-direction. The filled dots denote particles and the colors red and black denote diffusive and ballistic motion respectively. The arrows denote the direction of motion of the particles at asymptotic timescales ($t = t_f$) with the length of the arrow being proportional to the magnitude of the x component of their velocities, i.e., v_x. In the presence of only the driven background lattice V_B depicted in blue (setup I, upper panel), most particles exhibit diffusive/chaotic transport towards right, hence the average transport is along the positive x-direction. On superimposing a finite lattice of 2D Gaussian barriers V_{G1} (in green), most particles undergo a conversion from diffusive to ballistic motion leading to a reversal of their average transport direction (setup II, middle panel). Their velocities can be reversed once again due to the superposition of a second identical lattice of Gaussian barriers V_{G2}, thus leading to a second current reversal. The external driving force is along the x-direction. (**b**) Mean transport velocity of the ensemble along the x-direction as a function of time for the three different setups. $U_G(\mathbf{R}_{mn}) = 0$ for all (m, n) in setup I. For the setup II, $U_G(\mathbf{R}_{mn}) = 5$ for $5 \times 10^3 < m < 10^4$ and vanishes elsewhere whereas for setup III, $U_G(\mathbf{R}_{mn}) = 5$ for $5 \times 10^3 < |m| < 10^4$ and zero elsewhere. Remaining parameters: $U_B = 1.0$, $\beta = 5$, $d = 0.5$.

3. Results

To explore the transport properties of our setup, we initialize $N = 10^4$ particles within a square region $x, y \in [-5, 5] \times [-5, 5]$ with small random velocities $v_x, v_y \in [-0.1, 0.1] \times [-0.1, 0.1]$. The initial velocities of the particles are chosen randomly within the low velocity regime such that their initial kinetic energies are small compared to the potential heights of the lattices. Subsequently we time evolve our ensemble up to time $t = t_f = 4 \times 10^4$ T by numerical integration of Equation (1) using a Runge-Kutta Dormand Prince integrator [53]. The background lattice is large enough such that the ensemble never leaves the lattice throughout the duration of the simulation; hence no boundary conditions are imposed on the particles. We now discuss the transport properties of our setup characterized by the average velocity $\bar{v}_x$ of the particle ensemble along the x-direction.

In the presence of only the background lattice V_B (setup I in Figure 1a), the particles exhibit directed transport along the positive x-direction with an asymptotic transport velocity $\bar{v}_x \simeq 1.3$ (Figure 1b). In the setup II we consider a spatially localized lattice of Gaussian barriers V_{G1} superimposed on the lattice V_B (Figure 1a), such that $U_G(\mathbf{R}_{mn}) = 5$ for $5 \times 10^3 < m < 10^4$ and $U_G(\mathbf{R}_{mn}) = 0$ everywhere else. We define $x_1 = 5 \times 10^3 - \epsilon$ and $x_2 = 10^4 + \epsilon$ with $\epsilon = 5L$ as the left and right 'edges' of the lattice V_{G1}, since the force on the particles due to the Gaussian barriers is negligible for $x < x_1$ and $x > x_2$. In this case, we observe an initial directed transport along the positive x-direction with $\bar{v}_x > 0$ (Figure 1b). However, the transport velocity starts to decelerate and at $t \simeq 3.1 \times 10^3$ T, the transport completely vanishes. Thereafter, the ensemble is transported along the negative x-direction with $\bar{v}_x < 0$ and the transport velocity finally saturates to $\bar{v}_x \simeq -7.1$. Hence, a superimposed spatially localized lattice of Gaussian barriers can trigger a current reversal with the reversal timescale in this case given by $t_{r1} = 3.1 \times 10^3$ T, i.e., when $\bar{v}_x$ changes its sign.

In the third setup (setup III), we consider a second identical lattice of Gaussian barriers V_{G2} superimposed on the lattice V_B between $x = -x_1$ and $x = -x_2$, such that now $U_G(\mathbf{R}_{mn}) = 5$ for $5 \times 10^3 < |m| < 10^4$ and $U_G(\mathbf{R}_{mn}) = 0$ elsewhere (Figure 1a). Up to $t \simeq 4.6 \times 10^3 T$, the transport velocity exhibits a similar behavior as that observed in setup II (Figure 1b). Thereafter, instead of asymptotically attaining a negative value, the velocity increases steadily, exhibiting a second current

reversal at $t = t_{r2} = 5.6 \times 10^3$ T before finally attaining a constant value $\bar{v}_x \simeq 4.7$. The timescales of current reversal can be controlled by the locations of the lattices V_{G1} and V_{G2}. Overall, this demonstrates a controllable scheme to generate multiple reversals of directed particle transport by superimposing spatially localized lattices of 2D Gaussian barriers over a background lattice.

4. Discussion

The mechanism behind such controllable multiple current reversals in our setup crucially depends on the structure of the phase space underlying the system. Since the particles are non-interacting and can move along both x and y directions, the single particle phase space in our externally driven lattice setup is five-dimensional (5D); characterized by (x, p_x, y, p_y, t). However in the regions where the lattices V_{G1} and V_{G2} are absent, the particle dynamics along x and y directions can be completely decoupled. Hence the dynamics of the particles moving only through the background lattice V_B driven along the x-direction can be described in terms of a three-dimensional (3D) phase space characterized by (x, p_x, t) along x and a 2D phase space characterized by (y, p_y) along y direction. Since we are only interested in the transport along the x-direction, we would henceforth only refer to the 3D phase space along the x-direction in the course of our discussion.

4.1. Directed Transport in Background Lattice

First, we discuss the directed transport of particles in the positive x-direction in the presence of only the lattice V_B and the driving force. To do so, it is necessary to understand the phase space underlying our setup I by taking stroboscopic snapshots of particle trajectories $x(t), v_x(t)$ at $t = nT (n \in \mathbb{N})$ with each particle having different initial conditions. This leads to the 2D Poincaré surface of sections (PSOS): $\{x(nT) \bmod L, v_x(nT)\}$, which provide a representative overview of the structure of the complete 3D phase space (Figure 2a). Due to the broken P_x and S_t symmetries, the PSOS do not possess any reflection symmetry about $v_x = 0$. The PSOS is characterized by a single chaotic manifold or 'chaotic sea' bounded by the two first invariant spanning curves (FISC) at $v_x \simeq 10$ and $v_x \simeq -6$. The chaotic sea correspond to trajectories undergoing diffusive motion through the lattice. The large regular island embedded in the chaotic sea denotes trapped particles oscillating near the potential minima of the lattice. The particles with speed $|v_x|$ higher than the speed of the respective FISC at positive and negative velocities correspond to ballistic unidirectional motion through the lattice along positive or negative x-directions.
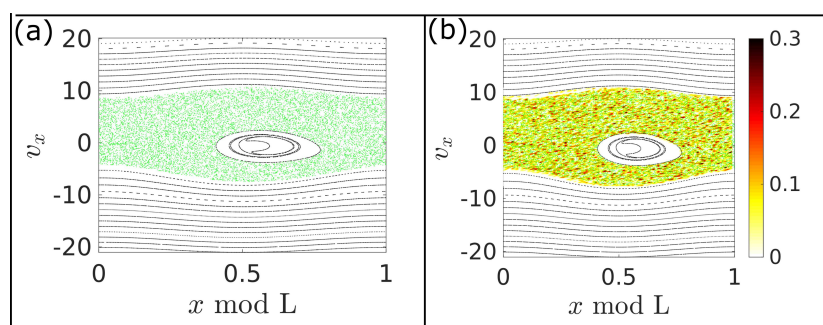

Figure 2. (**a**) The stroboscopic 2D Poincaré surface of sections (PSOS) in the (x, v_x) plane corresponding to the driven background lattice V_B. The regular islands and invariant curves (in black) denote trapped oscillations and ballistic motion respectively. The chaotic sea (in green) denotes diffusive motion. (**b**) The asymptotic particle distribution as a function of position $x \bmod L$ and v_x (in colormap) of all the $N = 10^4$ particles propagating in the setup I superimposed on the PSOS shown in Figure 2a. The parameters are the same as in Figure 1.

The low energy initial coordinates of our particle ensemble correspond to trajectories in the chaotic sea. Hence in the course of their time evolution, they ergodically populate the entire chaotic sea. This can be observed from (Figure 2b), where we project the snapshot of the ensemble population

distribution as a function of the particle coordinates (x, v_x) at time $t = t_f$ onto the PSOS. This leads to a converged value of the ensemble velocity which is equal to the transport velocity of the chaotic manifold [16]. Physically this signifies that these particles undergo diffusive motion through the lattice which is however asymmetric about $v_x = 0$ due to the broken symmetries. Hence, the asymptotic average velocity of the ensemble is non-zero and the particles exhibit directed transport along x-direction with $\bar{v}_x \simeq 1.3$ as observed in Figure 1b.

4.2. First Current Reversal

Next, we discuss why the transport velocity is reversed due to the superposition of a localized lattice of 2D Gaussian barriers V_{G1} on the background lattice V_B as in the setup II. Here, the particle dynamics is governed by the 2D PSOS (Figure 2a) in the region where only the lattice V_B is present, but by the full 5D phase space in the region $x_1 < x < x_2$ due to the presence of both the lattices V_B and V_{G1}. Although this 5D phase space cannot be straightforwardly visualized, it turns out that the cause of current reversal can be explained solely on the basis of the ensemble population in the 2D PSOS in Figure 2a. Since the ensemble is initialized near the origin $(0,0)$, the particles initially experience the spatial potential only due to the lattice V_B and hence their initial dynamics is exactly the same as described for setup I in the previous subsection. As a result the initial transport velocity is $\bar{v}_x \simeq 1.3$.

Since the transport velocity is positive, the particles reach $x = x_1$ in the course of time where they encounter the lattice V_{G1} in addition to V_B. In the region $x_1 < x < x_2$, since the particle dynamics is no longer governed by the 2D PSOS, the particles are now no longer confined to the central chaotic sea and can access higher velocities beyond the FISC. In fact, the higher potential heights of the Gaussian barriers ensure that most of the particles perform chaotic diffusive motion even at higher velocities corresponding to the full 5D phase space of our setup. This leads to an interesting conversion process between diffusive and ballistic motion of the particles at the left edge of the lattice V_{G1}, i.e., at $x = x_1$, which is the key mechanism behind the current reversal. A diffusive particle close to the left edge but with $x > x_1$ can cross this edge in the course of time back to $x < x_1$ with $v_x < 0$. However, its velocity v_x immediately after crossing back can be either $\gtrsim -6$ in which case it lies in the chaotic sea performing diffusive motion or $\lesssim -6$ which means it moves away ballistically from the lattice V_{G1} towards the negative x-direction. For the particles with $v_x \lesssim -6$, such a conversion from diffusive to ballistic motion ensures that they perform unidirectional ballistic flights towards the negative x-direction, thus attaining a permanent negative velocity. On the other hand, since the particles with $v_x \gtrsim -6$ perform diffusive motion they can again enter the region $x_1 < x < x_2$ in course of time. They would then undergo the same conversion mechanism until all the particles undergo the conversion from diffusive to ballistic motion with $v_x \lesssim -6$. This can be observed in Figure 3a where we plot the asymptotic distribution of the ensemble over the 2D PSOS. Most of the particles are located on the invariant curves $v_x \lesssim -6$ moving ballistically in the negative x-direction. This results in the asymptotic ensemble transport velocity $\bar{v}_x \simeq -7.1$. The dynamical change in the transport direction leads to the current reversal at $t_{r1} = 3.1 \times 10^3$ T.
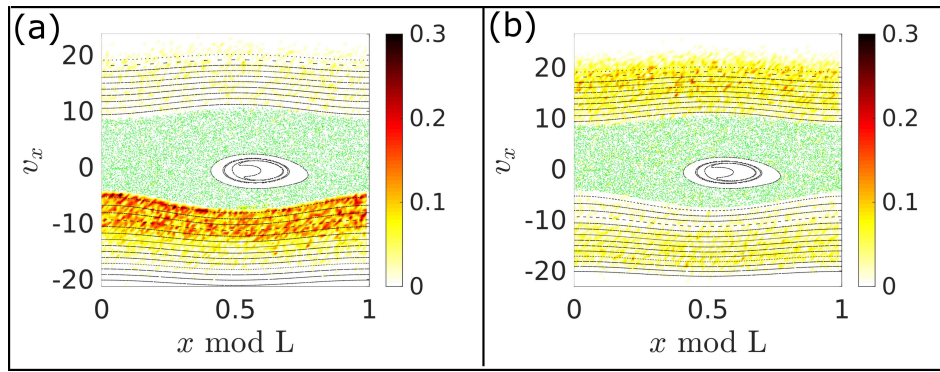
Figure 3. The asymptotic particle distribution as a function of position x mod L and v_x (in colormap) of all the $N = 10^4$ particles propagating in the (**a**) setup II and (**b**) setup III projected on to the PSOS shown in Figure 2a. The parameters are the same as in Figure 1.

4.3. Second Current Reversal

We now discuss why the transport can be reversed once again by superimposing a second identical lattice of Gaussian barriers V_{G2} between $x = -x_1$ and $x = -x_2$ as in the setup III. Initially since the particles are initialized near the origin $(0,0)$, the ensemble drifts towards the positive x-direction and exhibit the same dynamics as in the setup II. As a result, the transport velocity is initially positive till the first current reversal occurs at $t_{r1} = 3.1 \times 10^3$ T and then continues to be negative until $t \simeq 4.6 \times 10^3$ T. Thereafter, the particle dynamics undergo another conversion process due to which the transport velocity is reversed again.

Unlike the situation in setup II, the particles in the setup III moving ballistically with negative v_x after $t = t_{r1}$ cannot keep moving through the lattice V_B for all longer timescales. Instead at some point, they interact with the lattice V_{G2} in the region $-x_2 < x < -x_1$. Due to the high kinetic energy of the particles (since $|v_x| \gtrsim 6$), some of them can pass through the region and continue their ballistic flights for longer timescales through the lattice V_B. This can be seen from the asymptotic ensemble distribution projected on to the 2D PSOS in Figure 3b, showing that even at $t = t_f$ a considerable fraction of the ensemble moves with $v_x \lesssim -6$.

However, once a particle enters the region $-x_2 < x < -x_1$, its dynamics is no longer confined to the region $v_x \lesssim -6$ of the 2D PSOS and can explore the different regions of the 5D phase space. Hence most of the particles attain $v_x > 0$ which in turn allow them to cross the right edge of the lattice V_{G2} at $x = -x_1$ back into the region $-x_1 < x < x_1$ where only the lattice V_B is present. After crossing to this region, these particles can either belong to the chaotic sea or to the invariant spanning curves with velocity higher than the FISC at $v_x \simeq 10$ of the 2D PSOS in Figure 2a. The particles with $v_x \gtrsim 10$ perform unidirectional ballistic flights in the positive x-direction. Due to their significantly higher kinetic energy, most of these particles are not 'reflected' further by the lattice V_{G1} in the region $x_1 < x < x_2$; instead, after crossing this region, they continue moving ballistically through the lattice V_B with $v_x \gtrsim 10$. This can be observed from the significant distribution of particles with $v_x \gtrsim 10$ in Figure 3b at $t = t_f$. As the velocities of more and more particles undergo the conversion from $v_x \lesssim -6$ to $v_x \gtrsim 10$, the transport velocity increases steadily after $t \simeq 4.6 \times 10^3$ T, leading to a second current reversal at $t = t_{r2} = 5.6 \times 10^3$ T (Figure 1b). On the other hand, the particles in the chaotic layer would eventually again encounter the lattices V_{G1} or V_{G2} so that their chaotic dynamics is eventually converted to ballistic motion either with $v_x \gtrsim 10$ or with $v_x \lesssim -6$. Due to the overall higher number of particles moving asymptotically with $v_x \gtrsim 10$ compared to those with $v_x \lesssim -6$ (see Figure 3b), the asymptotic transport velocity is $\bar{v}_x \simeq 4.7$.

It is worth stressing that the conversion from chaotic to ballistic dynamics of the particles is possible solely due to the 2D nature of the potential generated by the superimposed Gaussian barriers. This ensures that the particle dynamics is coupled in the x and y directions upon entering the regions $x_1 < |x| < x_2$ (where the Gaussian barriers are present) whereas it is uncoupled in all other regions.

In Figure 4a, we show the typical trajectory of a particle in our setup III undergoing such a conversion process. The particle exhibits diffusive motion in the x direction through the lattice V_B until it reaches the left edge of the lattice V_{G1} at $t \approx 5 \times 10^3$ T. However, since its motion in the y direction is completely decoupled from the x direction, its velocity component v_y shows a regular oscillatory behaviour until $t \approx 5 \times 10^3$ T. The interaction with the 2D Gaussian barriers couples the x and y motion of the particle leading to a change in both the velocity components v_x and v_y. It then undergo ballistic motion with negative v_x between $t \approx 5 \times 10^3$ T and $t \approx 6 \times 10^3$ T. Between $t \approx 6 \times 10^3$ T and $t \approx 8 \times 10^3$ T, it interacts with the lattice V_{G2} exhibiting diffusive motion coupled in x and y directions. Finally, it undergoes a second conversion from diffusive to ballistic motion at $t \approx 8 \times 10^3$ T as it exits the right edge of the lattice V_{G2} and ballistically moves with a positive v_x thereafter. It is important to note that the individual timescales of such conversion processes vary for different particles. Some particles may even undergo multiple conversions between diffusive and ballistic dynamics over long timescales as shown for another typical trajectory in Figure 4b.
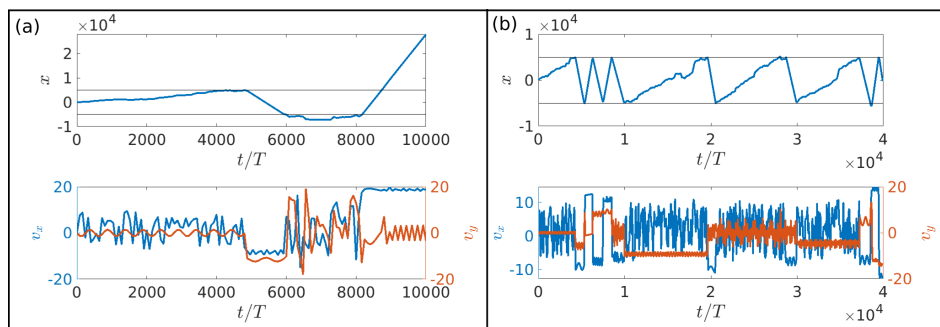

Figure 4. (**a**,**b**) Trajectories of two typical particles depicting the conversion between diffusive and ballistic dynamics in the setup III. The horizontal black lines at $x = x_1$ and $x = -x_1$ in the upper panels denote the left and right edges of the lattices V_{G1} and V_{G2} respectively. The particle in (**a**) is reflected twice by these two lattices due to the conversion between diffusive and ballistic dynamics. However, the particle in (**b**) undergoes such conversions multiple times over long timescales. The parameters are the same as in Figure 1.

5. Experimental Realization

Our scheme of multiple current reversal can be experimentally realized using cold atoms or colloids with optical lattices [14,32,38] and lattices designed using holographic trapping techniques [37,54–57]. The background lattice can be formed by 2D optical lattices where the periodic potential is generated by counterpropagating laser beams of perpendicular polarization. The spatially localized lattices of 2D Gaussian barriers can be obtained by reflecting a linearly polarized laser beam onto a spatial light modulator (SLM) displaying a computer generated hologram. The external driving force can be realized using a piezo-modulator [37].

Translating our parameters to experimentally relevant quantities for an optical lattice setup with cold rubidium (Rb[87]) atoms and 780 nm lasers, we obtain the lattice height $\tilde{V}_B \sim 5E_r$, the width $\frac{1}{\sqrt{\alpha}} \sim$ 350 nm, and the driving frequency $\omega \sim \omega_r$ and the driving amplitude $a \sim 0.003 \ E_r/$nm, where E_r and ω_r are the recoil energy and recoil frequency of the atom respectively. The timescales of the current reversals can be controlled by the spatial locations of the two lattices of Gaussian barriers. Further away the lattices are from the origin, i.e., near the initial location of the ensemble, the larger would be the reversal timescales. In contrast to Brownian ratchets, our mechanism does not depend on noise and operates in the purely Hamiltonian regime. The effect of weak noise typical for ratchet experiments with cold atoms and underdamped colloids [10,58] represent minor fluctuations of the average velocity of the ensemble and this does not affect the functionality of the current reversal mechanism. Interaction and disorder have been shown to enhance accumulation of particles within the regular regions of the

phase space [33,59,60], which would aid the conversion of chaotic to ballistic dynamics of particles. This would possibly decrease the reversal timescales.

6. Brief Conclusions

We provided a scheme to realize time dependent multiple reversals of directed transport in a two dimensional driven lattice setup by superimposing 'spatially localized lattices' on top of a 'global background lattice'. In contrast to most other current reversal schemes, the reversal of transport here occurs dynamically and the timescales of reversal can be controlled by controlling the spatial location of the localized lattices. The scheme is generic in the sense that the only requirement is a mixed phase space corresponding to the underlying background lattice and hence can be applied to a variety of physical systems, for e.g, cold atoms and colloids.

References

1. Ait-Haddou, R.; Herzog, W. Brownian Ratchet Models of Molecular Motors. *Cell Biochem. Biophys.* **2003**, *38*, 191–214. [CrossRef]
2. Astumian, R.D.; Hänggi, P. Brownian Motors. *Phys. Today* **2002**, *55*, 33. [CrossRef]
3. Astumian, R.D. Thermodynamics and Kinetics of a Brownian Motor. *Science* **1997**, *276*, 917–922. [CrossRef] [PubMed]
4. Jülicher, F.; Ajdari, A.; Prost, J. Modeling Molecular Motors. *Rev. Mod. Phys.* **1997**, *69*, 1269–1282. [CrossRef]
5. Bartussek, R.; Hänggi, P.; Kissner, J.G. Periodically Rocked Thermal Ratchets. *Europhys. Lett.* **1994**, *28*, 459–464. [CrossRef]
6. Cubero, D.; Renzoni, F. *Brownian Ratchets*; Cambridge University Press: Cambridge, UK, 2016. [CrossRef]
7. Denisov, S.; Flach, S.; Hänggi, P. Tunable Transport with Broken Space–Time Symmetries. *Phys. Rep.* **2014**, *538*, 77–120. [CrossRef]
8. Faucheux, L.P.; Bourdieu, L.S.; Kaplan, P.D.; Libchaber, A.J. Optical Thermal Ratchet. *Phys. Rev. Lett.* **1995**, *74*, 1504–1507. [CrossRef]
9. Hänggi, P.; Marchesoni, F.; Nori, F. Brownian Motors. *Ann. Phys.* **2005**, *14*, 51. [CrossRef]
10. Hänggi, P.; Marchesoni, F. Artificial Brownian Motors: Controlling Transport on the Nanoscale. *Rev. Mod. Phys.* **2009**, *81*, 387–442. [CrossRef]
11. Magnasco, M.O. Forced Thermal Ratchets. *Phys. Rev. Lett.* **1993**, *71*, 1477–1481. [CrossRef]
12. Prost, J.; Chauwin, J.F.; Peliti, L.; Ajdari, A. Asymmetric Pumping of Particles. *Phys. Rev. Lett.* **1994**, *72*, 2652–2655. [CrossRef]
13. Reichhardt, C.J.O.; Reichhardt, C. Ratchet Effects in Active Matter Systems. *Annu. Rev. Condens. Matter Phys.* **2017**, *8*, 51. [CrossRef]
14. Renzoni, F. *Driven Ratchets in Cold Atoms*; Elsevier: Amsterdam, The Netherlands, 2009.
15. Flach, S.; Yevtushenko, O.; Zolotaryuk, Y. Directed Current Due to Broken Time-Space Symmetry. *Phys. Rev. Lett.* **2000**, *84*, 2358–2361. [CrossRef]
16. Schanz, H.; Dittrich, T.; Ketzmerick, R. Directed Chaotic Transport in Hamiltonian Ratchets. *Phys. Rev. E* **2005**, *71*, 026228. [CrossRef]

17. Matthias, S.; Müller, F. Asymmetric Pores in a Silicon Membrane Acting as Massively Parallel Brownian Ratchets. *Nature* **2003**, *424*, 53. [CrossRef]

18. Mukhopadhyay, A.K.; Liebchen, B.; Schmelcher, P. Simultaneous Control of Multispecies Particle Transport and Segregation in Driven Lattices. *Phys. Rev. Lett.* **2018**, *120*, 218002. [CrossRef]

19. Wambaugh, J.F.; Reichhardt, C.; Olson, C.J. Ratchet-Induced Segregation and Transport of Nonspherical Grains. *Phys. Rev. E* **2002**, *65*, 031308. [CrossRef]

20. Petri, C.; Lenz, F.; Liebchen, B.; Diakonos, F.; Schmelcher, P. Formation of Density Waves via Interface Conversion of Ballistic and Diffusive Motion. *Europhys. Lett.* **2011**, *95*, 30005. [CrossRef]

21. Wulf, T.; Petri, C.; Liebchen, B.; Schmelcher, P. Analysis of Interface Conversion Processes of Ballistic and Diffusive Motion in Driven Superlattices. *Phys. Rev. E* **2012**, *86*, 016201. [CrossRef]

22. Falo, F.; Martínez, P.J.; Mazo, J.J.; Cilla, S. Ratchet Potential for Fluxons in Josephson-Junction Arrays. *Europhys. Lett.* **1999**, *45*, 700–706. [CrossRef]

23. Zolotaryuk, Y. Asymmetric Ac Fluxon Depinning in a Josephson Junction Array: A Highly Discrete Limit. *Phys. Rev. E* **2012**, *86*, 026604. [CrossRef]

24. Ai, B. Ratchet Transport Powered by Chiral Active Particles. *Sci. Rep.* **2016**, *6*, 18740. [CrossRef]

25. Spiechowicz, J.; Łuczka, J. SQUID Ratchet: Statistics of Transitions in Dynamical Localization. *Chaos Interdiscip. J. Nonlinear Sci.* **2019**, *29*, 013105. [CrossRef]

26. Spiechowicz, J.; Łuczka, J. Efficiency of the SQUID Ratchet Driven by External Current. *New J. Phys.* **2015**, *17*, 023054. [CrossRef]

27. Zapata, I.; Bartussek, R.; Sols, F.; Hänggi, P. Voltage Rectification by a SQUID Ratchet. *Phys. Rev. Lett.* **1996**, *77*, 2292–2295. [CrossRef]

28. Faltermeier, P.; Budkin, G.V.; Unverzagt, J.; Hubmann, S.; Pfaller, A.; Bel'Kov, V.V.; Golub, L.E.; Ivchenko, E.L.; Adamus, Z.; Karczewski, G.; et al. Magnetic Quantum Ratchet Effect in (Cd,Mn)Te- and CdTe-Based Quantum Well Structures with a Lateral Asymmetric Superlattice. *Phys. Rev. B* **2017**, *95*, 155442. [CrossRef]

29. Lebedev, V.; Renzoni, F. Two-Dimensional Rocking Ratchet for Cold Atoms. *Phys. Rev. A* **2009**, *80*, 023422. [CrossRef]

30. Schiavoni, M.; Sanchez-Palencia, L.; Renzoni, F.; Grynberg, G. Phase Control of Directed Diffusion in a Symmetric Optical Lattice. *Phys. Rev. Lett.* **2003**, *90*, 094101. [CrossRef]

31. Salger, T.; Kling, S.; Hecking, T.; Geckeler, C.; Morales-Molina, L.; Weitz, M. Directed Transport of Atoms in a Hamiltonian Quantum Ratchet. *Science* **2009**, *326*, 1241–1243. [CrossRef]

32. Brown, M.; Renzoni, F. Ratchet Effect in an Optical Lattice with Biharmonic Driving: A Numerical Analysis. *Phys. Rev. A* **2008**, *77*, 033405. [CrossRef]

33. Liebchen, B.; Diakonos, F.K.; Schmelcher, P. Interaction-Induced Current-Reversals in Driven Lattices. *New J. Phys.* **2012**, *14*, 103032. [CrossRef]

34. Schanz, H.; Otto, M.F.; Ketzmerick, R.; Dittrich, T. Classical and Quantum Hamiltonian Ratchets. *Phys. Rev. Lett.* **2001**, *87*, 070601. [CrossRef] [PubMed]

35. Cubero, D.; Renzoni, F. Control of Transport in Two-Dimensional Systems via Dynamical Decoupling of Degrees of Freedom with Quasiperiodic Driving Fields. *Phys. Rev. E* **2012**, *86*, 056201. [CrossRef] [PubMed]

36. Denisov, S.; Zolotaryuk, Y.; Flach, S.; Yevtushenko, O. Vortex and Translational Currents Due to Broken Time-Space Symmetries. *Phys. Rev. Lett.* **2008**, *100*, 224102. [CrossRef]

37. Arzola, A.V.; Villasante-Barahona, M.; Volke-Sepúlveda, K.; Jákl, P.; Zemánek, P. Omnidirectional Transport in Fully Reconfigurable Two Dimensional Optical Ratchets. *Phys. Rev. Lett.* **2017**, *118*, 138002. [CrossRef]

38. Arzola, A.V.; Volke-Sepúlveda, K.; Mateos, J.L. Experimental Control of Transport and Current Reversals in a Deterministic Optical Rocking Ratchet. *Phys. Rev. Lett.* **2011**, *106*, 168104. [CrossRef]

39. Dandogbessi, B.; Akin-Ojo, O.; Kenfack, A. Controlling Current Reversals in Chaotic Ratchet Transport. *Phys. Scr.* **2015**, *90*, 055206. [CrossRef]

40. Schreier, M.; Reimann, P.; Hänggi, P.; Pollak, E. Giant Enhancement of Diffusion and Particle Selection in Rocked Periodic Potentials. *Europhys. Lett.* **1998**, *44*, 416–422. [CrossRef]

41. Wickenbrock, A.; Cubero, D.; Wahab, N.A.A.; Phoonthong, P.; Renzoni, F. Current Reversals in a Rocking Ratchet: The Frequency Domain. *Phys. Rev. E* **2011**, *84*, 021127. [CrossRef]

42. Dinis, L.; Quintero, N.R. Nonsinusoidal Current and Current Reversals in a Gating Ratchet. *Phys. Rev. E* **2015**, *91*, 032920. [CrossRef]

43. Zeng, C.; Wang, H.; Nie, L. Multiple Current Reversals and Diffusion Enhancement in a Symmetrical Periodic Potential. *Chaos Interdiscip. J. Nonlinear Sci.* **2012**, *22*, 033125. [CrossRef]
44. Kostur, M.; Łuczka, J. Multiple Current Reversal in Brownian Ratchets. *Phys. Rev. E* **2001**, *63*, 021101. [CrossRef]
45. Chen, R.; Zhang, G.; Wang, C.; Nie, L.; Chen, C. Current Reversal in a Symmetric Periodic Potential. *Chaos Solitons Fractals* **2017**, *98*, 205–209. [CrossRef]
46. Rana, S.; Goswami, S.; Chatterjee, S.; Pradhan, P. Current Reversal in Interacting Colloids under Time-Periodic Drive. *Phys. Rev. E* **2018**, *98*, 052142. [CrossRef]
47. Da Silva, R.M.; Manchein, C.; Beims, M.W. Optimal Ratchet Current for Elastically Interacting Particles. *Chaos Interdiscip. J. Nonlinear Sci.* **2019**, *29*, 111101. [CrossRef]
48. De Souza Silva, C.C.; Van de Vondel, J.; Morelle, M.; Moshchalkov, V.V. Controlled Multiple Reversals of a Ratchet Effect. *Nature* **2006**, *440*, 651–654. [CrossRef]
49. Marconi, V.I. Rocking Ratchets in Two-Dimensional Josephson Networks: Collective Effects and Current Reversal. *Phys. Rev. Lett.* **2007**, *98*, 047006. [CrossRef]
50. Mateos, J.L. Chaotic Transport and Current Reversal in Deterministic Ratchets. *Phys. Rev. Lett.* **2000**, *84*, 258–261. [CrossRef]
51. Mukhopadhyay, A.K.; Xie, T.; Liebchen, B.; Schmelcher, P. Dimensional Coupling-Induced Current Reversal in Two-Dimensional Driven Lattices. *Phys. Rev. E* **2018**, *97*, 050202. [CrossRef]
52. Mukhopadhyay, A.K.; Liebchen, B.; Wulf, T.; Schmelcher, P. Freezing, Accelerating, and Slowing Directed Currents in Real Time with Superimposed Driven Lattices. *Phys. Rev. E* **2016**, *93*, 052219. [CrossRef]
53. Dormand, J.R.; Prince, P.J. A Family of Embedded Runge-Kutta Formulae. *J. Comput. Appl. Math.* **1980**, *6*, 19. [CrossRef]
54. Barredo, D.; de Léséleuc, S.; Lienhard, V.; Lahaye, T.; Browaeys, A. An Atom-by-Atom Assembler of Defect-Free Arbitrary Two-Dimensional Atomic Arrays. *Science* **2016**, *354*, 1021–1023. [CrossRef]
55. Kim, H.; Lee, W.; Lee, H.G.; Jo, H.; Song, Y.; Ahn, J. In Situ Single-Atom Array Synthesis Using Dynamic Holographic Optical Tweezers. *Nat. Commun.* **2016**, *7*, 13317. [CrossRef]
56. Nogrette, F.; Labuhn, H.; Ravets, S.; Barredo, D.; Béguin, L.; Vernier, A.; Lahaye, T.; Browaeys, A. Single-Atom Trapping in Holographic 2D Arrays of Microtraps with Arbitrary Geometries. *Phys. Rev. X* **2014**, *4*, 021034. [CrossRef]
57. Stuart, D.; Kuhn, A. Single-Atom Trapping and Transport in DMD-Controlled Optical Tweezers. *New J. Phys.* **2018**, *20*, 023013. [CrossRef]
58. Cubero, D.; Lebedev, V.; Renzoni, F. Current Reversals in a Rocking Ratchet: Dynamical versus Symmetry-Breaking Mechanisms. *Phys. Rev. E* **2010**, *82*, 041116. [CrossRef]
59. Liebchen, B.; Schmelcher, P. Interaction Induced Directed Transport in Ac-Driven Periodic Potentials. *New J. Phys.* **2015**, *17*, 083011. [CrossRef]
60. Wulf, T.; Liebchen, B.; Schmelcher, P. Disorder Induced Regular Dynamics in Oscillating Lattices. *Phys. Rev. Lett.* **2014**, *112*, 034101. [CrossRef]

3.6 Controlling vortical motion of particles in two-dimensional driven superlattices

Controlling vortical motion of particles in two-dimensional driven superlattices

Aritra K. Mukhopadhyay [1,*] and Peter Schmelcher[1,2,†]

[1]*Zentrum für Optische Quantentechnologien, Fachbereich Physik, Universität Hamburg,*
Luruper Chaussee 149, 22761 Hamburg, Germany
[2]*The Hamburg Centre for Ultrafast Imaging, Universität Hamburg, Luruper Chaussee 149, 22761 Hamburg, Germany*

We demonstrate the control of vortical motion of neutral classical particles in driven superlattices. Our superlattice consists of a superposition of individual lattices whose potential depths are modulated periodically in time but with different phases. This driving scheme breaks the spatial reflection symmetries and allows an ensemble of particles to rotate with an average angular velocity. An analysis of the underlying dynamical attractors provides an efficient method to control the angular velocities of the particles by changing the driving amplitude. As a result, spatially periodic patterns of particles showing different vortical motions can be created. Possible experimental realizations include holographic optical lattice based setups for colloids or cold atoms.

I. INTRODUCTION

Due to their experimental controllability, driven lattice potentials have become an important test bed for the exploration of nonequilibrium physical phenomena [1–3]. The inherent nonlinearity and tunable symmetries in these systems allow us to realize different nonequilibrium transport phenomena, the "ratchet effect" being one of them [4–15]. A ratchet rectifies random particle motion into unidirectional particle transport in an unbiased nonequilibrium environment. Certain spatiotemporal symmetries of the system need to be broken in order to realize it [16–18]. This leads to numerous applications across different disciplines, such as controlling the transport of atomic ensembles in ac-driven optical lattices [19,20] in both the ultracold quantum [1] and classical regimes [2,12], colloidal transport in driven holographic optical lattices [21], particle separation based on physical properties [22–24], and motion of vortices in type-II superconductors [25–27]. Due to the widespread applicability of such directed transport, there has been extensive research to control the strength and direction of the ratchet current. Setups using one-dimensional (1D) driven lattices have been shown to effectively accelerate, slow down, or even completely reverse the direction of transport [18,28,29]. Two-dimensional (2D) driven lattices, on the other hand, offer a higher variability in terms of transport direction and for particles to be transported parallel to, orthogonal to, or at any arbitrary angle with respect to the direction of the driving force [21,30,31].

In contrast to 1D, the 2D driven lattice based ratchet setups also allow for the possibility to convert random particle motion into rotational or vortical motion leading to nonzero angular velocity of the particles. This is particularly interesting since it provides a method to realize rotational motion of neutral particles analogous to the motion of charged particles

in a magnetic field without explicitly rotating the system. In fact, similar setups have been used to generate artificial magnetic fields for exploring topological quantum states with cold neutral atoms in periodically modulated lattices [32,33]. However, the extensive research on symmetry-breaking-induced directed transport in the classical regime has mostly focused on translational currents, and the control of rotational currents has remained largely unexplored. The few existing setups either lead to a diffusive rotational motion over an extended space in the presence of an elliptical ac drive, introducing an inherent rotational bias [34], or require specially tailored potentials [35,36] and temporally correlated colored noise [37,38]. Furthermore, due to the lack of spatial tunability of the underlying lattice potential, these setups do not allow patterns of multiple vortices in space analogous to the different spatial configurations of artificial magnetic fluxes in the quantum regime [39].

Here, we address these key limitations and present a setup to realize controllable rotational motion of classical particles along closed spatial paths in driven superlattices without any explicit rotational bias. The individual lattices are modeled by a periodic arrangement of Gaussian potential wells whose depths can be individually modulated in a time-periodic manner, leading to a "spatiotemporally" driven lattice setup [40,41]. We show that modulating different wells with the same driving amplitude but different driving phases allows us to break the relevant symmetries and generate nonzero average angular velocities for an ensemble of particles. The angular velocities of individual trajectories can be controlled by varying the driving amplitude. Additionally, we demonstrate periodic spatial arrangements of different types of rotational motion by modulating the different potential wells with different driving amplitudes and phases.

II. SETUP

We consider N noninteracting classical particles of mass m in a 2D potential landscape $V(\mathbf{r} \equiv (x, y, 0), t) =$

---

*Aritra.Mukhopadhyay@physnet.uni-hamburg.de
†Peter.Schmelcher@physnet.uni-hamburg.de

$\sum_{m,n=-\infty}^{+\infty} \tilde{U}_{mn}(t)e^{-\beta(\mathbf{r}-\mathbf{r}_{mn})^2}$ formed by a lattice of 2D Gaussian wells centered at positions $\mathbf{r}_{mn} = (mL, nL, 0)$, $m, n \in \mathbb{Z}$. The depths of the wells are modulated periodically in time by the site-dependent driving law $\tilde{U}_{mn}(t) = \tilde{V}_{mn}[\cos(\omega t + \phi_{mn}) - 1]$ with driving frequency ω, driving amplitude $\tilde{V}_{mn}$, and a temporal phase shift ϕ_{mn}. We consider the setup to be dissipative, with the dissipation coefficient of the particles being denoted by $\tilde{\gamma}$. The source of dissipation can be different for different systems, e.g., viscous drag forces for colloidal particles or optical molasses for cold atoms [42]. Introducing dimensionless variables $\mathbf{r}' = \frac{\mathbf{r}}{L}$ and $t' = \omega t$ and dropping the primes for simplicity, the equation of motion for a single particle at position $\mathbf{r} = (x, y, 0)$ with velocity $\dot{\mathbf{r}} = (\dot{x}, \dot{y}, 0)$ reads

$$\ddot{\mathbf{r}} + \gamma \dot{\mathbf{r}} = \sum_{m,n=-\infty}^{+\infty} 2\alpha U_{mn}(t)(\mathbf{r} - \mathbf{R}_{mn})e^{-\alpha(\mathbf{r}-\mathbf{R}_{mn})^2} + \xi(t),$$

(1)

where $U_{mn}(t) = V_{mn}[\cos(t + \phi_{mn}) - 1]$ is the effective site-dependent driving law with time period $T = 2\pi$ and driving amplitude $V_{mn} = \frac{\tilde{V}_{mn}}{m\omega^2 L^2}$. $\mathbf{R}_{mn} = (m, n, 0)$ denotes the positions of the Gaussian wells, $\gamma = \frac{\tilde{\gamma}}{m\omega}$ is the effective dissipation coefficient, and the parameter $\alpha = \beta L^2$ is a measure of the widths of the wells. $\xi(t) = (\xi_x, \xi_y, 0)$ denotes thermal fluctuations modeled by Gaussian white noise of zero mean with the property $\langle \xi_i(t)\xi_j(t') \rangle = 2D\delta_{ij}\delta(t - t')$, where $i, j \in x, y$ and $D = \frac{\tilde{\gamma} k_B \mathcal{T}}{m^2 \omega^2 L^2}$ is the dimensionless noise strength, with $\mathcal{T}$ and k_B denoting the temperature and Boltzmann constant, respectively. Unless mentioned otherwise, we choose $V_{mn} = V$ for all the wells, $\alpha = 3$, and $\gamma = 0.1$. The set of all wells arranged periodically in space with a specific value of the driving phase ϕ_{mn} forms a sublattice of our system. Our setup is hence a driven superlattice formed by the superposition of different sublattices, each driven by a distinct driving phase ϕ_{mn}. Possible experimental realizations of such a 2D potential include holographic optical lattices [21,43–46] and optical superlattices [47] with the lattice depth modulated via standard amplitude modulation techniques [48,49]. The rotational dynamics of particles in such a setup could be observed with colloidal particles or with cold atoms in the classically describable regime of microkelvin temperatures [12,21]. In colloidal experimental setups with polystyrene microspheres [21], our parameter values would correspond to typical well widths of $\sim 10\,\mu$m at room temperatures, and the value of V can be flexibly controlled by the intensity of light.

III. ROTATIONAL CURRENT DUE TO SYMMETRY BREAKING

The asymptotic dynamics of particles in our setup can be confined within either a lattice unit cell such as in linear oscillatory motion or vortical motion along arbitrary closed spatial curves. There can also be unconfined diffusive or ballistic motion throughout the lattice. Different particles exhibiting vortical motion can, in general, possess different angular velocities. Hence, in order to distinguish vortical motion of a trajectory from ballistic, diffusive, and vortical dynamics of other trajectories, we use the angular velocity
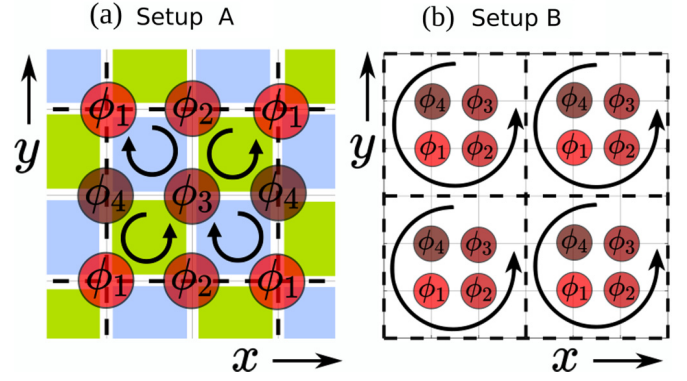

FIG. 1. Schematic representation of superlattice setups A and B formed by the superposition of four square sublattices driven with an amplitude V but at different phases $\phi_i = \frac{(i-1)\pi}{2}$, $i = 1, 2, 3, 4$. Each red circle denotes the position of an individual Gaussian well. The thick black dashed lines denote the boundary of the lattice unit cells. The spatial period of setup A is $(2,2,0)$, whereas that of setup B is $(3,3,0)$ due to the presence of empty sites without any wells. The blue and green regions in (a) denote plaquettes with clockwise and counterclockwise chiralities with respect to the spatial orientation of the wells with driving phases ϕ_i. The remaining parameters are $V = 0.41$, $\alpha = 3$, $\gamma = 0.1$.

$\mathbf{\Omega}(t) = [\dot{\mathbf{r}}(t) \times \ddot{\mathbf{r}}(t)]/\dot{\mathbf{r}}^2(t)$, which is equivalent to the definition of curvature of planar curves measuring the speed of rotation of the velocity vector about the origin [34,50]. Since the particle dynamics is confined to the xy plane, the only possible nonzero component of $\mathbf{\Omega}(t)$ is along $\hat{\mathbf{z}}$, the unit vector along the z direction. The mean angular velocity of a trajectory is defined as $\bar{\mathbf{\Omega}} = \frac{1}{t} \lim_{t \to \infty} \int_0^t \mathbf{\Omega}(t')dt'$. For trajectories rotating along a closed spatial curve with period ηT, the mean angular velocity can be expressed as $\bar{\mathbf{\Omega}} = \frac{2\pi\tau}{\eta T}\hat{\mathbf{z}} = \frac{\tau}{\eta}\hat{\mathbf{z}}$ (since $T = 2\pi$), where $2\pi\tau$ denotes the *total curvature* of the curve with the *turning number* τ defined as the number of times the velocity vector winds about its origin [51]. The net rotational current, defined as the mean angular velocity of an ensemble of particles with different initial conditions, is given by $\mathbf{J}_{\mathbf{\Omega}} = \langle \bar{\mathbf{\Omega}} \rangle$, where $\langle \cdots \rangle$ denotes the average over all trajectories. Since the only possible nonzero components of $\mathbf{\Omega}(t)$, $\bar{\mathbf{\Omega}}$, and $\mathbf{J}_{\mathbf{\Omega}}$ are along $\hat{\mathbf{z}}$, we drop the symbol $\hat{\mathbf{z}}$ henceforth.

The necessary condition for any setup to exhibit a net rotational current is to break the symmetries, which keeps the system invariant but changes the sign of the angular velocity $\mathbf{\Omega}(t)$ [34]. There are only two symmetry transformations which can change the sign of $\mathbf{\Omega}(t)$: (i) time reversal together with optional spatial inversion and space-time translations S_t, $t \longrightarrow -t + t'$, $\mathbf{r} \longrightarrow \pm\mathbf{r} + \delta$, and (ii) parity or reflection $\mathcal{P}$ about any plane perpendicular to the xy plane with optional spatial rotation $\mathcal{R}$ in the xy plane and space-time translations S_p, $\mathbf{r} \longrightarrow \mathcal{R}(\mathcal{P}\mathbf{r}) + \delta$, $t \longrightarrow t + t'$. Since our setup is dissipative, S_t is broken independent of our choice of the lattice potential $V(\mathbf{r}, t)$. However, the superlattice potential allows us to preserve or break the symmetry S_p by controlling the driving phases of the underlying sublattices. In order to illustrate this, we consider two setups, A and B [Figs. 1(a) and 1(b)], each consisting of four square sublattices with the same driving amplitude $V = 0.41$ but different phases

$\phi_i = \frac{(i-1)\pi}{2}$, $i = 1, 2, 3, 4$. The sublattices in setup A have lattice vectors $(2,0,0)$ and $(0,2,0)$; hence, the setup has a spatial period $\mathbf{L_A} = (2, 2, 0)$. In contrast, setup B has a spatial period $\mathbf{L_B} = (3, 3, 0)$, with the lattice vectors being $(3,0,0)$ and $(0,3,0)$. As shown in Fig. 1(a), the arrangement of the sublattices allows us to consider the unit cell of setup A as a collection of four distinct spatial domains or plaquettes. The plaquettes are characterized by clockwise or counterclockwise arrangement of Gaussian wells with driving phase ϕ_i, i.e., of opposite chirality. Since the parity transformation S_p reverses chirality, each of these plaquettes breaks the S_p symmetry. However, since the unit cell has an equal number of plaquettes with opposite chiralities (two clockwise and two counterclockwise), the unit cell and hence the entire setup A are symmetric with respect to S_p. This implies that although setup A might allow trajectories with different mean angular velocities $\bar{\boldsymbol{\Omega}}$, the net rotational current $\mathbf{J_\Omega}$ must be zero. In contrast, the entire unit cell of setup B has a counterclockwise chirality which can be reversed by S_p, and hence, setup B breaks S_p symmetry. As a result one can expect $\mathbf{J_\Omega}$ to be nonzero.

In order to verify our symmetry analysis and explore the behavior of rotational current in our system, we initialize $N = 10^4$ particles randomly within a square region $x, y \in [-100, 100] \times [-100, 100]$ in both setups A and B with small random velocities $v_x, v_y \in [-0.1, 0.1]$. Subsequently, we time evolve our ensemble up to time $t_f = 10^4 T$ by numerical integration of Eq. (1) for different noise strengths D. In the deterministic limit $D = 0$, all particles in setup A exhibit only rotational motion along closed curves with mean angular velocity $\bar{\boldsymbol{\Omega}} = \frac{1}{2}$ (vortex) or $-\frac{1}{2}$ (antivortex). Figure 2(a) shows a typical trajectory in this setup having $\bar{\boldsymbol{\Omega}} = -\frac{1}{2}$. The velocity vector winds around its origin in the clockwise direction once during the period of rotation $2T$; hence, $\tau = -1$, and $\eta = 2$. The vortical motion persists as the noise strength is increased to $D = 0.001$. However, most importantly, there exists an equal number of trajectories possessing $\bar{\boldsymbol{\Omega}} = -\frac{1}{2}$ and $\bar{\boldsymbol{\Omega}} = \frac{1}{2}$, signifying that the net rotational current $\mathbf{J_\Omega} = 0$ [Fig. 2(b)], as predicted by our symmetry analysis. Even for higher noise strength up to $D = 0.003$, such a symmetry-related cancellation of vortex-antivortex pairs with equal and opposite angular velocities persists, leading to a zero net rotational current. Beyond $D > 0.003$, the vortical motion is destroyed, resulting in a symmetric distribution of particles around $\bar{\boldsymbol{\Omega}} = 0$ and hence $\mathbf{J_\Omega} = 0$. The particles in setup B also exhibit rotational motion; however, unlike in setup A, all the particles in setup B possess a mean angular velocity $\bar{\boldsymbol{\Omega}} = \frac{3}{5} = 0.6$. An example trajectory in setup B in the deterministic limit can be seen in Fig. 2(c). The velocity vector makes four counterclockwise (at the four corners of the curve) and one clockwise (corresponding to one full rotation along the curve) windings around its origin during one period of rotation $5T$; hence, $\tau = 3$, and $\eta = 5$. For $D \leqslant 0.002$, the vortical motion is quite stable, and almost all the particles in the setup rotate with $\bar{\boldsymbol{\Omega}} = 0.6$, resulting in $\mathbf{J_\Omega} = 0.6$ [Fig. 2(d)] in accordance with our symmetry analysis. For $D > 0.002$, the particles perform diffusive motion through the lattice, and the vortical motion is gradually destroyed, thus decreasing the value of $\mathbf{J_\Omega}$.
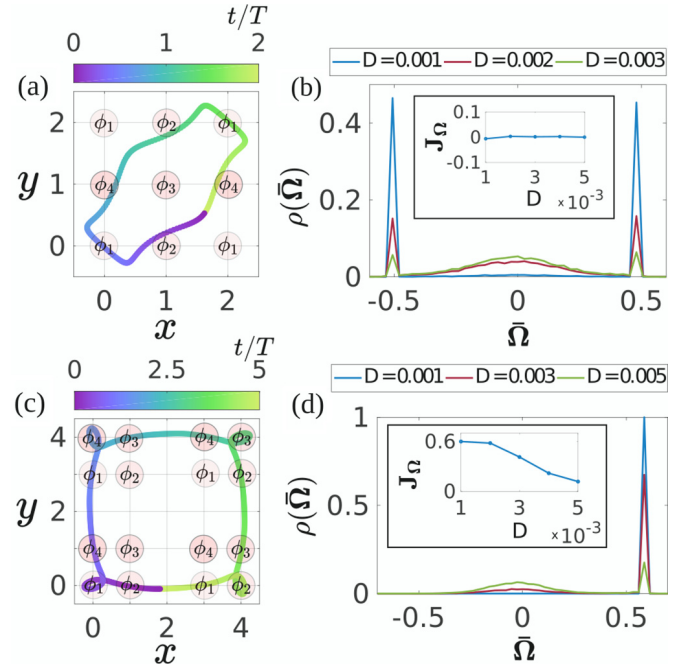

FIG. 2. Typical trajectories exhibiting rotational motion in (a) setup A and (c) setup B over one time period of rotation (color bars). The colored circles denote the positions of individual Gaussian wells with different driving phases ϕ_i. (b) and (d) The fraction of particles $\rho(\bar{\boldsymbol{\Omega}})$ possessing mean angular velocity $\bar{\boldsymbol{\Omega}}$ for different noise strengths D in setups A and B, respectively. The insets show the variation of the net rotational current $\mathbf{J_\Omega}$ with D. The remaining parameters are the same as in Fig. 1.

IV. CONTROL OF ROTATIONAL CURRENT

The question that naturally arises is that once we design a driven superlattice which breaks the S_p symmetry, e.g., our setup B, can we predict the value of $\mathbf{J_\Omega}$ *a priori*? Specifically, how does the mean angular velocity $\bar{\boldsymbol{\Omega}}$ of the trajectories depend on the system parameters? For a driven dissipative nonlinear system like the present one, this can be answered by analyzing the asymptotic $t \to \infty$ particle dynamics in the deterministic limit $D = 0$. The asymptotic dynamics of the particles is governed by the set of attractors underlying the phase space of the system, which can be of two types: (i) *regular* attractors denoting ballistic, linear oscillatory and rotational motions and (ii) *chaotic* attractors denoting diffusive motion. In order to distinguish between attractors corresponding to rotational motion compared to the others, we introduce a slightly modified angular velocity vector $\boldsymbol{\Omega}'(t) = [\dot{\mathbf{r}}(t) \times \ddot{\mathbf{r}}(t)]/[|\dot{\mathbf{r}}(t)||\ddot{\mathbf{r}}(t)|]$. Note that $\boldsymbol{\Omega}'(t) = \sin \vartheta(t) \, \hat{\mathbf{z}}$, where $\vartheta(t)$ denotes the instantaneous angle between the velocity and acceleration vectors of the particle. $\boldsymbol{\Omega}'(t)$ transforms under S_p and S_t in exactly the same way as $\boldsymbol{\Omega}(t)$. However, since the values of $\boldsymbol{\Omega}'(t)$ are bounded in the interval $[-1, 1]$, as opposed to $\boldsymbol{\Omega}(t)$, which becomes large for small values of $\dot{\mathbf{r}}(t)$, it is a good quantity to differentiate between chaotic and regular rotational dynamics of particles. To illustrate this, we inspect the *bifurcation diagram* of $\boldsymbol{\Omega}'(t)$ in Fig. 3(a) as a function of the driving amplitude V for our setup B by initializing particles with random positions and velocities and stroboscopically monitoring $\boldsymbol{\Omega}'(t)$ after an
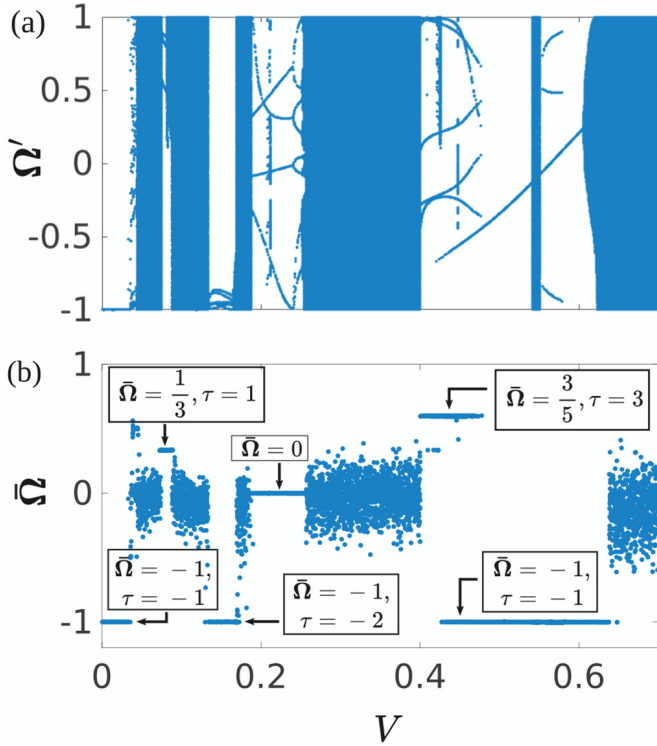
FIG. 3. (a) Bifurcation diagram of $\mathbf{\Omega}'(t)$ as a function of the driving amplitude V depicting the chaotic (broad blue bands) and regular (thin blue lines) attractors of setup B [see Fig. 1(b)]. (b) The mean angular velocity $\bar{\mathbf{\Omega}}$ of the attractors in Fig. 3(a) as a function of V. The values of $\bar{\mathbf{\Omega}}$ for the regular attractors denoting rotational motion and the turning number τ of the corresponding closed curves are labeled with arrows. The remaining parameters are the same as in Fig. 1(b).

initial transient [52]. For certain ranges of values of V, all the particles in the setup exhibit chaotic motion [broad blue bands in Fig. 3(a)] such that $\mathbf{\Omega}'(t)$ takes all possible values in the range $[-1, 1]$. For all other values of V, they perform regular periodic motion, resulting in only specific values of $\mathbf{\Omega}'(t)$. Most of these periodic motions correspond to particles performing rotational motion with different nonzero $\bar{\mathbf{\Omega}}$ (except for $0.19 \lesssim V \lesssim 0.25$) depending on the value of V, as shown in Fig. 3(b). This provides an efficient method to design and control the angular velocities of the trajectories in our setup by simply choosing the desired driving amplitude V. Our previous results [see Figs. 2(c) and 2(d)] give such an example for setup B with $V = 0.41$.

V. MULTIPLE VORTICES

The ability to control the angular momentum of the particles with different driving amplitude V allows us to design lattices with spatially periodic arrangements of multiple vortices. In order to illustrate this, we consider the specific setup shown in Fig. 4(a). It is designed such that the unit cell consists of a collection of four plaquettes, $\mathcal{D}_1$, $\mathcal{D}_2$, $\mathcal{D}_3$, and $\mathcal{D}_4$. Each plaquette consists of four Gaussian wells driven at different phases $\phi_i = \frac{(i-1)\pi}{2}$, $i = 1, 2, 3, 4$. The plaquettes $\mathcal{D}_1$ and $\mathcal{D}_4$ possess a counterclockwise chirality, whereas $\mathcal{D}_2$ and $\mathcal{D}_3$ have clockwise chirality with respect to the spatial
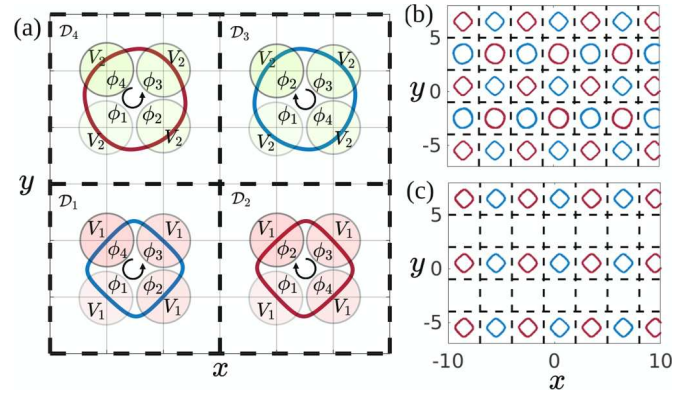

FIG. 4. (a) Schematic representation of one unit cell of our setup consisting of four plaquettes, $\mathcal{D}_1$, $\mathcal{D}_2$, $\mathcal{D}_3$, and $\mathcal{D}_4$, with the thick dashed lines denoting the plaquette boundaries. The shaded circles denote the positions of individual Gaussian wells driven with amplitudes $V_1 = 0.51$ or $V_2 = 0.078$ and phases ϕ_i. $\mathcal{D}_1$ and $\mathcal{D}_4$ ($\mathcal{D}_2$ and $\mathcal{D}_3$) have counterclockwise (clockwise) chirality with respect to the spatial orientation of the wells with driving phases ϕ_i. Trajectories of particles exhibiting vortical motion for $D = 0$ with positive (red) and negative (blue) $\bar{\mathbf{\Omega}}$ have been superimposed on the unit cell. The trajectories in $\mathcal{D}_1$, $\mathcal{D}_2$, $\mathcal{D}_3$, and $\mathcal{D}_4$ have $\bar{\mathbf{\Omega}} = -1$, 1, $-\frac{1}{3}$, and $\frac{1}{3}$, respectively. (b) and (c) An extract of the spatial arrangements of the trajectories exhibiting vortical motion within different plaquettes for $D = 10^{-4}$ and $D = 10^{-3}$, respectively. The remaining parameters are the same as in Fig. 1.

arrangement of the wells with driving phases ϕ_i. Additionally, the wells in $\mathcal{D}_1$ and $\mathcal{D}_2$ are driven with amplitude $V_1 = 0.51$, and those in $\mathcal{D}_3$ and $\mathcal{D}_4$ are driven with $V_2 = 0.078$. Note that these specific values of driving amplitude are chosen by consulting the bifurcation diagram in Fig. 3 to allow only vortex trajectories with specific angular momenta. We initialize $N = 10^4$ particles randomly in this setup within a square region $x, y \in [-50, 50] \times [-50, 50]$ with small random velocities $v_x, v_y \in [-0.1, 0.1]$ and propagate the ensemble up to time $t_f = 10^4 T$. For $D = 0$, the particles exhibit vortical motion at long timescales, with their angular velocity being governed by the plaquette they are trapped within, as shown in Fig. 4(a). The particles in $\mathcal{D}_1$ and $\mathcal{D}_4$ rotate with $\bar{\mathbf{\Omega}} = -1$ and $\bar{\mathbf{\Omega}} = \frac{1}{3}$, respectively, as predicted by Fig. 3(b). Note that plaquettes $\mathcal{D}_2$ and $\mathcal{D}_3$ can be obtained by a spatial parity transformation on $\mathcal{D}_1$ and $\mathcal{D}_4$, respectively. Hence, the mean angular velocity of the particles in $\mathcal{D}_2$ and $\mathcal{D}_3$ has a sign opposite that of the particles in $\mathcal{D}_1$ and $\mathcal{D}_4$, respectively. Even for $D = 10^{-4}$, such rotational motion persists, and we obtain a periodic arrangement of particles in space rotating with different angular momenta [Fig. 4(b)]. For a higher strength $D = 10^{-3}$, the vortical motion of particles with $\bar{\mathbf{\Omega}} = \pm\frac{1}{3}$ is destroyed, and only the ones with $\bar{\mathbf{\Omega}} = \pm 1$ remain, yielding a different periodic arrangement [Fig. 4(c)]. Noise strengths $D \geqslant 4 \times 10^{-3}$ eventually destroy all the vortex trajectories.

VI. CONCLUSIONS

We have demonstrated that superlattices of periodically driven localized wells provide highly controllable setups to realize different patterns of rotational motion of particles. The

spatial arrangement of the lattices is responsible for breaking the relevant symmetries, thus allowing for the nonzero average angular momentum of an ensemble of particles. Our analysis of the underlying nonlinear dynamical attractors provides an efficient method to control the angular momentum of the particles as well as to create a variety of periodic arrangements of vortical motion with different angular momenta. This might be useful for technological applications too. For example, an extension of this scheme with a mixture of two particle species differing in mass or size would allow us to segregate them in different spatial plaquettes with each species rotating

with different angular momenta. Future perspectives include investigation of rotational dynamics of particles operating in the purely Hamiltonian regime without dissipation, as well as in the quantum regime with the possibility to realize spatially varying artificial magnetic fluxes.

ACKNOWLEDGMENTS

[1] T. Salger, S. Kling, T. Hecking, C. Geckeler, L. Morales-Molina, and M. Weitz, Science **326**, 1241 (2009).

[2] M. Brown and F. Renzoni, Phys. Rev. A **77**, 033405 (2008).

[3] T. Dittrich and F. L. Dubeibe, Phys. Rev. Lett. **114**, 094101 (2015).

[4] R. D. Astumian and P. Hänggi, Phys. Today **55**(11), 33 (2002).

[5] R. Bartussek, P. Hänggi, and J. G. Kissner, Europhys. Lett. **28**, 459 (1994).

[6] D. Cubero and F. Renzoni, *Brownian Ratchets* (Cambridge University Press, Cambridge, 2016).

[7] L. P. Faucheux, L. S. Bourdieu, P. D. Kaplan, and A. J. Libchaber, Phys. Rev. Lett. **74**, 1504 (1995).

[8] P. Hänggi, F. Marchesoni, and F. Nori, Ann. Phys. (Berlin, Ger.) **14**, 51 (2005).

[9] M. O. Magnasco, Phys. Rev. Lett. **71**, 1477 (1993).

[10] J. Prost, J. F. Chauwin, L. Peliti, and A. Ajdari, Phys. Rev. Lett. **72**, 2652 (1994).

[11] C. J. O. Reichhardt and C. Reichhardt, Annu. Rev. Condens. Matter Phys. **8**, 51 (2017).

[12] F. Renzoni, *Driven Ratchets in Cold Atoms* (Elsevier, Amsterdam, 2009).

[13] P. Reimann, Phys. Rep. **361**, 57 (2002).

[14] P. Hänggi and F. Marchesoni, Rev. Mod. Phys. **81**, 387 (2009).

[15] A. K. Mukhopadhyay, T. Xie, B. Liebchen, and P. Schmelcher, Phys. Rev. E **97**, 050202(R) (2018).

[16] S. Denisov, S. Flach, and P. Hänggi, Phys. Rep. **538**, 77 (2014).

[17] S. Flach, O. Yevtushenko, and Y. Zolotaryuk, Phys. Rev. Lett. **84**, 2358 (2000).

[18] H. Schanz, T. Dittrich, and R. Ketzmerick, Phys. Rev. E **71**, 026228 (2005).

[19] V. Lebedev and F. Renzoni, Phys. Rev. A **80**, 023422 (2009).

[20] M. Schiavoni, L. Sanchez-Palencia, F. Renzoni, and G. Grynberg, Phys. Rev. Lett. **90**, 094101 (2003).

[21] A. V. Arzola, M. Villasante-Barahona, K. Volke-Sepúlveda, P. Jákl, and P. Zemánek, Phys. Rev. Lett. **118**, 138002 (2017).

[22] S. Matthias and F. Müller, Nature (London) **424**, 53 (2003).

[23] A. K. Mukhopadhyay, B. Liebchen, and P. Schmelcher, Phys. Rev. Lett. **120**, 218002 (2018).

[24] J. F. Wambaugh, C. Reichhardt, and C. J. Olson, Phys. Rev. E **65**, 031308 (2002).

[25] C.-S. Lee, B. Jankó, I. Derényi, and A.-L. Barabási, Nature (London) **400**, 337 (1999).

[26] C. Reichhardt, D. Ray, and C. J. Olson Reichhardt, Phys. Rev. B **91**, 184502 (2015).

[27] C. Reichhardt and C. J. Olson Reichhardt, Phys. Rev. B **93**, 064508 (2016).

[28] A. K. Mukhopadhyay, B. Liebchen, T. Wulf, and P. Schmelcher, Phys. Rev. E **93**, 052219 (2016).

[29] B. Liebchen, F. K. Diakonos, and P. Schmelcher, New J. Phys. **14**, 103032 (2012).

[30] A. K. Mukhopadhyay and P. Schmelcher, Phys. Rev. Research **2**, 013290 (2020).

[31] C. Reichhardt and C. J. Olson Reichhardt, Phys. Rev. E **68**, 046102 (2003).

[32] G. Jotzu, M. Messer, R. Desbuquois, M. Lebrat, T. Uehlinger, D. Greif, and T. Esslinger, Nature (London) **515**, 237 (2014).

[33] J. Struck, C. Ölschläger, M. Weinberg, P. Hauke, J. Simonet, A. Eckardt, M. Lewenstein, K. Sengstock, and P. Windpassinger, Phys. Rev. Lett. **108**, 225304 (2012).

[34] S. Denisov, Y. Zolotaryuk, S. Flach, and O. Yevtushenko, Phys. Rev. Lett. **100**, 224102 (2008).

[35] H. Tutu and Y. Hoshino, Phys. Rev. E **84**, 061119 (2011).

[36] H. Tutu and S. Nagata, Phys. Rev. E **87**, 022144 (2013).

[37] A. W. Ghosh and S. V. Khare, Phys. Rev. E **67**, 056110 (2003).

[38] A. W. Ghosh and S. V. Khare, Phys. Rev. Lett. **84**, 5243 (2000).

[39] P. Hauke, O. Tieleman, A. Celi, C. Ölschläger, J. Simonet, J. Struck, M. Weinberg, P. Windpassinger, K. Sengstock, M. Lewenstein, and A. Eckardt, Phys. Rev. Lett. **109**, 145301 (2012).

[40] C. Petri, F. Lenz, F. K. Diakonos, and P. Schmelcher, Phys. Rev. E **81**, 046219 (2010).

[41] B. Liebchen, C. Petri, F. Lenz, and P. Schmelcher, Europhys. Lett. **94**, 40001 (2011).

[42] G. Grynberg and C. Robilliard, Phys. Rep. **355**, 335 (2001).

[43] D. Barredo, S. de Léséleuc, V. Lienhard, T. Lahaye, and A. Browaeys, Science **354**, 1021 (2016).

[44] H. Kim, W. Lee, H. G. Lee, H. Jo, Y. Song, and J. Ahn, Nat. Commun. **7**, 13317 (2016).

[45] F. Nogrette, H. Labuhn, S. Ravets, D. Barredo, L. Béguin, A. Vernier, T. Lahaye, and A. Browaeys, Phys. Rev. X **4**, 021034 (2014).

[46] D. Stuart and A. Kuhn, New J. Phys. **20**, 023013 (2018).

[47] M. Lohse, C. Schweizer, O. Zilberberg, M. Aidelsburger, and I. Bloch, Nat. Phys. **12**, 350 (2016).

[48] A. Alberti, G. Ferrari, V. V. Ivanov, M. L. Chiofalo, and G. M. Tino, New J. Phys. **12**, 065037 (2010).

[49] M. Arnal, V. Brunaud, G. Chatelain, C. Cabrera-Gutiérrez, E. Michon, P. Cheiney, J. Billy, and D. Guéry-Odelin, Phys. Rev. A **100**, 013416 (2019).

[50] J. J. Stoker, *Differential Geometry* (Wiley, New York, 1989).

[51] M. Berger and B. Gostiaux, *Differential Geometry: Manifolds, Curves, and Surfaces: Manifolds, Curves, and Surfaces*, Graduate Texts in Mathematics (Springer, New York, 1988).

[52] M. Tabor, *Chaos and Integrability in Nonlinear Dynamics: An Introduction* (Wiley, New York, 1989).

4

Conclusion and Outlook

In this cumulative thesis, we have explored the controllability of directed transport in driven lattices which operate in the underdamped or purely Hamiltonian regime. The essential aim was to understand the particle dynamics in these systems in terms of the underlying phase space, which would allow us to control the transport phenomena by engineering the phase space structures. A second closely related objective was to better understand the occurrence of directed transport in two dimensional setups, including rotational or vortical currents. In this chapter, we would give brief summary of our findings and provide perspectives for future research.

In $[A1]$, we have shown that particles in a 2D driven optical lattice type potential can be transported at different angles depending on their physical properties like mass or size. Specifically, we have demonstrated how the average velocities of the underlying ballistic attractors in the phase space depend on these physical properties and the potential height of the lattice. This provided an efficient scheme to segregate more than two species of particles differing in their mass or size simultaneously and this was illustrated with examples of colloidal particles and cold atoms. From the perspectives of ratchet physics, this demonstrates that a periodically driven 2D dissipative lattice can induce ballistic directed transport of particles simultaneously at different angles in a species-selective manner. From the point of view of technical applications, the simultaneous separation of multiple species constitutes a significant improvement over the existing ratchet based segregation schemes in 1D, which can only separate binary mixtures at a time. Furthermore, owing to the inherently deterministic character of the mechanism and non-requirement of an overdamped setup, the scheme can be potentially ap-

plied to particles with larger sizes too, for e.g. granular particles. A potential future extension would be to realize such a segregation scheme in 2D Hamiltonian systems. In this case, particle-particle interaction or disordered potentials could play the role of dissipation which might induce transition of particles dynamics from chaotic to ballistic with their average velocities characterized by their physical properties [95, 113].

The investigation of the transport properties of underdamped particles continued in $[A2]$, where we have shown that they can be transported at specific directions in different types of 2D Bravais lattices driven by unbiased external forces. This is indeed one of the very few works where directed transport is achieved in a 2D spatially periodic system driven out of equilibrium only by unbiased ac-forces [13, 23, 56]. One of the most important feature of this setup is that the required breaking of spatial inversion symmetry is achieved solely due to the structure and geometry of the lattice. The velocity of the ballistic attractors underlying the setup can be controlled by the lattice geometry and the orientation of the oscillating ac-drive. This allow us to realize directed transport parallel, perpendicular and oblique to the drive orientation depending on the lattice geometry. A remarkable result is that it is possible to explain the direction of transport even in the lattices without any lines of reflection symmetry, for e.g. oblique lattices, which is in general impossible using the standard symmetry arguments. Future perspectives include the investigation of the role lattice geometry plays in directed transport of particles in purely Hamiltonian setups.

In $[A3 - A5]$, we shifted our focus to 1D and 2D driven lattice setups which operate in purely Hamiltonian regime without any dissipation. Specifically, the aim was to devise methods to control the directed transport of ensembles in these setups in a time-dependent manner. In $[A3]$, we have demonstrated that two superimposed 1D driven optical lattices can be used to accelerate, freeze and reverse the transport on demand by a time-dependent switch of either the potential height or driving phase of one of the lattices. These parameter switches are shown to induce characteristic changes in the underlying phase space, which allow us to control the particle velocities. The key requirement is that the phase space should be 'mixed', i.e. have both chaotic and regular components separated by cantori structures. Such a generic requirement makes this scheme applicable for different physical systems, one of them being cold atoms in ac-driven optical lattices.

In $[A4]$ and $[A5]$, we have shown that a time-dependent change of the transport direction can also occur without any explicit time-dependent switch of a system

parameter. In [A4], we have demonstrated that the direction of transport in a 2D driven lattice can be reversed dynamically due to the strong coupling of underlying lattice potential in the two dimensions. The timescale of current reversal can be controlled by changing the strength of the dimensional coupling. In [A5], such a dynamical current reversal is achieved by superimposing spatially localized lattices over a 'global' background lattice. Interestingly, we can induce multiple current reversals in the setup by using more than one localized lattice at different positions. The timescales of these reversals can be controlled by adjusting the spatial locations of the superimposed lattices. The key principle behind both these processes is a precise control of the underlying phase spaces, which allow the particles to access regions of phase space which are inaccessible otherwise. Cold atomic ensembles in optical lattices operating in an extremely weak dissipative regime form an ideal test bed for these effects.

Unlike in [A1 − A5] where the focus is on translational currents, in [A6] we study the rotational or vortical transport of particles in 2D driven lattices. Here we demonstrate that superlattices of periodically driven localized potential wells provide a highly controllable setup to achieve rotational transport of an ensemble. One of the key findings is that the spatial arrangement of the potential wells having different driving phases can be used to design setups which break the reflection symmetries, thus allowing such rotational motion of particles. The angular velocities of the particles can be controlled by the potential depths of the wells, which allow us to realize a variety of spatial arrangements of particles having different angular velocities. Such rotational motion of neutral particles in driven lattices is quite interesting since it provides an analogous method to mimic the behavior of charged particles in a magnetic field. An interesting future perspective could be the investigation of the particle dynamics in the analogous quantum setup with the possibility to realize spatially varying artificial magnetic fluxes [114–118].

One of the major outcome of this thesis is the ability to break different spatio-temporal symmetries by designing setups composed of individually driven barriers or wells. The fact that the symmetries of the setup depends highly on how these barriers or wells are arranged in space and how they are driven with time allow us to flexibly control not only the global but also the local symmetries of the setup. A second important outcome is the ability to control the large scale phase space structures underlying the system, for e.g. the ballistic islands, cantori and chaotic sea for the Hamiltonian setups or the attractors in presence of dissipation.

Besides allowing a high degree of control over the transport in both 1D and 2D setups, this also helps us understand the effect of different parameters like lattice geometry or physical properties of particles on the transport. The ability to tune the setup symmetries and the phase space presents promising opportunities to realize many novel transport phenomena in future. One of them is the investigation of the impact of local symmetries on the global transport in driven lattice setups. It has been shown that locally symmetric structures can play an important role in the context of wave propagation in both one and two dimensions [119–122]. The concept of local symmetries can be extended to driven lattice setups by considering periodic arrangements of locally driven potential wells or barriers, with spatial domains which are locally symmetric with respect to certain symmetry transformations. Indeed, we have presented such a setup in [A6] where the unit-cell of our setup could be broken down into multiple spatial domains which are connected by a spatial parity transformation. It would be interesting to see what effect these locally symmetric domains have on the phase space of the entire system. Could the global translational transport in such systems be decomposed in terms of certain 'local' components governed by the symmetries of these spatial domains? This might allow targeted design of setups allowing specific values of transport velocities through a bottom-up approach by combining different locally symmetric potentials.

In contrast to setups where each potential barrier in the lattice is driven by the same time-dependent driving force, the setups where each barrier can be driven differently allow us to design 'block' superlattices [47, 48]. The idea is to arrange the barriers in spatially periodic groups or blocks with all the barriers in each block being driven by a specific driving law. This promises another interesting perspective for future research, which is the investigation of particle dynamics in 2D block superlattices. Similar setups in 1D has been shown to introduce new phenomena like the conversion of an initially diffusive particle ensemble into a pulsed particle beam [47] or the formation of density wave like structures in space [48]. One of the major reasons behind the occurrence of these phenomena is the conversion of particle dynamics from diffusive to ballistic and vice-versa at the junctions of two consecutive blocks in space. In contrast to the 1D setup where each block has only two edges, the blocks in the 2D setup can be designed such that they have multiple edges through which the particles can enter or leave a specific block. This would allow multiple conversions of particle dynamics at the different block edges leading to potentially richer density distributions of parti-

cles over the 2D space. Furthermore, by choosing an appropriate driving law for a specific block, one can induce directed transport of particles in this block at a specific direction. By proper arrangement of different blocks in space with different driving laws, one can in principle design many different transport patterns including transport along closed circular paths in space.

Another interesting perspective is to investigate how a spatially localized disordered potential impacts the dynamics of particles in the 2D driven lattices. For similar setups in 1D, it has been shown that localized disorder induces conversion of particle dynamics from diffusive to regular [113] and the efficiency of such a conversion process depends on the strength as well as the spatial extent of the disordered potential. In 2D, one can design different spatial distributions of such disordered potentials and this might lead to different types of modification in the particle dynamics which are not observed in the 1D counterparts. A particular aim could be to induce transition of particles from the chaotic sea to specific regular islands in the phase space by choosing specific profiles of the spatially localized disorder. Additionally, this kind of conversion process might help us classify the regular manifolds of the underlying phase space for 2D driven Hamiltonian setups, which is in general not easy to visualize due to its higher dimensionality.

Bibliography

[1] R. P. Feynman, R. B. Leighton, and M. Sands, *The Feynman Lectures on Physics, Vol. I: The New Millennium Edition: Mainly Mechanics, Radiation, and Heat* (Hachette UK, 2015).

[2] M. Smoluchowski, *"Experimentell nachweisbare, der üblichen Thermodynamik widersprechende Molekularphänomene,"* Pisma Mariana Smoluchowskiego **2**, 226 (1927).

[3] A. Ajdari and J. Prost, *"Mouvement induit par un potentiel périodique de basse symétrie : Diélectrophorèse pulsée,"* C. r. Acad. sci., Sér. 2 **315**, 1635 (1992).

[4] R. D. Astumian and P. Hänggi, *"Brownian Motors,"* Phys. Today **55**, 33 (2002).

[5] R. D. Astumian, *"Thermodynamics and Kinetics of a Brownian Motor,"* Science **276**, 917 (1997).

[6] M. O. Magnasco, *"Forced thermal ratchets,"* Phys. Rev. Lett. **71**, 1477 (1993).

[7] R. Bartussek, P. Hänggi, and J. G. Kissner, *"Periodically Rocked Thermal Ratchets,"* Europhys. Lett. **28**, 459 (1994).

[8] C. R. Doering, W. Horsthemke, and J. Riordan, *"Nonequilibrium fluctuation-induced transport,"* Phys. Rev. Lett. **72**, 2984 (1994).

[9] J. Prost, J. F. Chauwin, L. Peliti, and A. Ajdari, *"Asymmetric pumping of particles,"* Phys. Rev. Lett. **72**, 2652 (1994).

[10] P. Reimann, *"Brownian motors: Noisy transport far from equilibrium,"* Phys. Rep. **361**, 57 (2002).

[11] J. Rousselet, L. Salome, A. Ajdari, and J. Prost, *"Directional motion of brownian particles induced by a periodic asymmetric potential."* Nature **370**, 446 (1994).

[12] L. P. Faucheux, L. S. Bourdieu, P. D. Kaplan, and A. J. Libchaber, *"Optical Thermal Ratchet,"* Phys. Rev. Lett. **74**, 1504 (1995).

[13] S. H. Wu, N. Huang, E. Jaquay, and M. L. Povinelli, *"Near-Field, On-Chip Optical Brownian Ratchets,"* Nano Lett. **16**, 5261 (2016).

[14] R. Bartussek, P. Reimann, and P. Hänggi, *"Precise Numerics versus Theory for Correlation Ratchets,"* Phys. Rev. Lett. **76**, 1166 (1996).

[15] D. R. Chialvo and M. M. Millonas, *"Asymmetric unbiased fluctuations are sufficient for the operation of a correlation ratchet,"* Physics Letters A **209**, 26 (1995).

[16] I. Zapata, R. Bartussek, F. Sols, and P. Hänggi, *"Voltage Rectification by a SQUID Ratchet,"* Phys. Rev. Lett. **77**, 2292 (1996).

[17] F. Falo, P. J. Martínez, J. J. Mazo, and S. Cilla, *"Ratchet potential for fluxons in Josephson-junction arrays,"* Europhys. Lett. **45**, 700 (1999).

[18] E. Trías, J. J. Mazo, F. Falo, and T. P. Orlando, *"Depinning of kinks in a Josephson-junction ratchet array,"* Phys. Rev. E **61**, 2257 (2000).

[19] C.-S. Lee, B. Jankó, I. Derényi, and A.-L. Barabási, *"Reducing vortex density in superconductors using the 'ratchet effect',"* Nature **400**, 337 (1999).

[20] J. F. Wambaugh, C. Reichhardt, C. J. Olson, F. Marchesoni, and F. Nori, *"Superconducting Fluxon Pumps and Lenses,"* Phys. Rev. Lett. **83**, 5106 (1999).

[21] P. Jung, J. G. Kissner, and P. Hänggi, *"Regular and Chaotic Transport in Asymmetric Periodic Potentials: Inertia Ratchets,"* Phys. Rev. Lett. **76**, 3436 (1996).

[22] A. V. Arzola, K. Volke-Sepúlveda, and J. L. Mateos, *"Experimental Control of Transport and Current Reversals in a Deterministic Optical Rocking Ratchet,"* Phys. Rev. Lett. **106**, 168104 (2011).

[23] K. Loutherback, J. Puchalla, R. H. Austin, and J. C. Sturm, *"Deterministic Microfluidic Ratchet,"* Phys. Rev. Lett. **102**, 045301 (2009).

[24] J. L. Mateos, *"Chaotic Transport and Current Reversal in Deterministic Ratchets,"* Phys. Rev. Lett. **84**, 258 (2000).

[25] M. Barbi and M. Salerno, *"Phase locking effect and current reversals in deterministic underdamped ratchets,"* Phys. Rev. E **62**, 1988 (2000).

[26] R. Salgado-García, M. Aldana, and G. Martínez-Mekler, *"Deterministic Ratchets, Circle Maps, and Current Reversals,"* Phys. Rev. Lett. **96**, 134101 (2006).

[27] A. Sarmiento and H. Larralde, *"Deterministic transport in ratchets,"* Phys. Rev. E **59**, 4878 (1999).

[28] M. Borromeo, G. Costantini, and F. Marchesoni, *"Deterministic ratchets: Route to diffusive transport,"* Phys. Rev. E **65**, 041110 (2002).

[29] Q. Guo, S. M. McFaul, and H. Ma, *"Deterministic microfluidic ratchet based on the deformation of individual cells,"* Phys. Rev. E **83**, 051910 (2011).

[30] T. Kulrattanarak, R. G. M. van der Sman, Y. S. Lubbersen, C. G. P. H. Schroën, H. T. M. Pham, P. M. Sarro, and R. M. Boom, *"Mixed motion in deterministic ratchets due to anisotropic permeability,"* Journal of Colloid and Interface Science **354**, 7 (2011).

[31] Y. S. Lubbersen, M. A. I. Schutyser, and R. M. Boom, *"Suspension separation with deterministic ratchets at moderate Reynolds numbers,"* Chemical Engineering Science **73**, 314 (2012).

[32] M. Salerno and Y. Zolotaryuk, *"Soliton ratchetlike dynamics by ac forces with harmonic mixing,"* Phys. Rev. E **65**, 056603 (2002).

[33] M. Borromeo and F. Marchesoni, *"Noise-assisted transport on symmetric periodic substrates,"* Chaos **15**, 026110 (2005).

[34] M. Borromeo, S. Giusepponi, and F. Marchesoni, *"Recycled noise rectification: An automated Maxwell's daemon,"* Phys. Rev. E **74**, 031121 (2006).

[35] S. Savel'ev, F. Marchesoni, P. Hänggi, and F. Nori, *"Nonlinear signal mixing in a ratchet device,"* EPL **67**, 179 (2004).

[36] S. Savel'ev, F. Marchesoni, P. Hänggi, and F. Nori, *"Transport via nonlinear signal mixing in ratchet devices,"* Phys. Rev. E **70**, 066109 (2004).

[37] F. Marchesoni, *"Harmonic mixing signal: Doubly dithered ring laser gyroscope,"* Physics Letters A **119**, 221 (1986).

[38] W. Wonneberger, *"Stochastic theory of harmonic microwave mixing in periodic potentials,"* Solid State Communications **30**, 511 (1979).

[39] S. Flach, O. Yevtushenko, and Y. Zolotaryuk, *"Directed Current due to Broken Time-Space Symmetry,"* Phys. Rev. Lett. **84**, 2358 (2000).

[40] S. Denisov, S. Flach, and P. Hänggi, *"Tunable transport with broken space–time symmetries,"* Phys. Rep. **538**, 77 (2014).

[41] T. Dittrich, R. Ketzmerick, M.-F. Otto, and H. Schanz, *"Classical and quantum transport in deterministic Hamiltonian ratchets,"* Annalen der Physik **9**, 755 (2000).

[42] H. Schanz, M. F. Otto, R. Ketzmerick, and T. Dittrich, *"Classical and Quantum Hamiltonian Ratchets,"* Phys. Rev. Lett. **87**, 070601 (2001).

[43] F. Renzoni, *Driven Ratchets in Cold Atoms* (Elsevier, Amsterdam, 2009).

[44] F. Renzoni, in *Adv. At. Mol. Opt. Phys.*, Vol. 57 (Elsevier, 2009) pp. 1–32.

[45] C. Petri, F. Lenz, F. Diakonos, and P. Schmelcher, *"Directed transport and localization in phase-modulated driven lattices,"* Phys. Rev. E **81**, 046219 (2010).

[46] B. Liebchen, C. Petri, F. Lenz, and P. Schmelcher, *"Patterned deposition of particles in spatio-temporally driven lattices,"* Europhys. Lett. **94**, 40001 (2011).

[47] T. Wulf, C. Petri, B. Liebchen, and P. Schmelcher, *"Analysis of interface conversion processes of ballistic and diffusive motion in driven superlattices,"* Phys. Rev. E **86**, 016201 (2012).

[48] C. Petri, F. Lenz, B. Liebchen, F. Diakonos, and P. Schmelcher, *"Formation of density waves via interface conversion of ballistic and diffusive motion,"* Europhys. Lett. **95**, 30005 (2011).

[49] S. Denisov, Y. Zolotaryuk, S. Flach, and O. Yevtushenko, *"Vortex and Translational Currents due to Broken Time-Space Symmetries,"* Phys. Rev. Lett. **100**, 224102 (2008).

[50] J. S. Bader, R. W. Hammond, S. A. Henck, M. W. Deem, G. A. McDermott, J. M. Bustillo, J. W. Simpson, G. T. Mulhern, and J. M. Rothberg, *"DNA transport by a micromachined Brownian ratchet device,"* PNAS **96**, 13165 (1999).

[51] L. P. Faucheux and A. Libchaber, *"Selection of Brownian particles,"* J. Chem. Soc., Faraday Trans. **91**, 3163 (1995).

[52] D. G. Grier and Y. Roichman, *"Holographic optical trapping,"* Appl. Opt. **45**, 880 (2006).

[53] D. G. Grier, *"A revolution in optical manipulation,"* Nature **424**, 810 (2003).

[54] K. Dholakia, M. P. MacDonald, P. Zemánek, and T. Čižmár, in *Methods in Cell Biology*, Laser Manipulation of Cells and Tissues, Vol. 82 (Academic Press, 2007) pp. 467–495.

[55] S.-H. Lee, K. Ladavac, M. Polin, and D. G. Grier, *"Observation of Flux Reversal in a Symmetric Optical Thermal Ratchet,"* Phys. Rev. Lett. **94**, 110601 (2005).

[56] A. V. Arzola, M. Villasante-Barahona, K. Volke-Sepúlveda, P. Jákl, and P. Zemánek, *"Omnidirectional Transport in Fully Reconfigurable Two Dimensional Optical Ratchets,"* Phys. Rev. Lett. **118**, 138002 (2017).

[57] C. Mennerat-Robilliard, D. Lucas, S. Guibal, J. Tabosa, C. Jurczak, J.-Y. Courtois, and G. Grynberg, *"Ratchet for Cold Rubidium Atoms: The Asymmetric Optical Lattice,"* Phys. Rev. Lett. **82**, 851 (1999).

[58] M. Schiavoni, L. Sanchez-Palencia, F. Renzoni, and G. Grynberg, *"Phase Control of Directed Diffusion in a Symmetric Optical Lattice,"* Phys. Rev. Lett. **90**, 094101 (2003).

[59] M. Brown and F. Renzoni, *"Ratchet effect in an optical lattice with biharmonic driving: A numerical analysis,"* Phys. Rev. A **77**, 033405 (2008).

[60] R. Gommers, S. Bergamini, and F. Renzoni, *"Dissipation-Induced Symmetry Breaking in a Driven Optical Lattice,"* Phys. Rev. Lett. **95**, 073003 (2005).

[61] R. Gommers, V. Lebedev, M. Brown, and F. Renzoni, *"Gating ratchet for cold atoms."* Phys. Rev. Lett. **100**, 040603 (2008).

[62] D. Cubero and F. Renzoni, *"Asymptotic theory of quasiperiodically driven quantum systems,"* Phys. Rev. E **97**, 062139 (2018).

[63] D. Cubero and F. Renzoni, *"Control of transport in two-dimensional systems via dynamical decoupling of degrees of freedom with quasiperiodic driving fields,"* Phys. Rev. E **86**, 056201 (2012).

[64] D. Cubero, V. Lebedev, and F. Renzoni, *"Current reversals in a rocking ratchet: Dynamical versus symmetry-breaking mechanisms,"* Phys. Rev. E **82**, 041116 (2010).

[65] D. Cubero and F. Renzoni, *"Hidden symmetries, instabilities, and current suppression in Brownian ratchets,"* Phys. Rev. Lett. **116**, 010602 (2016).

[66] V. Lebedev and F. Renzoni, *"Two-dimensional rocking ratchet for cold atoms,"* Phys. Rev. A **80**, 023422 (2009).

[67] A. Wickenbrock, D. Cubero, N. A. A. Wahab, P. Phoonthong, and F. Renzoni, *"Current reversals in a rocking ratchet: The frequency domain,"* Phys. Rev. E **84**, 021127 (2011).

[68] A. Wickenbrock, P. C. Holz, N. A. A. Wahab, P. Phoonthong, D. Cubero, and F. Renzoni, *"Vibrational mechanics in an optical lattice: Controlling transport via potential renormalization."* Phys. Rev. Lett. **108**, 020603 (2012).

[69] D. Cubero and F. Renzoni, *Brownian Ratchets* (Cambridge University Press, Cambridge, 2016).

[70] I. Derényi and R. Dean Astumian, *"Ac separation of particles by biased Brownian motion in a two-dimensional sieve,"* Phys. Rev. E **58**, 7781 (1998).

[71] S. Matthias and F. Müller, *"Asymmetric pores in a silicon membrane acting as massively parallel brownian ratchets,"* Nature **424**, 53 (2003).

[72] M. Cabodi, Y.-F. Chen, S. W. P. Turner, H. G. Craighead, and R. H. Austin, *"Continuous separation of biomolecules by the laterally asymmetric diffusion array with out-of-plane sample injection,"* ELECTROPHORESIS **23**, 3496 (2002).

[73] A. van Oudenaarden, *"Brownian Ratchets: Molecular Separations in Lipid Bilayers Supported on Patterned Arrays,"* Science **285**, 1046 (1999).

[74] F. Liu, L. Jiang, H. M. Tan, A. Yadav, P. Biswas, J. R. C. van der Maarel, C. A. Nijhuis, and J. A. van Kan, *"Separation of superparamagnetic particles through ratcheted Brownian motion and periodically switching magnetic fields,"* Biomicrofluidics **10**, 064105 (2016).

[75] C. J. O. Reichhardt and C. Reichhardt, *"Ratchet Effects in Active Matter Systems,"* Annu. Rev. Condens. Matter Phys. **8**, 51 (2017).

[76] B. Ai, *"Ratchet transport powered by chiral active particles,"* Sci. Rep. **6**, 18740 (2016).

[77] S. M. McFaul, B. K. Lin, and H. Ma, *"Cell separation based on size and deformability using microfluidic funnel ratchets,"* Lab Chip **12**, 2369 (2012).

[78] J. F. Wambaugh, C. Reichhardt, and C. J. Olson, *"Ratchet-induced segregation and transport of nonspherical grains,"* Phys. Rev. E **65**, 031308 (2002).

[79] J. Spiechowicz and J. \Luczka, *"SQUID ratchet: Statistics of transitions in dynamical localization,"* Chaos An Interdiscip. J. Nonlinear Sci. **29**, 013105 (2019).

[80] J. Spiechowicz and J. \Luczka, *"Efficiency of the SQUID ratchet driven by external current,"* New J. Phys. **17**, 023054 (2015).

[81] Y. Zolotaryuk, *"Asymmetric ac fluxon depinning in a Josephson junction array: A highly discrete limit,"* Phys. Rev. E **86**, 026604 (2012).

[82] C. C. de Souza Silva, J. Van de Vondel, M. Morelle, and V. V. Moshchalkov, *"Controlled multiple reversals of a ratchet effect,"* Nature **440**, 651 (2006).

[83] C. Reichhardt, D. Ray, and C. J. O. Reichhardt, *"Reversible ratchet effects for vortices in conformal pinning arrays,"* Phys. Rev. B **91**, 184502 (2015).

[84] C. Reichhardt and C. J. O. Reichhardt, *"Transverse ac-driven and geometric ratchet effects for vortices in conformal crystal pinning arrays,"* Phys. Rev. B **93**, 064508 (2016).

[85] M. M. Millonas and M. I. Dykman, *"Transport and current reversal in stochastically driven ratchets,"* Physics Letters A **185**, 65 (1994).

[86] B. Dandogbessi, O. Akin-Ojo, and A. Kenfack, *"Controlling current reversals in chaotic ratchet transport,"* Phys. Scr. **90**, 055206 (2015).

[87] M. Schreier, P. Reimann, P. Hänggi, and E. Pollak, *"Giant enhancement of diffusion and particle selection in rocked periodic potentials,"* Europhys. Lett. **44**, 416 (1998).

[88] L. Dinis and N. R. Quintero, *"Nonsinusoidal current and current reversals in a gating ratchet,"* Phys. Rev. E **91**, 032920 (2015).

[89] C. Zeng, H. Wang, and L. Nie, *"Multiple current reversals and diffusion enhancement in a symmetrical periodic potential,"* Chaos **22**, 033125 (2012).

[90] M. Kostur and J. Łuczka, *"Multiple current reversal in Brownian ratchets,"* Phys. Rev. E **63**, 021101 (2001).

[91] R. Chen, G. Zhang, C. Wang, L. Nie, and C. Chen, *"Current reversal in a symmetric periodic potential,"* Chaos, Solitons & Fractals **98**, 205 (2017).

[92] S. Rana, S. Goswami, S. Chatterjee, and P. Pradhan, *"Current reversal in interacting colloids under time-periodic drive,"* Phys. Rev. E **98**, 052142 (2018).

[93] R. M. da Silva, C. Manchein, and M. W. Beims, *"Optimal ratchet current for elastically interacting particles,"* Chaos **29**, 111101 (2019).

[94] V. I. Marconi, *"Rocking Ratchets in Two-Dimensional Josephson Networks: Collective Effects and Current Reversal,"* Phys. Rev. Lett. **98**, 047006 (2007).

[95] B. Liebchen, F. K. Diakonos, and P. Schmelcher, *"Interaction-induced current-reversals in driven lattices,"* New J. Phys. **14**, 103032 (2012).

[96] A. K. Mukhopadhyay, T. Xie, B. Liebchen, and P. Schmelcher, *"Dimensional coupling-induced current reversal in two-dimensional driven lattices,"* Phys. Rev. E **97**, 050202 (2018).

[97] A. K. Mukhopadhyay, B. Liebchen, T. Wulf, and P. Schmelcher, *"Freezing, accelerating, and slowing directed currents in real time with superimposed driven lattices,"* Phys. Rev. E **93**, 052219 (2016).

[98] C. Berghaus, U. Kahlert, and J. Schnakenberg, *"Current reversal induced by a cyclic stochastic process,"* Physics Letters A **224**, 243 (1997).

[99] M. Bier, *"Reversals of noise induced flow,"* Physics Letters A **211**, 12 (1996).

[100] D. Dan, M. C. Mahato, and A. M. Jayannavar, *"Multiple current reversals in forced inhomogeneous ratchets,"* Phys. Rev. E **63**, 056307 (2001).

[101] R. Tammelo, R. Mankin, and D. Martila, *"Three and four current reversals versus temperature in correlation ratchets with a simple sawtooth potential,"* Phys. Rev. E **66**, 051101 (2002).

[102] B. Lindner, L. Schimansky-Geier, P. Reimann, P. Hänggi, and M. Nagaoka, *"Inertia ratchets: A numerical study versus theory,"* Phys. Rev. E **59**, 1417 (1999).

[103] C. J. Olson, C. Reichhardt, B. Jankó, and F. Nori, *"Collective Interaction-Driven Ratchet for Transporting Flux Quanta,"* Phys. Rev. Lett. **87**, 177002 (2001).

[104] C. Reichhardt and C. J. Olson Reichhardt, *"Absolute transverse mobility and ratchet effect on periodic two-dimensional symmetric substrates,"* Phys. Rev. E **68**, 046102 (2003).

[105] C. Reichhardt, C. J. O. Reichhardt, and M. B. Hastings, *"Nonlinear dynamics, rectification, and phase locking for particles on symmetrical two-dimensional periodic substrates with dc and circular ac drives,"* Phys. Rev. E **69**, 056115 (2004).

[106] C. Reichhardt and C. J. Olson Reichhardt, *"Ratchet effect and nonlinear transport for particles on random substrates with crossed ac drives,"* Phys. Rev. E **73**, 011102 (2006).

[107] C. Reichhardt, C. J. Olson, and M. B. Hastings, *"Rectification and Phase Locking for Particles on Symmetric Two-Dimensional Periodic Substrates,"* Phys. Rev. Lett. **89**, 024101 (2002).

[108] L. Machura, M. Kostur, P. Talkner, J. \Luczka, and P. Hänggi, *"Absolute Negative Mobility Induced by Thermal Equilibrium Fluctuations,"* Phys. Rev. Lett. **98**, 040601 (2007).

[109] H. Tutu and Y. Hoshino, *"Design of two-tooth unidirectional rotary-ratchet molecular machines driven by linearly polarized ac fields,"* Phys. Rev. E **84**, 061119 (2011).

[110] H. Tutu and S. Nagata, *"Robust unidirectional rotation in three-tooth Brownian rotary ratchet systems,"* Phys. Rev. E **87**, 022144 (2013).

[111] A. W. Ghosh and S. V. Khare, *"Breaking of general rotational symmetries by multidimensional classical ratchets,"* Phys. Rev. E **67**, 056110 (2003).

[112] A. W. Ghosh and S. V. Khare, *"Rotation in an Asymmetric Multidimensional Periodic Potential due to Colored Noise,"* Phys. Rev. Lett. **84**, 5243 (2000).

[113] T. Wulf, B. Liebchen, and P. Schmelcher, *"Disorder Induced Regular Dynamics in Oscillating Lattices,"* Phys. Rev. Lett. **112**, 034101 (2014).

[114] G. Jotzu, M. Messer, R. Desbuquois, M. Lebrat, T. Uehlinger, D. Greif, and T. Esslinger, *"Experimental realization of the topological Haldane model with ultracold fermions,"* Nature **515**, 237 (2014).

[115] J. Struck, C. Ölschläger, M. Weinberg, P. Hauke, J. Simonet, A. Eckardt, M. Lewenstein, K. Sengstock, and P. Windpassinger, *"Tunable Gauge Potential for Neutral and Spinless Particles in Driven Optical Lattices,"* Phys. Rev. Lett. **108**, 225304 (2012).

[116] M. Aidelsburger, S. Nascimbene, and N. Goldman, *"Artificial gauge fields in materials and engineered systems,"* Comptes Rendus Physique Quantum Simulation / Simulation Quantique, **19**, 394 (2018).

[117] M. Aidelsburger, *"Artificial gauge fields and topology with ultracold atoms in optical lattices,"* J. Phys. B: At. Mol. Opt. Phys. **51**, 193001 (2018).

[118] J. Dalibard, F. Gerbier, G. Juzeliūnas, and P. Öhberg, *"Colloquium: Artificial gauge potentials for neutral atoms,"* Rev. Mod. Phys. **83**, 1523 (2011).

[119] P. A. Kalozoumis, C. V. Morfonios, F. K. Diakonos, and P. Schmelcher, *"Invariant currents and scattering off locally symmetric potential landscapes,"* Annals of Physics **362**, 684 (2015).

[120] P. A. Kalozoumis, C. Morfonios, F. K. Diakonos, and P. Schmelcher, *"Local symmetries in one-dimensional quantum scattering,"* Phys. Rev. A **87**, 032113 (2013).

[121] P. A. Kalozoumis, C. Morfonios, F. K. Diakonos, and P. Schmelcher, *"Invariants of Broken Discrete Symmetries,"* Phys. Rev. Lett. **113**, 050403 (2014).

[122] M. Röntgen, C. V. Morfonios, F. K. Diakonos, and P. Schmelcher, *"Nonlocal currents and the structure of eigenstates in planar discrete systems with local symmetries,"* Annals of Physics **380**, 135 (2017).

Acknowledgments

First of all, I would like to thank Prof. Dr. Peter Schmelcher for providing me the opportunity to carry out my PhD in his research group, supervising me and introducing me to this beautiful research topic. His constant support, motivation and guidance immensely helped me to enjoy my research and learn from my mistakes.

I thank Prof. Dr. Benno Liebchen, Dr. Thomas Wulf and Dr. Tianting Xie for the scientific collaborations and exchanges throughout the first few years of this thesis. Many thanks to Benno and Thomas for helping me understand many of the scientific and numerical techniques of non-linear dynamics used in this thesis.

My sincere thanks to Deutscher Akademischer Austauschdienst (DAAD) for supporting me through a PhD scholarship.

Thanks to all my current and past colleagues in the group, including my office mates Andrea, Jie, Thomas, Friethjof and Ansgar for the many enjoyable moments over these years. Through those long late evening scientific discussions with Jie or the lunchtime discussions with Malte, Christian Morfonios, Maxim and Koushik, I learnt a lot! Thanks to Malte for being such a wonderful and patient German language teacher, and for encouraging me to speak the language. I am also grateful to Markus, Valentin and Fabian for helping me out with so many technical problems and to Anja for all her help in administrative matters.

This thesis wouldn't have been possible without those hundreds of developers designing and maintaining the wonderful numerical tools/softwares which I have used. Thanks to them and the scores of people on online forums like Stack-Exchange, who code snippets have solved many of my problems which would have otherwise taken days to solve.

Outside my direct scientific environment, I am thankful to my friends for being there and supporting me in all difficulties. Thanks to Jhilik, Anand, Swathi, Mariyam, Anchita, Malte, Indranil *da*, Bodhaditya *da* and Suranita *di* for making my life in Hamburg so memorable. Thanks to Harshit and Ankan for always checking on me and discussing problems, both in and beyond science. I am grateful to Mr. Rolf and Mrs. Ursula Auersch for not only providing me a great place to live in Hamburg but also warmly helping me in all possible ways to make me feel at home in a new country. For me, good food is a source of creativity and sink of all depressions! Hence, I can't thank enough the persons in charge of my three often visited restaurants in Hamburg, Mr. Bo (of 'Mr. Dam'), Mr. Makhdum (of 'Samarkhand') and Mr. Josan (of 'Badshah'), not only for excellent lunch/dinners

Eidesstattliche Versicherung (Declaration on oath)

Hiermit versichere ich an Eides statt, die vorliegende Dissertationsschrift selbst verfasst und keine anderen als die angegebenen Hilfsmittel und Quellen benutzt zu haben. Die eingereichte schriftliche Fassung entspricht der auf dem elektronischen Speichermedium. Die Dissertation wurde in der vorgelegten oder einer ähnlichen Form nicht schon einmal in einem früheren Promotionsverfahren angenommen oder als ungenügend beurteilt.

I hereby affirm in lieu of oath that I have written this dissertation myself and not to have used any aids and sources other than those indicated. The written version submitted corresponds to that on the electronic storage medium. The dissertation in the submitted or a similar form has not already been a previous doctoral procedure or was assessed as insufficient.

Hamburg, den